3-15-2021

Applications of Quantum Optics: From the Quantum Internet to Analogue Gravity

Anthony Brady
Louisiana State University and Agricultural and Mechanical College

APPLICATIONS OF QUANTUM OPTICS: FROM THE QUANTUM INTERNET TO ANALOGUE GRAVITY

A Dissertation

Submitted to the Graduate Faculty of the
Louisiana State University and
Agricultural and Mechanical College
in partial fulfillment of the
requirements for the degree of
Doctor of Philosophy

in

The Department of Physics and Astronomy

by
Anthony Brady
B.S., University of North Georgia, 2016
May 2021

I dedicate this work to my family – to my beautiful daughters, Willow, Leigha, and our newest addition, Clover; and to my better half, Autumn. Especially to Autumn, who held down the fort while I was in "thesis mode". I love you all, dearly.

ACKNOWLEDGEMENTS

Foremost, I want to take this opportunity to acknowledge my mother who passed away this past Fall (October 2020). Under difficult circumstances, she set my "life's stage" up remarkably and was the most supportive person I have ever known. She persistently encouraged my sister and I to pursue our dreams, as if there was no other way to go about life, and had zero doubt that we would be successful in doing so. Even if we ended up failing, she was always there to catch us and heal our wounds. I owe almost everything to my mother.

I also want to acknowledge my late advisor, Jonathan P. Dowling, who passed away this past Summer (June 2020). I was extremely fortunate to know Jon and have him as my advisor. He gave me so much support and freedom in my research and trusted me, almost as a colleague rather than a graduate student. The amount of freedom and support that I felt while working with Jon reminds me of the freedom and support that I had with my mother, even though these two personalities were starkly different. There is nothing comparable to having that kind of support system in your family life as well as in your career. I am forever grateful to Jon for illuminating the fact that the workplace can be so human.

I want to thank my current advisor, Ivan Agullo, for reaching out to me after Jon's passing and extending an invitation to "pick me up" as a graduate student, as well as for welcoming my research style and approach to physics. I can only hope for more smooth-sailing from here. I want to thank my first collaborator, Sumeet Khatri. My first real research project was in collaboration with Sumeet, and by observing and working closely with him, I learned how to properly and precisely do research, write papers, and work collaboratively. This lesson was invaluable. I would also like to thank a current post-doc here at LSU and my good friend, Lior Cohen, for being present and extremely supportive during this last year or two. It is also good to see another "family man" in the office! I would also like to thank Stav Haldar for allowing me to play the role of mentor and letting me drag him along my research endeavors. It has been fun, and hopefully, we can explore some more. I would like to thank some specific members of the Quantum Science and Technologies (QST) group, Eneet Kaur and Kunal Sharma, that I have befriended though did not get the pleasure to work with. I would like to thank them both for bringing fun into the office and outside the office as well. I would also like to thank *all* the prior and present members of the QST group which have met me and somehow tolerated my shenanigans without complaining too much. And last, but certainly not least, I would like to thank Siddharth Soni for not only being my first friend at LSU but also for becoming a life-long best friend. I hope that we get to explore the world a bit in the upcoming years.

TABLE OF CONTENTS

ABSTRACT

The aim of this thesis is to highlight applications of quantum optics in two very distinct fields: space-based quantum communication and the Hawking effect in analogue gravity.

Regarding the former: We simulate and analyze a constellation of satellites, equipped with entangled photon-pair sources, which provide on-demand entanglement distribution services to terrestrial receiver stations. Satellite services are especially relevant for long-distance quantum-communication scenarios, as the loss in satellite-based schemes scales more favorably with distance than in optical fibers or in atmospheric links, though establishing quantum resources in the space-domain is expensive. We thus develop an optimization technique which balances both the number of satellites in the constellation and the entanglement-distribution rates that they provide. Comparisons to ground-based quantum-repeater rates are also made. Overall, our results suggest that satellite-based quantum networks are a viable option for establishing the backbone of future quantum internet.

Regarding the latter: The Hawking effect was discussed in the astrophysical context of the spontaneous decay of black holes into blackbody radiation, i.e. Hawking radiation. However, this effect seems to be universal, appearing anywhere that an event horizon (a region which restricts the flow of information to one direction) forms. Here, we analyze the Hawking effect in an optical-analogue gravity system, building on prior theoretical results regarding this effect in dielectric media. We provide a simplification of the process via the Bloch-Messiah reduction, which allows us to decompose the Hawking effect into a discrete set of elementary processes. With this simplification and leveraging the positivity of partial transpose (PPT) criteria, we examine the quantum correlations of the stimulated Hawking effect, explicitly showing that an environmental background temperature, along with backscattering, can lead to entanglement "sudden-death", even when the number of entangled Hawking-pairs is comparatively large. We also discuss the prospect of enhancing and "reviving" entanglement pre-mortem using single-mode, non-classical resources at the input. Though much of the discussion is phrased in terms of an optical-analogue model, the methods used and results obtained apply just as well to a variety of other systems supporting this effect. Finally, we provide Bloch-Messiah reductions of more exotic scenarios consisting of e.g. a white-hole–black-hole pair which share an interior region.

CHAPTER 1. INTRODUCTION

I think it is not too uncommon (pardon the double negative) in physics to constrain oneself to a particular (sub-)field, along with its (sub-)set of principles and its technical machinery, and explore the surrounding world (or universe) through this lens, contributing valuable research to one's field along the way. However, this is not the route I have taken. I have chosen to focus, up to this point, on one particular system instead – the quantum electromagnetic field, photons, flying quantum oscillators, whatever one wants to call them(!) – and asked, "What can one say about various fields or sub-fields in the language of photons? And how do the principles of such fields translate?" This has taken me down various exploratory paths – from space-based quantum communication (see [1] and Section 3) to linear-optical simulation of quantum gravity [2] to Hawking radiation in optical analogue-gravity systems (see Section 4). Perhaps this winding path of mine is due in part to the wandering history and modern meandering of light itself.

For instance, it was experiments with light in the early 20th century which e.g. (i) resolved the "ultra-violet catastrophe" (the classical prediction that black-bodies are unstable at high frequencies) and sparked the quantum revolution through the postulated existence of photons by Einstein (following Planck's lead) [3], (ii) refuted the existence of the luminiferous aether, providing implicit support for Einstein's special theory of relativity [4],[1] and (iii) provided initial support for Einstein's theory of general relativity through early observations of the bending of light by the gravitational field of the sun [5, 6].[2] In the latter half of the 20th century (and very early 21st century), experiments with photons have, as examples, provided the first experimental support for the intrinsic non-locality of quantum mechanics [7, 8] as well as aspects of wave-particle duality at the level of individual quanta [9]. In more modern times, optical interferometers are measuring distortions in space-time induced by gravitational waves (a prediction of the general theory of relativity), even utilizing quantum states of light to enhance the sensitivity of detection events [10]; networks of linear-optical components, together with single-photon sources and detectors, are actively being developed to work as quantum simulators and even universal quantum computers [11, 12]; and photons serve as an essential ingredient for long-distance quantum communication and are crucial for building large-scale, inter-connected quantum networks [13, 14, 15, 16].

This meandering of light through time, subsequently translating into my own research endeavors, has made writing a coherent and comprehensible thesis a bit challenging. In order to facilitate some order of coherency, I have structured this thesis into a few digestible parts:

- The first part, Chapter 2, lays out the mathematical formalism used to describe photons and their dynamics, in general terms and in a simplified fashion, and serves as the basis for later chapters.

- The second part, Chapter 3, is (with a few additional intricacies) an application of the formalism introduced in Chapter 2, to the domain of space-based entanglement-distribution. It is based on my published work [1].

[1] It was Einstein's theoretical investigations of light which brought him to the special theory of relativity. Indeed, one of the postulates has to do with the invariance of the speed of light under changes of reference.

[2] There is a lot of "Einstein" here, but of course, he was not the only one!

- The third and final part, Chapter 4, is another application of the formalism introduced in Chapter 2, now applied in the context of Hawking radiation in optical analogue-gravity systems. This work is still in development, though nearing its completion, with many of the main results appearing in this chapter for the first time.

In this thesis, one should view Chapters 3 and 4 simply as physical (though remarkably distinct) applications of photons and the underlying formalism used to describe them, since this perspective adds a bit of coherency to the document as a whole.

As a final remark, I note that I have also completed other works, which fall under this broad category of "applications of quantum optics", but which I have not included in this thesis. For example, I (and collaborators) have investigated the prospect of simulating/computing transition amplitudes in loop quantum-gravity (an exotic quantum description of general relativity) with a linear-optical quantum simulator [2]. In another work, I and a fellow graduate student investigated aspects of local, geometric quantum-optics in curved space-time, for the purpose of exploring potential overlaps between classical general relativity and seminal quantum-interference experiments in quantum optics (see reference [17]; currently under review). These topics could have just as well served as Chapters 5 and 6 of this thesis, but I did not include them for the sake of brevity and in hopes to avoid any more meandering than necessary.

CHAPTER 2. FUNDAMENTALS

The chapter serves as a pedagogical introduction to many of the concepts and techniques used throughout the thesis. The emphasis is on photons: what to do with them and how to analyze them in various scenarios, in a simplistic and, more or less, generalized framework.

My approach is to provide what I deem interesting, pedagogical, and/or essential in order to comprehend the bulk of this thesis. It is not my concern to dive into the history of the photon nor provide philosophical insights into what a photon is, only to say that it is the quantum (bundle of energy, particle, etc.) of the electromagnetic field, and I provide only an overly-simplistic mathematical description of what that means, at the level of the quantum harmonic oscillator, and how to formally deal with it, at the level of Fock spaces, symplectic transformations, etc.

This chapter is broken into three parts. Section 2.1 introduces photons through quantization of the simple harmonic oscillator. After a thorough discussion of the harmonic oscillator, we swiftly transition to fields, providing a more satisfactory and "closer to reality" description of the quantized electromagnetic field. This section is meant only to develop some familiarity with the structure of quantum fields and set notation. Section 2.2 introduces photon dynamics, restricting to quadratic interactions (the "Gaussian sector") and posed in the form of scattering-like processes. Though this focus seems quite restrictive and perhaps trivial at times, it is rich enough to encompass a variety of phenomena in markedly distinct scenarios – from e.g. photon scattering in the atmosphere in quantum-optical communication to linear-optical quantum-computation to the spontaneous decay of astrophysical black holes, etc. Gaussian states/systems and the Gaussian formalism is also introduced in this section. Finally, in section 2.3, I introduce some basic concepts from quantum information theory with a focus on photonic encoding. Quantum entanglement is also discussed, with focus on the positivity of partial transpose (PPT) criteria for the separability of quantum states. Since much of what I write in this chapter is "textbook material", I will limit the references to textbooks for the most part, a list of which can be found at the beginning of each subsection, as needed.

2.1 Quantum oscillators and photons

The quantum harmonic oscillator

At the most primitive level, the electromagnetic field can be thought of as a sea of massless harmonic oscillators, with an oscillator positioned at each point in space vibrating at some frequency. Thus, to understand the physics and quantum properties of the electromagnetic field, it is sufficient to grasp the corresponding properties of a single, point-like quantum harmonic oscillator. We do this by first characterizing a classical oscillator, which we do so by deriving the equations of motion in the Lagrangian formalism and by also introducing the *canonical variables* for the oscillator. The latter provides an easy route to quantization. After solving the equations of motion, we proceed to quantize the oscillator modes via canonical quantization, which will naturally lead us to extend these notions to fields.

Basic notions regarding the Lagrangian and Hamiltonian formalisms can be found in

Goldstein's classic book [18]. Discussions on the method of canonical quantization can be found in Dirac's classic book [19].

The classical oscillator

I first provide general methods of analyzing physical systems via the Lagrangian and Hamiltonian formalisms. We then apply such to a point-like, simple harmonic oscillator.

Consider the action functional for a (non-relativistic) point-like particle in one dimension,

$$S[x] = \int \mathrm{d}t \mathscr{L}(x, \dot{x}), \tag{2.1}$$

where $\mathscr{L}$ is the *Lagrangian* for the system, x is the position of the particle in space (relative to some origin, taken at $x = 0$), and the overdot represents a derivative with respect to time. The equation of motion is then found through Hamilton's principle, which states that the evolution of the system is governed by the path, $x(t)$, which extremizes the action (e.g., $\delta S = 0$). For a general Lagrangian, the extremization of the action (assuming vanishing boundary conditions) implies the *Euler-Lagrange equations of motion*,

$$\delta S = 0 \implies \frac{\partial \mathscr{L}}{\partial x} - \frac{\mathrm{d}}{\mathrm{d}t}\left(\frac{\partial \mathscr{L}}{\partial \dot{x}}\right) = 0. \tag{2.2}$$

Proof. We prove the preceding implication assuming vanishing endpoints for the variation. Consider the following set of equalities,

$$\begin{aligned}
\delta S &= \int \mathrm{d}t \delta \mathscr{L}(x, \dot{x}) \\
&= \int \mathrm{d}t \left(\frac{\partial \mathscr{L}}{\partial x}\delta x + \frac{\partial \mathscr{L}}{\partial \dot{x}}\delta \dot{x}\right) \\
&= \int \mathrm{d}t \left(\frac{\partial \mathscr{L}}{\partial x}\delta x + \frac{\mathrm{d}}{\mathrm{d}t}\left(\frac{\partial \mathscr{L}}{\partial \dot{x}}\delta x\right) - \frac{\mathrm{d}}{\mathrm{d}t}\left(\frac{\partial \mathscr{L}}{\partial \dot{x}}\right)\delta x\right) \\
&= \frac{\partial \mathscr{L}}{\partial \dot{x}}\delta x\Big|_{t_0}^{t_f} + \int \mathrm{d}t \left(\frac{\partial \mathscr{L}}{\partial x} - \frac{\mathrm{d}}{\mathrm{d}t}\left(\frac{\partial \mathscr{L}}{\partial \dot{x}}\right)\right)\delta x \\
&\overset{\text{def}}{=} 0.
\end{aligned}$$

The final equality follows from Hamilton's principle. The first term in the penultimate equality vanishes by assumption of fixed endpoints (a vanishing boundary condition), while the second term vanishes if and only if the Euler-Lagrange equations hold [eq. (2.2)]. □

Let us now introduce the Hamiltonian formalism and the canonical (or phase-space) variables. After which, we come to our oscillator example, and solve everything in a few strokes.

Given a Lagrangian, $\mathscr{L}$, defined in terms of configuration variables $(x, \dot{x})$, the Hamiltonian, H, defined in terms of the canonical variables (x, p), can be found via the Legendre transform of the Lagrangian – i.e.,

$$H(x, p) = \dot{x}p - \mathscr{L}, \tag{2.3}$$

with

$$p = \frac{\partial \mathscr{L}}{\partial \dot{x}}, \tag{2.4}$$

being the *conjugate momentum*. By definition, the Hamiltonian is solely a function of the canonical variables, (x, p).

Proof. We prove the last statement by variation,

$$\begin{aligned}
\delta H &= \frac{\partial H}{\partial x}\delta x + \frac{\partial H}{\partial p}\delta p \\
&= p\delta\dot{x} + \dot{x}\delta p - \delta\mathscr{L} \\
&= p\delta\dot{x} + \dot{x}\delta p - \frac{\partial \mathscr{L}}{\partial x}\delta x - \frac{\partial \mathscr{L}}{\partial \dot{x}}\delta\dot{x} \\
&= \left(p - \frac{\partial \mathscr{L}}{\partial \dot{x}}\right)\delta\dot{x} + \dot{x}\delta p - \frac{\partial \mathscr{L}}{\partial x}\delta x.
\end{aligned}$$

Setting $p = \partial\mathscr{L}/\partial\dot{x}$ completes the proof. □

Some immediate corollaries follow from this. By virtue of the Euler-Lagrange equations, equation (2.2), and by definition of the momentum, equation (2.4), it follows from the preceding proof that,

$$\dot{x} = \frac{\partial H}{\partial p} \quad \text{and} \quad \dot{p} = -\frac{\partial H}{\partial x}, \tag{2.5}$$

which are known as *Hamilton's equations*. We see that the Hamiltonian is intimately related to the time evolution, the dynamics of the canonical variables. This observation can generalized to arbitrary functions; for, consider a generic function of canonical variables, $f(x, p)$,[1] which can be used to describe any given property of our system under question. Using equation (2.5), we have,

$$\begin{aligned}
\mathrm{d}f(x,p) &= \frac{\partial f}{\partial x}\mathrm{d}x + \frac{\partial f}{\partial p}\mathrm{d}p \\
&= \left(\frac{\partial f}{\partial x}\dot{x} + \frac{\partial f}{\partial p}\dot{p}\right)\mathrm{d}t \\
&= \left(\frac{\partial f}{\partial x}\frac{\partial H}{\partial p} - \frac{\partial f}{\partial p}\frac{\partial H}{\partial x}\right)\mathrm{d}t \\
&\stackrel{\text{def}}{=} \{f, H\}_{\mathrm{PB}}\,\mathrm{d}t.
\end{aligned} \tag{2.6}$$

Hence, the Hamiltonian is the generator of infinitesimal time translations through the *Poisson bracket*, which has been implicitly defined as,

$$\{f, g\}_{\mathrm{PB}} \stackrel{\text{def}}{=} \frac{\partial f}{\partial x}\frac{\partial g}{\partial p} - \frac{\partial f}{\partial p}\frac{\partial g}{\partial x}. \tag{2.7}$$

where f and g are functions of the canonical variables, (x, p).

[1] Ignoring explicit time dependence for brevity.

The Poisson bracket is important, as it will give us a direct route to the quantum theory via the correspondence principle. For later convenience, we list the most pertinent bracket relations,

$$\{f, H\}_{\mathrm{PB}} = \dot{f} \tag{2.8}$$
$$\{x, p\}_{\mathrm{PB}} = 1 \tag{2.9}$$
$$\{x, x\}_{\mathrm{PB}} = \{p, p\}_{\mathrm{PB}} = 0. \tag{2.10}$$

The second equation – also known as the (classical) *canonical commutation relation* – is perhaps the most prominent, as its quantum counterpart forms the basis of quantum theory.

We now apply the preceding formalism to solve the simple harmonic oscillator. Consider the Lagrangian for a simple harmonic oscillator,

$$\mathscr{L} = \frac{1}{2}m\dot{x}^2 - \frac{1}{2}m\omega^2 x^2, \tag{2.11}$$

where m is the mass of the oscillator and ω is its characteristic frequency of oscillation. We first find the conjugate momentum,

$$p = m\dot{x}, \tag{2.12}$$

which, unsurprisingly, is just the mass of the oscillator times its velocity. From here and the Legendre transform, equation (2.3), the Hamiltonian is derived,

$$H = \frac{p^2}{2m} + \frac{1}{2}m\omega^2 x^2. \tag{2.13}$$

As one recalls from elementary mechanics, this is just the energy of the oscillator. Hamilton's equations are then found,

$$\dot{x} = p/m \quad \text{and} \quad \dot{p} = -\omega^2 x., \tag{2.14}$$

which are a coupled set of first-order differential equations. We quickly solve these equations for the pair (x_t, p_t),

$$x_t = x_0 \cos\omega t + \frac{p_0}{m\omega}\sin\omega t \tag{2.15}$$
$$p_t = p_0 \cos\omega t - m\omega x_0 \sin\omega t, \tag{2.16}$$

where x_0 is the initial position of the oscillator and $p_0 = m\dot{x}(0)$ is the initial momentum. As an aside, let me remark that: If we regard (x_0, p_0) as canonical variables and define the Poisson bracket with respect to these variables, such that canonical commutation relations for them hold [equations (2.9)-(2.10)] by definition, Hamiltonian dynamics then preserves these relations for any and all times, t, i.e. $\{x_t, p_t\}_{\mathrm{PB}} = \{x_0, p_0\}_{\mathrm{PB}} = 1$ with the Poisson bracket taken with respect to (x_0, p_0).[2]

Another way to write this solution is in terms of (complex) plane-wave solutions, $u_t = N\exp(-\mathrm{i}\omega t)$ (also called the *mode functions*). Here, $N \in \mathbb{R}^+$ is a to-be-determined normalization constant. In these terms,

$$\begin{aligned} x_t &= \alpha u_t + \alpha^* u_t^* \\ &= N\left(\alpha \mathrm{e}^{-\mathrm{i}\omega t} + \alpha^* \mathrm{e}^{\mathrm{i}\omega t}\right), \end{aligned} \tag{2.17}$$

[2]I mention this here because similar properties appear in quantum theory, where unitary evolution generated by a Hamiltonian operator preserves the commutator between the canonical operators.

where α and α^* are dimensionless, complex coefficients. These coefficients play a prominent role in the quantum theory, where they take on the form of creation and annihilation operators, but more on this later.

We can extract the coefficients, α and α^*, directly by introducing the so-called Klein-Gordon inner product, which we define just below and which will be useful later when we discuss fields and quantization of such. Consider two complex solutions to the equations of motion, f and g, and define $\pi_f = m\,\mathrm{d}f/\mathrm{d}t$ (and similarly for g). Then, the *Klein-Gordon inner product* between f and g is defined as,

$$(f, g)_{\mathrm{KG}} \stackrel{\mathrm{def}}{=} \mathrm{i}\left(f^*\pi_g - g\pi_f^*\right), \tag{2.18}$$

Some generic observations are in order:

- The Klein-Gordon inner product is not an inner product in the strict sense, since it is not positive definite: if $(f, g)_{\mathrm{KG}} > 0$, then $(f^*, g^*)_{\mathrm{KG}} = -(f, g)_{\mathrm{KG}} < 0$.[3] (Note that all real solutions have vanishing Klein-Gordon inner product.)
- The Klein-Gordon inner product is conserved for solutions to the equations of motion, i.e. $\mathrm{d}(f, g)_{\mathrm{KG}}/\mathrm{d}t = 0$, which one can quickly check using the formalism above and the definition of the Klein-Gordon inner product.
- $(f, f^*)_{\mathrm{KG}} = 0$.

The last property is immediately useful as it gives us a way to distinguish the mode functions, u_t and u_t^*, since $(u_t, u_t^*)_{\mathrm{KG}} = 0$. We can also use this property to extract the coefficient α from equation (2.17). First, however, let us normalize the mode functions with respect to this inner product such that,

$$(u_t, u_t)_{\mathrm{KG}} \stackrel{\mathrm{def}}{=} 1 \quad \text{and} \quad (u_t^*, u_t^*)_{\mathrm{KG}} \stackrel{\mathrm{def}}{=} -1. \tag{2.19}$$

For our oscillator example, normalizing the mode functions in this manner gives us the normalization constant, $N = 1/\sqrt{2m\omega}$.

Proof. We prove the preceding statement. Observe that $\pi_u = m\,\mathrm{d}u_t/\mathrm{d}t = -\mathrm{i}m\omega u_t$ by definition of $u_t = N\exp(-\mathrm{i}\omega t)$, where $\omega > 0$. Then,

$$\begin{aligned}(u_t, u_t)_{\mathrm{KG}} &= \mathrm{i}\left(u_t^*\pi_u - u_t\pi_u^*\right) \\ &= \mathrm{i}\left(-\mathrm{i}m\omega|u_t|^2 - \mathrm{i}m\omega|u_t|^2\right) \\ &= 2m\omega|N|^2 \\ &\stackrel{\mathrm{def}}{=} 1.\end{aligned}$$

The final definition then holds for $N = 1/\sqrt{2m\omega}$. □

[3] Although, it will allow us to define a basis of complex solutions, which we will useful only when we discuss fields.

With the normalization of the mode functions in hand and using equation (2.17), we find the complex coefficients, α and α^*, in terms of the Klein-Gordon inner product,

$$\alpha = (u_t, x_t)_{\rm KG} \quad \text{and} \quad \alpha^* = -(u_t^*, x_t)_{\rm KG}. \tag{2.20}$$

Thus, the oscillator system has been formally solved, but we continue the discussion to make more connections with the quantum theory.

For curiosity's sake, let us compute the Poisson bracket between α and α^* by using equation (2.20). We find that,[4]

$$\{\alpha, \alpha^*\}_{\rm PB} = -{\rm i}(u_t, u_t)_{\rm KG} = -{\rm i} \tag{2.21}$$

where the last equality follows from the normalization of the mode functions with respect to the Klein-Gordon inner product. A similar relation will carry over to the quantum theory where α and α^* will be replaced by the creation and annihilation operators.

Proof. We prove the preceding equations. Consider the following set of equalities,

$$\begin{aligned}
\{\alpha, \alpha^*\}_{\rm PB} &= -\big\{(u_t, x_t)_{\rm KG}, (u_t^*, x_t)_{\rm KG}\big\}_{\rm PB} \\
&= -\big\{{\rm i}\,(u_t^* p_t - x_t \pi_u^*)\,, {\rm i}\,(u_t p_t - x_t \pi_u)\,\big\}_{\rm PB} \\
&= \big\{\,(u_t^* p_t - x_t \pi_u^*)\,, u_t p_t\big\}_{\rm PB} - \big\{\,(u_t^* p_t - x_t \pi_u^*)\,, x_t \pi_u\big\}_{\rm PB} \\
&= -u_t \pi_u^* \big\{x_t, p_t\big\}_{\rm PB} - u_t^* \pi_u \big\{p_t, x_t\big\}_{\rm PB} \\
&= (u_t^* \pi_u - u_t \pi_u^*)\,\big\{x_t, p_t\big\}_{\rm PB} \\
&= -{\rm i}(u_t, u_t)_{\rm KG}.
\end{aligned}$$

In the first equality, we used equation (2.20). In the second and third equalities, we expanded the Klein-Gordon inner product and then used the linearity of the Poisson bracket. For the remaining equalities, we used the anti-symmetry of the Poisson bracket to gather like terms, assumed the canonical commutation relations, and introduced the Klein-Gordon inner product for the mode function, u. □

One can also extract the real coefficients x_0 and p_0, introduced in equations (2.15) and (2.16), by using the Klein-Gordon inner product. First we find the relations,

$$(u_t, \cos\omega t)_{\rm KG} = \sqrt{\frac{m\omega}{2}} \quad \text{and} \quad (u_t, \sin\omega t)_{\rm KG} = {\rm i}\sqrt{\frac{m\omega}{2}} \tag{2.22}$$

from which we compute,

$$\alpha = (u_t, x_t)_{\rm KG} \tag{2.23}$$

$$= (u_t, x_0 \cos\omega t + \frac{p_0}{m\omega}\sin\omega t)_{\rm KG} \tag{2.24}$$

$$= \sqrt{\frac{m\omega}{2}}\left(x_0 + {\rm i}\frac{p_0}{m\omega}\right). \tag{2.25}$$

[4]Note that, with this normalization, α has dimensions of $\sqrt{\text{action}}$ (square root of length times momentum) since the Poisson bracket itself has dimensions of one over action.

Observe that,

$$\omega|\alpha|^2 = \frac{p_0^2}{2m} + \frac{1}{2}m\omega^2 x_0^2, \tag{2.26}$$

which is just the energy of the oscillator. With quantum theory in mind, we see that, up to a factor of $\hbar$, the number $|\alpha|^2$ is the classical analogue to the number of particles (photons) in the system.

Recap: We took a somewhat odd approach to solving the classical harmonic oscillator, but this will allow us to 'go over' to the quantum theory with relative ease (especially in the case of fields). To summarize, let me distill the approach we took down to a handful of steps:

- Define a Lagrangian, $\mathscr{L}$, and find the canonical variables, (x, p), from the Lagrangian as well as the corresponding Hamiltonian, H.
- Establish the canonical commutation relations and dynamics (Hamilton's equations) via the Poisson bracket.
- Solve Hamilton's equations in terms of the mode functions, u.
- Define the Klein-Gordon inner product and find the complex coefficients, α, thereby solving Hamilton's equations in general.

These are almost the exact steps that we will take in order to describe and quantize a field; so it is beneficial to keep them in mind.

The quantum oscillator

We now set out to solve the quantum harmonic oscillator, but a bulk of the work has already been done! We need only make correspondence between the classical theory and quantum theory and then transition fully into quantum mechanics by describing the quantum states of the oscillator. This will allow us to ease our way into a quantum field and photons in later sections. But first, allow me to list some basic elements of quantum theory, which we will be implicitly or explicitly understood and applied in this thesis.

- *Quantum states:* The state of a quantum system is given by a vector, $|\psi\rangle$, which resides in a Hilbert space, $\mathscr{H}$ (a complex vector space, equipped with an inner product, $\langle\cdot|\cdot\rangle$; the "space of states") and which has unit norm, i.e. $\langle\psi|\psi\rangle = 1$. The vector space structure implies that a linear combination (a superposition) of quantum states is again a quantum state. That is, given two quantum states, $|\psi\rangle, |\varphi\rangle \in \mathscr{H}$, and complex coefficients, α and β, then $\alpha|\psi\rangle + \beta|\varphi\rangle \in \mathscr{H}$, with an extra algebraic condition on α and β in order to preserve unit norm for the superposed state. For example, assuming ψ and φ are orthogonal with respect to the inner product, $\langle\psi|\varphi\rangle = 0$, then $|\alpha|^2 + |\beta|^2 = 1$.
- *Density matrix:* More generically, we can form a density matrix, ρ, which is a convex combination (a probabilistic mixture) of pure quantum states. That is, given a set of

unit vectors, $\{|\psi_i\rangle\}$, which are not necessarily orthogonal, one can define the density matrix,

$$\rho = \sum_i p_i \, |\psi_i\rangle\langle\psi_i| \, , \tag{2.27}$$

where $\mathrm{Tr}\,\rho = \sum_i p_i = 1$ and $p_i \geq 0 \; \forall i$.

- *Composite Systems:* The quantum state for a composite system, consisting of subsystems A and B with respective Hilbert spaces $\mathscr{H}_A$ and $\mathscr{H}_B$, is a vector in the tensor product space, i.e. $|\Psi\rangle \in \mathscr{H}_A \otimes \mathscr{H}_B$. Note that, for $|\Psi\rangle \in \mathscr{H}_A \otimes \mathscr{H}_B$, it is not generally true that $|\Psi\rangle = |\psi\rangle \otimes |\varphi\rangle$ for some $|\psi\rangle \in \mathscr{H}_A$ and $\varphi \in \mathscr{H}_B$, which only holds when the subsystems are separable (independent, no correlations).

- *Observables*: Every observable, O, in the classical theory corresponds to a Hermitian ('real') operator, $\hat{O}$, in the quantum theory, which act on quantum states in the Hilbert space and which has mean value $\langle\psi|\hat{O}|\psi\rangle$, with respect to the quantum state ψ. Independent realizations/measurements of the observable O take on values from the spectrum (the eigenvalues) of $\hat{O}$ and occur with a frequency, determined by probability of occurrence for a given quantum states. These probabilities formally correspond to the squared coefficients of the quantum state ψ written in the eigen-basis of $\hat{O}$.

With some basic elements of quantum mechanics in hand, we now 'go over' to quantum theory from the classical theory in one stroke by the method of *canonical quantization*. That is, we make the physical correspondence between Poisson brackets, taken between observables in the classical Hamiltonian theory, and commutators, taken between the observable's Hermitian-operator-counterparts in the quantum theory. Given two classical functions of canonical variables, A and B, and their operator counterparts, $\hat{A}$ and $\hat{B}$, we assume the correspondence (up to operator-ordering ambiguities),

$$\{A, B\}_{\mathrm{PB}} \to \frac{[\hat{A}, \hat{B}]}{\mathrm{i}\hbar}, \tag{2.28}$$

where $[\hat{A}, \hat{B}] = \hat{A}\hat{B} - \hat{B}\hat{A}$ is the commutator and $\hbar$ is Planck's reduced constant. We now apply this correspondence to our classical system discussed previously: given the canonical variables (x, p) and Hamiltonian H, define the Hermitian operators $x \to \hat{x}$, $p \to \hat{p}$, and $H \to \hat{H}$. Applying the correspondence to the Poisson bracket relations, equations (2.8)-(2.10), we have,

$$\frac{\mathrm{d}\hat{f}}{\mathrm{d}t} = \frac{1}{\mathrm{i}\hbar}[\hat{f}, \hat{H}] \tag{2.29}$$

$$[\hat{x}, \hat{p}] = \mathrm{i}\hbar\mathbb{I} \tag{2.30}$$

$$[\hat{x}, \hat{x}] = [\hat{p}, \hat{p}] = 0, \tag{2.31}$$

where $\hat{f}$ is some function of the *canonical operators*, $\hat{x}$ and $\hat{p}$, and $\mathbb{I}$ is the identity operator (which we will drop for brevity).

As to our primary example, consider the Hamiltonian for a quantum harmonic oscillator,

$$\hat{H} = \frac{\hat{p}^2}{2m} + \frac{1}{2}m\omega^2\hat{x}^2. \tag{2.32}$$

We find Hamilton's equations in operator form by the commutation relations (2.29)-(2.31),

$$\frac{\mathrm{d}\hat{x}_t}{\mathrm{d}t} = \hat{p}_t/m \quad \text{and} \quad \frac{\mathrm{d}\hat{p}_t}{\mathrm{d}t} = -m\omega^2\hat{x}_t, \tag{2.33}$$

which is, as in the classical case, a coupled set of first-order differential equations for the canonical operators $\hat{x}$ and $\hat{p}$. These equations are easily solved,

$$\hat{x}_t = \hat{x}\cos\omega t + \frac{\hat{p}}{m\omega}\sin\omega t \tag{2.34}$$

$$\hat{p}_t = \hat{p}\cos\omega t - m\omega\hat{x}\sin\omega t. \tag{2.35}$$

One can check that evolution under the Hamiltonian operator, $\hat{H}$, preserves the canonical commutator, i.e. $[\hat{x}_t, \hat{p}_t] = \mathrm{i}\hbar$.

One can rewrite these operator equations in terms of complex mode functions,

$$\hat{x}_t = \hat{a}u_t + \hat{a}^\dagger u_t^*, \tag{2.36}$$

where $u_t = N\exp(-\mathrm{i}\omega t)$ is the mode function and $\hat{a}$ and $\hat{a}^\dagger$ are non-Hermitian operators (generalized from complex numbers, α and α^*), called the *annihilation creation operators*, respectively. We extract these operator coefficients via the Klein-Gordon inner product, as before, but before doing so, we re-scale our previous definition, equation (2.18), by the factor $\hbar$ in order to makes the creation and annihilation operators dimensionless.

Given two complex solutions to the classical equations of motion, f and g, and defining $\pi_f = m\,\mathrm{d}f/\mathrm{d}t$ (and likewise for g), the re-defined Klein-Gordon inner product between f and g reads,

$$(f,g)_{\mathrm{KG}} \overset{\mathrm{def}}{=} \frac{\mathrm{i}}{\hbar}\left(f^*\pi_g - g\pi_f^*\right). \tag{2.37}$$

Normalizing the mode functions with respect to this re-scaled version, we have, $N = \sqrt{\hbar/2m\omega}$, such that, $(u_t, u_t)_{\mathrm{KG}} = 1$. Then,

$$\hat{a} = (u_t, \hat{x}_t)_{\mathrm{KG}} \quad \text{and} \quad \hat{a}^\dagger = -(u_t^*, \hat{x}_t)_{\mathrm{KG}}. \tag{2.38}$$

From which we find the commutator,

$$[\hat{a}, \hat{a}^\dagger] = 1. \tag{2.39}$$

Proof. We prove the last equality. Given the relations (2.38), consider the following set of equalities,

$$\begin{aligned}
[\hat{a}, \hat{a}^\dagger] &= -[(u_t, \hat{x}_t)_{\mathrm{KG}}, (u_t^*, \hat{x}_t)_{\mathrm{KG}}] \\
&= -(\mathrm{i}/\hbar)^2[(u_t^\star\hat{p}_t - \hat{x}_t\pi_u^*), (u_t\hat{p}_t - \hat{x}_t\pi_u)] \\
&= (1/\hbar^2)\big([(u_t^*\hat{p}_t - \hat{x}_t\pi_u^*)\,, u_t\hat{p}_t] - [(u_t^*\hat{p}_t - \hat{x}_t\pi_u^*)\,, \hat{x}_t\pi_u]\big) \\
&= -(1/\hbar^2)\big(u_t\pi_u^*[\hat{x}_t, \hat{p}_t] + u_t^*\pi_u[\hat{p}_t, \hat{x}_t]\big) \\
&= (1/\hbar^2)(u_t^*\pi_u - u_t\pi_u^*)[\hat{x}_t, \hat{p}_t] \\
&= (\mathrm{i}/\hbar)(u_t^*\pi_u - u_t\pi_u^*) \\
&= (u_t, u_t)_{\mathrm{KG}}.
\end{aligned}$$

In the first equality, we used equation (2.38). In the second and third equalities, we expanded the Klein-Gordon inner product and then used the linearity of the commutator. For the remaining equalities, we used the anti-symmetry of the commutator to gather like terms, assumed the canonical commutation relations (Hamiltonian evolution preserves these relations), and introduced the Klein-Gordon inner product for the mode function, u. Normalizing the mode function then establishes the equality which was to be shown. □

As before, one can find a relation between the annihilation and creation operators, $\hat{a}$ and $\hat{a}^\dagger$, and the canonical operators, $\hat{x}$ and $\hat{p}$ via the Klein-Gordon inner product. I simply write down the result,

$$\hat{a} = \sqrt{\frac{m\omega}{2\hbar}}\left(\hat{x} + \mathrm{i}\frac{\hat{p}}{m\omega}\right). \tag{2.40}$$

Observe that,

$$\begin{aligned}\hbar\omega\hat{a}^\dagger\hat{a} &= \frac{\hat{p}^2}{2m} + \frac{1}{2}m\omega^2\hat{x}^2 + \frac{\mathrm{i}\hbar\omega}{2}[\hat{x},\hat{p}] \\ &= \frac{\hat{p}^2}{2m} + \frac{1}{2}m\omega^2\hat{x}^2 - \hbar\omega/2,\end{aligned}$$

which, after rearranging, gives us the Hamiltonian operator in terms of creation and annihilation operators,

$$\hat{H} = \hbar\omega(\hat{a}^\dagger\hat{a} + 1/2). \tag{2.41}$$

This is similar to the classical energy, equation (2.26), up to factor of $\hbar$ and an extra term $\hbar\omega/2$, which is known as the vacuum energy. The vacuum in this case being the ground state of the above Hamiltonian, with energy $\hbar\omega/2$. The quantum vacuum is starkly different from the "classical vacuum", which has trivial properties (zero energy, etc.).

At this stage, we have some clear definitions for the observables of our theory: they are given as general functions of the canonical operators, $\hat{x}$ and $\hat{p}$. The quantum oscillator system is only half-solved at this point, however, because we have not yet determined the quantum states to which these observables are measured with respect to. This is now our goal.

From the quantum vacuum, all other quantum states originate. This is because we can build a basis of quantum states (the Fock basis), which are eigenvectors of the Hamiltonian operator, by successive applications of the creation operator to the vacuum state. This basis spans an infinite dimensional Hilbert space (the Fock space), which any quantum state can then be written in terms of by superposition. To show this, let us first argue that there exists a ground state – the vacuum state, $|0\rangle$ – with energy $\hbar\omega/2$ and which satisfies $\hat{a}\,|0\rangle = 0$.

Physicist's proof. We prove the preceding statement. Define the *number operator*, $\hat{n} \stackrel{\text{def}}{=} \hat{a}^\dagger\hat{a}$, such that

$$\hat{H} = \hbar\omega(\hat{n} + 1/2), \tag{2.42}$$

Now, define the vacuum state, $|0\rangle$, to be the minimum energy state of the Hamiltonian operator, and thus the minimum eigenvector of the number operator; i.e.,

$$\hat{n}\,|0\rangle = \mu\,|0\rangle\,, \tag{2.43}$$

with μ being the smallest eigenvalue of $\hat{n}$. We argue that $\mu = 0$ on the grounds of stability for the physical system (on the assumption for the existence of a minimum energy state) and that $\hat{a}\,|0\rangle = 0$. We argue by contradiction.

Consider the unnormalized state,

$$|\psi_a\rangle = \hat{a}\,|0\rangle\,. \tag{2.44}$$

Then,

$$\hat{a}\hat{n}\,|0\rangle = \mu\,|\psi_a\rangle\,. \tag{2.45}$$

Now,

$$\hat{a}\hat{n}\,|0\rangle = \hat{a}\hat{a}^\dagger\hat{a}\,|0\rangle \tag{2.46}$$

$$= (\hat{n} + \mathbb{I})\,|\psi_a\rangle\,, \tag{2.47}$$

which, from equation (2.45), implies that,

$$(\hat{n} + \mathbb{I})\,|\psi_a\rangle = \mu\,|\psi_a\rangle \implies \hat{n}\,|\psi_a\rangle = (\mu - 1)\,|\psi_a\rangle\,. \tag{2.48}$$

But this contradicts our assumption that there exists a ground state, unless $\mu = 0$ to begin with. Furthermore, for our assumption to generally hold, it must also be so that the state ψ_a is the trivial state, i.e. $\hat{a}\,|0\rangle = 0$. □

We now define the Fock basis, which serve as a basis for the Hilbert/Fock space, $\mathscr{F}$, from which all quantum states can be built from by superposition. I list the most important properties and definitions and then prove various claims:

- The set of orthonormal basis vectors $\{|n\rangle\}$, for $n \in \mathbb{N}$, define a basis for the Fock space, $\mathscr{F}$. They satisfy,
$$\langle m|n\rangle = \delta_{mn}, \tag{2.49}$$
with δ_{mn} being the Kronecker delta-function, such that $\delta_{mn} = 1$ for $m = n$ and 0 otherwise.

- The basis states (also called Fock states or number states), $|n\rangle$, can be constructed from the vacuum by successive applications of the creation operator, $\hat{a}^\dagger$, such that
$$|n\rangle = \frac{\hat{a}^{\dagger n}}{\sqrt{n!}}\,|0\rangle\,. \tag{2.50}$$

- Fock states are eigenstates of the number operator, and thus the oscillator Hamiltonian, equation (2.42), such that,
$$\hat{n}\,|n\rangle = n\,|n\rangle \implies E_n = \hbar\omega(n + 1/2), \tag{2.51}$$
with E_n being the eigenvalue of $\hat{H}$.

- The set of quantum states are then defined as,
$$\left\{\, |\psi\rangle \;\middle|\; |\psi\rangle = \sum_{n=0}^{\infty} c_n\,|n\rangle \in \mathscr{F} \text{ with } \langle\psi|\psi\rangle = \sum_n |c_n|^2 = 1 \quad \text{and} \quad c_n = \langle n|\psi\rangle \,\right\}. \tag{2.52}$$

We now prove the first three statements.

Proofs. We first show that the single-particle state (defined below) is an eigenstate of the number operator, with eigenvalue equal to 1. We then show, by induction, that the vector, $|n\rangle$, constructed by n-successive applications of $\hat{a}^\dagger$ to the vacuum state, is an eigenstate of the number operator, with eigenvalue equal to n. Orthonormality of the vectors $\{|n\rangle\}$ is then proven.

Consider the single-particle state,

$$|1\rangle = \hat{a}^\dagger |0\rangle , \tag{2.53}$$

and observe that,

$$\begin{aligned}
\hat{n}|1\rangle &= \hat{n}\hat{a}^\dagger |0\rangle \\
&= [\hat{n}, \hat{a}^\dagger] |0\rangle \\
&= [\hat{a}^\dagger \hat{a}, \hat{a}^\dagger] |0\rangle \\
&= \hat{a}^\dagger [\hat{a}, \hat{a}^\dagger] |0\rangle \\
&= \hat{a}^\dagger |0\rangle \\
&= |1\rangle .
\end{aligned}$$

For the second and third equalities, we used $\hat{n}|0\rangle = 0$ and expanded the number operator in terms of creation and annihilation operators. For the fourth equality, we used the commutator property $[\hat{f}\hat{g}, \hat{h}] = \hat{f}[\hat{g}, \hat{h}] + [\hat{f}, \hat{h}]\hat{g}$ together with $[\hat{a}^\dagger, \hat{a}^\dagger] = 0$. For the last set of equalities, we used the relation $[\hat{a}, \hat{a}^\dagger] = 1$ and the definition of the single-particle state. Thus, one sees that the single-particle state is an eigenstate of the number operator, with eigenvalue equal to one.

We now prove a similar relation for the two-particle state. The generalization to the n-particle state will follow by induction. Consider the two-particle state,

$$|2\rangle = N_2 \hat{a}^{\dagger 2} |0\rangle , \tag{2.54}$$

where N_2 is some normalization constant such that $\langle 2|2\rangle = 1$. Observe that,

$$\begin{aligned}
\hat{n}|2\rangle &= N_2 \hat{n}\hat{a}^{\dagger 2} |0\rangle \\
&= N_2 [\hat{n}, \hat{a}^{\dagger 2}] |0\rangle \\
&= N_2 [\hat{a}^\dagger \hat{a}, \hat{a}^{\dagger 2}] |0\rangle \\
&= N_2 \hat{a}^\dagger [\hat{a}, \hat{a}^{\dagger 2}] |0\rangle \\
&= N_2 \hat{a}^\dagger \left(\hat{a}^\dagger [\hat{a}, \hat{a}^\dagger] + [\hat{a}, \hat{a}^{\dagger 2}] \hat{a}^\dagger \right) |0\rangle \\
&= 2 N_2 \hat{a}^{\dagger 2} |0\rangle \\
&= 2 |2\rangle .
\end{aligned}$$

Thus, the two-particle state is an eigenstate of the number operator, with eigenvalue equal to 2. The generalization to the n-particle state, $|n\rangle = N_n \hat{a}^{\dagger n} |0\rangle$, follows by a repeated

application of the above set of equalities. Thus, the n-partidle Fock state, $|n\rangle$, is an eigenstate of the number (Hamiltonian) operator with eigenvalue equal to n [$E_n = \hbar\omega(n + 1/2)$].

We now prove orthonormality of the Fock states and provide the normalization constant, N_n, while doing so. Consider the Fock states $|n\rangle$ and $|m\rangle$ and take $n > m$ without loss of generality. Then, consider the following set of equalities,

$$\begin{aligned}
\langle m|n\rangle \propto\ & \langle 0|\hat{a}^m \hat{a}^{\dagger n}|0\rangle \\
=\ & \langle 0|\hat{a}^{m-1}[\hat{a}, \hat{a}^{\dagger n}]|0\rangle \\
=\ & \langle 0|\hat{a}^{m-1}\left(\hat{a}^\dagger[\hat{a}, \hat{a}^{\dagger n-1}] + [\hat{a}, \hat{a}^{\dagger n-1}]\hat{a}^\dagger\right)|0\rangle \\
& \vdots \\
=\ & n\,\langle 0|\hat{a}^{m-1}\hat{a}^{\dagger n-1}|0\rangle \\
=\ & n\,\langle 0|\hat{a}^{m-2}[\hat{a}, \hat{a}^{\dagger n-1}]|0\rangle \\
& \vdots \\
=\ & n(n-1)\,\langle 0|\hat{a}^{m-2}\hat{a}^{\dagger n-2}|0\rangle \\
& \vdots \\
=\ & n(n-1)\ldots(n-m)\,\langle 0|\hat{a}^{\dagger n-m}|0\rangle\,.
\end{aligned}$$

For $n \neq m$, the last equality is zero by virtue of $\hat{a}^k\,|0\rangle = 0$ for any $k \neq 0$. For $n = m$, the last equality is equal to $n!$ (assuming $\langle 0|0\rangle = 1$). Therefore, setting $N_n = 1/\sqrt{n!}$ gives $\langle m|n\rangle = \delta_{mn}$, as was to be shown. As an aside, note that there is no upper-bound for the value of n. It thus follows that the Fock space is an infinite dimensional Hilbert space. □

With the dynamics of the observables thus solved and the quantum states of the system in hand, our job is complete.

Recap: We were able to solve the quantum harmonic oscillator with swiftness via canonical quantization, which effectively allowed us to take most of our results from the classical theory and apply them directly to the quantum system. The only missing ingredient (and altogether absent in our classical discussion) was to find the quantum states of our system. I lay out the procedure we took for quick reference:

- Given the classical, Hamiltonian description of the system, 'go over' to the quantum theory by canonical quantization, i.e.

$$\{A, B\}_{\text{PB}} \to \frac{[\hat{A}, \hat{B}]}{\mathrm{i}\hbar}.$$

  Here, A and B are classical observables, which are general functions of the canonical variables, x and p, and $\hat{A}$ and $\hat{B}$ are their Hermitian operator-counterparts and are operator-functions of the canonical operators, $\hat{x}$ and $\hat{p}$.

- Solve the operator form of Hamilton's equations for the canonical variables,

$$\frac{\mathrm{d}\hat{x}}{\mathrm{d}t} = \frac{1}{\mathrm{i}\hbar}[\hat{x}, \hat{H}] \quad \text{and} \quad \frac{\mathrm{d}\hat{p}}{\mathrm{d}t} = \frac{1}{\mathrm{i}\hbar}[\hat{p}, \hat{H}], \tag{2.55}$$

thereby determining the time evolution for any observable, $\hat{A}(\hat{x}, \hat{p})$. Note that, the solutions of these equations are, more or less, equivalent to the classical equations of motion.

- Determine the quantum states of the system. For the quantum harmonic oscillator, this was found by constructing the Fock basis, $\{|n\rangle\}$, which was formed by successive applications of the creation operator to the quantum vacuum, $|0\rangle$ – i.e.,

$$|n\rangle = \frac{\hat{a}^{\dagger n}}{\sqrt{n!}} |0\rangle \,. \tag{2.56}$$

  Thus, for oscillator-like systems, construct the Fock basis from the vacuum, from which any quantum state can written in terms of by linearity.

Photons

We are almost in the position to discuss the quantum of electromagnetic field – i.e., photons. Formally, we must transition from point-like systems to systems described by fields – entities which take on a value at each point in space and time. This will require some slight rewiring of out thought processes when discussing the formalism but will nonetheless follow analogous steps we took earlier in describing point-like systems.

Quantizing the electromagnetic field also presents some complexities and mathematical maneuvering, owing to complications when dealing with the polarization of the field. We will bypass these difficulties, however, by considering a simple model for the electromagnetic field: a *massless scalar field*. This approximation will be sufficient for our purposes, and almost everything we have to say later about photons can be thought of directly in terms of the formalism and concepts presented therefrom.

We start by presenting the Lagrangian and Hamiltonian formalisms for a classical scalar field in one dimension. We will apply this formalism to solve the equations of motion for a free, massless scalar-field (the massless Klein-Gordon field), and then move on to a quantum description of the field via canonical quantization. We will see many similarities with the oscillator system along the way, and hopefully, these similarities will make the presentation seem familiar and make the quantum description of the field seem like a natural extension.

For background on (relativistic) quantum field theories, in general, see David Tong's lectures [20]. With respect to the quantized electromagnetic field and its place "in the lab", see the many books on quantum optics, e.g. [21, 22]. We will use the calculus of variations at the level of, e.g., functional derivatives when discussing fields. For background on this, see Gelfand's book [23].

The classical field

For the point-like oscillator, one thought of x as both a canonical variable describing the physical system and a coordinate. For fields however, the field, $\phi(x)$, itself is a canonical variable and x is just a coordinate (which plays no pivotal role) at which point the field takes on a particular value. Hence fields are the primary objects, not coordinates, and we must learn how to handle them in the context of the Lagrangian and Hamiltonian formalisms.

Recall that, in our prior endeavours, we took variations with respect to the variables $x, \dot{x}, p$, etc. In our current situation, we will be taking variations with respect to the field, ϕ, and its conjugate momentum, π, which are themselves functions of coordinates. To make the transition from point particles to fields more efficient, we take a short detour into functionals and their variation.

- *Functionals:* In simple terms, a functional is a function of a function. We define a functional, F, of the "field variable", ϕ, which is itself a function of coordinates, $\mathbf{x}$, in the following manner,

$$F[\phi] = \int \mathrm{d}\mathbf{x}\ f(\phi(\mathbf{x}), \partial_{\mathbf{x}}\phi), \tag{2.57}$$

  where $f(\phi, \partial_{\mathbf{x}}\phi)$ is typically a polynomial in ϕ and its first derivatives. This can be extended to functions of higher-order derivatives, but it will not be useful for us.

- *Variation of a functional:* The variation of a functional, F, with respect to a field, ϕ, assuming vanishing boundary conditions, is given by,

$$\begin{aligned}
\delta F[\phi] &= \int \mathrm{d}\mathbf{x}\ \delta f(\phi(\mathbf{x}), \partial_{\mathbf{x}}\phi) \\
&= \int \mathrm{d}\mathbf{x} \left(\frac{\partial f}{\partial \phi}\delta\phi + \frac{\partial f}{\partial(\partial_{\mathbf{x}}\phi)}\delta(\partial_{\mathbf{x}}\phi) \right) \\
&= \int \mathrm{d}\mathbf{x} \left(\frac{\partial f}{\partial \phi} - \partial_{\mathbf{x}} \left(\frac{\partial f}{\partial(\partial_{\mathbf{x}}\phi)} \right) \right) \delta\phi + \underbrace{\int \mathrm{d}\mathbf{x} \partial_{\mathbf{x}} \left(\frac{\partial f}{\partial(\partial_{\mathbf{x}}\phi)}\delta\phi \right)}_{=0},
\end{aligned}$$

  from which we define the *functional derivative* of F with respect to $\phi(\mathbf{x})$ as,

$$\frac{\delta F}{\delta \phi} \overset{\text{def}}{=} \frac{\partial f}{\partial \phi} - \partial_{\mathbf{x}} \left(\frac{\partial f}{\partial(\partial_{\mathbf{x}}\phi)} \right), \tag{2.58}$$

  where coordinate dependence on $\mathbf{x}$ is understood.

We now take on fields. Consider the action functional, $S[\phi]$, for a scalar field, $\phi(x,t)$, which we write in terms of the Lagrangian density, $\mathcal{L}$,

$$S[\phi] = \int \mathrm{d}t\mathrm{d}x \mathcal{L}[\phi, \dot{\phi}, \partial_x\phi], \tag{2.59}$$

where the space-time dependence of the Lagrangian density is implicit. Observe that the Lagrangian density is only a function of ϕ and its first derivatives. The equations of motion for the system are found via Hamilton's principle, i.e. by extremizing the action with respect to the field ϕ. Generically, the extremization of the action with respect to the field (assuming fixed endpoints) implies the Euler-Lagrange equations of motion,

$$\delta S[\phi] = 0 \implies \frac{\partial \mathcal{L}}{\partial \phi} - \frac{\partial}{\partial t}\left(\frac{\partial \mathcal{L}}{\partial \dot{\phi}} \right) - \frac{\partial}{\partial x}\left(\frac{\partial \mathcal{L}}{\partial(\partial_x \phi)} \right) = 0. \tag{2.60}$$

Proof. We prove the preceding implication assuming. First, note that,

$$\delta S = \int \mathrm{d}t\mathrm{d}x \frac{\delta S}{\delta \phi}\delta\phi(x,t). \tag{2.61}$$

by definition of the variation of a functional. Hamilton's principle, $\delta S \stackrel{\text{def}}{=} 0$, then implies $\delta S/\delta\phi = 0$ from the previous equation. Now, assuming that the Lagrangian density is only a function of ϕ and its first derivatives and assuming vanishing boundary conditions for the field variations, we have that the functional derivative of the action is given by,

$$\frac{\delta S}{\delta \phi} = \frac{\partial \mathcal{L}}{\partial \phi} - \frac{\partial}{\partial t}\left(\frac{\partial \mathcal{L}}{\partial \dot{\phi}}\right) - \frac{\partial}{\partial x}\left(\frac{\partial \mathcal{L}}{\partial(\partial_x \phi)}\right), \tag{2.62}$$

which follows by application of equation (2.58). Therefore, the action is extremized if and only if the Euler-Lagrange equations (2.60) are satisfied. □

We now go the Hamiltonian formalism and introduce the canonical field variables. Given a Lagrange density, $\mathcal{L}$, defined in terms of the configuration variables, $(\phi, \dot{\phi})$, the Hamiltonian density, $\mathcal{H}$, defined in terms of the canonical field variables, (ϕ, π), can be found via the Legendre transform of the Lagrangian; i.e.,

$$\mathcal{H}[\phi(x), \pi(x)] = \dot{\phi}\pi - \mathcal{L}, \tag{2.63}$$

with,

$$\pi(x,t) = \frac{\partial \mathcal{L}}{\partial \dot{\phi}}, \tag{2.64}$$

being the *conjugate field momentum*. The Hamiltonian density is related to the Hamiltonian functional, H, by integration,

$$H[\phi, \pi] = \int \mathrm{d}x \mathcal{H}[\phi(x,t), \pi(x,t)] \tag{2.65}$$

$$= \int \mathrm{d}x \big(\dot{\phi}\pi - \mathcal{L}\big). \tag{2.66}$$

Observe that the canonical variables and associated Hamiltonian are defined at a specific instance in time. By varying the Hamiltonian and making connection with the Euler-Lagrange equations, we find Hamilton's equations,

$$\dot{\phi} = \frac{\delta H}{\delta \pi} \quad \text{and} \quad \dot{\pi} = -\frac{\delta H}{\delta \phi}. \tag{2.67}$$

Actually, we can find the time evolution of a generic functional, $F[\phi, \pi]$, by variation,

$$dF[\phi, \pi] = \int \mathrm{d}x \left(\frac{\delta F}{\delta \phi}\mathrm{d}\phi + \frac{\delta F}{\delta \pi}\mathrm{d}\pi\right) \tag{2.68}$$

$$= \mathrm{d}t \int \mathrm{d}x \left(\frac{\delta F}{\delta \phi}\dot{\phi} + \frac{\delta F}{\delta \pi}\dot{\pi}\right) \tag{2.69}$$

$$= \mathrm{d}t \int \mathrm{d}x \left(\frac{\delta F}{\delta \phi}\frac{\delta H}{\delta \pi} - \frac{\delta F}{\delta \pi}\frac{\delta H}{\delta \phi}\right) \tag{2.70}$$

$$= \mathrm{d}t\{F, H\}_{\mathrm{PB}}, \tag{2.71}$$

where the Poisson bracket between two functionals F and G has been implicitly defined as,

$$\{F, G\}_{\text{PB}} \stackrel{\text{def}}{=} \int \mathrm{d}x \left(\frac{\delta F}{\delta \phi} \frac{\delta G}{\delta \pi} - \frac{\delta F}{\delta \pi} \frac{\delta G}{\delta \phi} \right). \tag{2.72}$$

I list the most important Poisson bracket relations,

$$\dot{F} = \{F, H\}_{\text{PB}} \tag{2.73}$$

$$\{\phi(x), \pi(y)\}_{\text{PB}} = \delta(x - y) \tag{2.74}$$

$$\{\phi(x), \phi(y)\}_{\text{PB}} = \{\phi(x), \phi(y)\}_{\text{PB}} = 0, \tag{2.75}$$

where $\delta(x - y)$ is the Dirac-delta distribution. The second equation, the canonical commutation relation for the field, follows from the definition of the Poisson bracket and the fact that $\delta\phi(x)/\delta\phi(y) = \delta\pi(x)/\delta\pi(y) = \delta(x - y)$, which I show below.

Proof. We show that $\delta\phi(y)/\delta\phi(x) = \delta(x-y)$. By extension, a similar relation follows for π. Consider that,

$$\phi(x) = \int \mathrm{d}y \; \delta(x - y)\phi(y), \tag{2.76}$$

and thus $\delta(x-y)\phi(y)$ defines a functional density for the functional ϕ. But, by definition of the variation of a functional,

$$\delta\phi(x) \stackrel{\text{def}}{=} \int \mathrm{d}y \frac{\delta\phi(x)}{\delta\phi(y)} \delta\phi(y). \tag{2.77}$$

After taking a variation of the former equation and equating the result with the latter, we are led to conclude $\delta\phi(y)/\delta\phi(x) = \delta(x - y)$. The canonical commutation relations can be found by using this result and applying the definition of the Poisson bracket. □

We now apply this formalism to find and solve equations of motion for a free, massless, scalar field. We take the speed of light to be one in what follows. The Lagrangian density for a free, massless, scalar field is given by,

$$\mathcal{L} = \frac{1}{2}\dot{\phi}^2 - \frac{1}{2}(\partial_x \phi)^2, \tag{2.78}$$

From this, we find the canonical momentum,

$$\pi = \dot{\phi}, \tag{2.79}$$

and the Hamiltonian,

$$H = \int \mathrm{d}x \left(\frac{1}{2}\pi^2 + \frac{1}{2}(\partial_x \phi)^2 \right). \tag{2.80}$$

We find an Hamilton's equations by using the definition of the functional derivative for the above Hamiltonian,

$$\frac{\delta H}{\delta \phi} = \frac{\partial \mathcal{H}}{\partial \phi} - \frac{\partial}{\partial x} \left(\frac{\partial \mathcal{H}}{\partial(\partial_x \phi)} \right), \tag{2.81}$$

with $\mathcal{H}$ being the integrand in the equation before last. It then follows that

$$\dot{\phi} = \pi \quad \text{and} \quad \dot{\pi} = \partial_x^2 \phi, \tag{2.82}$$

which are a coupled set of partial differential equations. By taking a time derivative of Hamilton's equation for ϕ, we are led to one second-order partial differential equation,

$$\partial_t^2 \phi - \partial_x^2 \phi = 0, \tag{2.83}$$

also known as the (massless, free) Klein-Gordon equation. This is a wave equation, which we can readily solve in Fourier space. I write a generic solution in terms of the complex mode functions, $u_k(x,t)$,

$$\phi(x,t) = \int \mathrm{d}k \left(\alpha_k u_k(x,t) + \alpha_k^* u_k^*(x,t)\right) \tag{2.84}$$

$$\pi(x,t) = -\mathrm{i} \int \mathrm{d}k\, \omega_k \left(\alpha_k u_k(x,t) - \alpha_k^* u_k^*(x,t)\right) \tag{2.85}$$

where α_k are complex coefficients and $u_k = N_k \exp[-\mathrm{i}(\omega_k t - kx)]$ is the mode function, with N_k a to-be-determined normalization constant. Here, $\omega_k = |k|$ is the oscillation frequency of the Fourier modes and $k \in \mathbb{R}$ is the wave-number. This is similar to the classical oscillator solution, however, in this case, we have an infinite set of oscillators, one for every point x, which have a range of possible oscillation frequencies, ω_k.

We now define the Klein-Gordon inner product for generic solutions to the equations of motion. This will allow us to determine the coefficients α_k from the field ϕ and the mode functions $\{u_k\}$. Consider two generic (complex) solutions to the equations of motion, $f(x,t)$ and $g(x,t)$, and define $p_f = \dot{f}$ (and similarly for g). Then, the Klein-Gordon inner product between f and g is defined as,

$$(f,g)_{\mathrm{KG}} \stackrel{\mathrm{def}}{=} \mathrm{i} \int \mathrm{d}x \left(f^* p_g - g p_f^*\right). \tag{2.86}$$

This has the same properties as the Klein-Gordon inner product introduced in previous sections.

From this definition and the form of the mode functions, one can show that,

$$(u_k, u_l)_{\mathrm{KG}} = -(u_k^*, u_l^*)_{\mathrm{KG}} = \delta(k-l) \tag{2.87}$$

$$(u_k, u_l^*)_{\mathrm{KG}} = 0 \tag{2.88}$$

$$\implies \alpha_k = (u_k, \phi)_{\mathrm{KG}} \quad \text{and} \quad \alpha_k^* = -(u_k^*, \phi)_{\mathrm{KG}}, \tag{2.89}$$

where $\delta(k-l)$ is the Dirac-delta distribution in Fourier space and, for these equations to hold, $N_k = 1/\sqrt{4\pi\omega_k}$.

Proof. We prove the first equation and show $N_k = 1/\sqrt{4\pi\omega_k}$. The other equations can be found using similar methods. Let

$$u_k(x,t) = N_k \mathrm{e}^{-\mathrm{i}(\omega_k t - kx)}, \tag{2.90}$$

such that,

$$p_{u_k} = \partial_t u_k = -\mathrm{i}\omega_k u_k. \tag{2.91}$$

Then, computing the Klein-Gordon inner product between the mode functions u_k and u_l, the following set of equalities are found,

$$\begin{aligned}
(u_k, u_l)_{\mathrm{KG}} &= \mathrm{i}\int \mathrm{d}x \left(u_k^* p_{u_l} - u_l p_{u_k}^*\right) && (2.92)\\
&= \mathrm{i}\int \mathrm{d}x \left(u_k^*(-\mathrm{i}\omega_l u_l) - u_l(\mathrm{i}\omega_k u_k)\right) && (2.93)\\
&= (\omega_k + \omega_l)\int \mathrm{d}x\, u_k^* u_l && (2.94)\\
&= N_k N_l(\omega_k + \omega_l)\mathrm{e}^{-\mathrm{i}(\omega_l - \omega_k)t}\int \mathrm{d}x\, \mathrm{e}^{\mathrm{i}(l-k)x} && (2.95)\\
&= N_k^2 4\pi\omega_k \delta(k-l), && (2.96)
\end{aligned}$$

where I introduced the Dirac-delta distribution with the convention,

$$\delta(k-l) = \frac{1}{2\pi}\int \mathrm{d}x\, \mathrm{e}^{\mathrm{i}(l-k)x}. \tag{2.97}$$

Hence, setting $N_k = 1/\sqrt{4\pi\omega_k} \implies (u_k, u_l)_{\mathrm{KG}} = \delta(k-l)$. □

We now have a formal solution to the classical equations of motion, but we continue on, hoping to make more connections with the quantum theory to be discussed shortly. From these relations, one can find the Poisson bracket between α and α^*,

$$\begin{aligned}
\{\alpha_k, \alpha_l^*\}_{\mathrm{PB}} &= -\mathrm{i}(u_k, u_l)_{\mathrm{KG}} && (2.98)\\
&= -\mathrm{i}\delta(k-l). && (2.99)
\end{aligned}$$

Proof. We prove the preceding equation. Consider the following set of equalities,

$$\begin{aligned}
\{\alpha_k, \alpha_l^*\}_{\mathrm{PB}} &= -\{(u_k, \phi)_{\mathrm{KG}}, (u_l^*, \phi)_{\mathrm{KG}}\}_{\mathrm{PB}}\\
&= -\Big\{\mathrm{i}\int \mathrm{d}x \left(u_k^*(x)\pi(x) - \phi(x)p_{u_k}^*(x)\right), \mathrm{i}\int \mathrm{d}y \left(u_l(y)\pi(y) - \phi(y)p_{u_l}(y)\right)\Big\}_{\mathrm{PB}}\\
&= \int \mathrm{d}x\,\mathrm{d}y \Big\{\left(u_k^*(x)\pi(x) - \phi(x)p_{u_k}^*(x)\right), \left(u_l(y)\pi(y) - \phi(y)p_{u_l}(y)\right)\Big\}_{\mathrm{PB}}\\
&= \int \mathrm{d}x\,\mathrm{d}y \Big(u_k^*(x)p_{u_l}(y)\big\{\phi(y), \pi(x)\big\}_{\mathrm{PB}} - u_l(y)p_{u_k}^*(x)\big\{\phi(x), \pi(y)\big\}_{\mathrm{PB}}\Big)\\
&= \int \mathrm{d}x \left(u_k^* p_{u_l} - u_l p_{u_k}^*\right)\\
&= -\mathrm{i}(u_k, u_l)_{\mathrm{KG}}\\
&= -\mathrm{i}\delta(k-l).
\end{aligned}$$

The first and second equalities follow from equations (2.89) and by expanding the Klein-Gordon inner product. The third, fourth, and fifth equalities follow from linearity of the Poisson bracket and by using the canonical commutation relations, equations (2.74) and (2.75). The final two equalities follow from the definition of the Klein-Gordon inner product and the normalization of the mode functions. □

As a final calculation, let us write the Hamiltonian in terms of the complex coefficients, α and α^*. Using the definition of the Hamiltonian, equation (2.80), the classical solutions to Hamilton's equations, equations (2.84) and (2.85), and after a few integrals, one finds,

$$H = \int \mathrm{d}k\, \omega_k |\alpha_k|^2, \tag{2.100}$$

which, upon inspection, is just the sum of the energies of an infinite set of simple harmonic oscillators. As one should expect, a similar relation will hold in the quantum theory but with an extra (divergent) contribution from the quantum vacuum.

The quantum field

We now "go over" to the quantum theory in a similar manner as we did for the quantum harmonic oscillator. We need to take some care, however, when dealing with the quantum states, due to the continuous nature of fields and formally divergent quantities etc. I will do whatever is convenient and whatever gets us to the answers we need in the most efficient and sensible fashion (in my perspective).

Recall our procedure for producing a quantum theory from the classical theory, which I reproduce here for convenience:

- Given the classical, Hamiltonian description of the system, 'go over' to the quantum theory by canonical quantization, i.e.

$$\{A, B\}_{\mathrm{PB}} \to \frac{[\hat{A}, \hat{B}]}{\mathrm{i}\hbar}.$$

  Here, A and B are classical observables, which are general functions of the canonical variables, ϕ and π, and $\hat{A}$ and $\hat{B}$ are their Hermitian operator-counterparts and are operator-functions of the canonical operators, $\hat{\phi}$ and $\hat{\pi}$.

- Solve the operator form of Hamilton's equations for the canonical variables,

$$\frac{\mathrm{d}\hat{\phi}}{\mathrm{d}t} = \frac{1}{\mathrm{i}\hbar}[\hat{\phi}, \hat{H}] \quad \text{and} \quad \frac{\mathrm{d}\hat{\pi}}{\mathrm{d}t} = \frac{1}{\mathrm{i}\hbar}[\hat{\pi}, \hat{H}], \tag{2.101}$$

  thereby determining the time evolution for any observable, $\hat{A}(\hat{\phi}, \hat{\pi})$. Note that, the solutions of these equations are, more or less, equivalent to the classical equations of motion.

- Determine the quantum states of the system. For the quantum harmonic oscillator, this was found by constructing the Fock basis, $\{|n\rangle\}$, which was formed by successive applications of the creation operator to the quantum vacuum, $|0\rangle$ – i.e.,

$$|n\rangle = \frac{\hat{a}^{\dagger n}}{\sqrt{n!}}|0\rangle\,. \tag{2.102}$$

  Thus, for oscillator-like systems, construct the Fock basis from the vacuum, from which any quantum state can written in terms of by linearity.

We follow this procedure to a tee. We start by writing out the canonical commutation relations. Let $\hat{\phi}$ and $\hat{\pi} = \partial_t\hat{\phi}$ be the canonical field operators for the massless, scalar field. Then,

$$\frac{\mathrm{d}\hat{F}}{\mathrm{d}t} = \frac{1}{\mathrm{i}\hbar}[\hat{F}, \hat{H}] \tag{2.103}$$

$$[\hat{\phi}(x), \hat{\pi}(y)] = \mathrm{i}\hbar\delta(x-y) \tag{2.104}$$

$$[\hat{\phi}(x), \hat{\phi}(y)] = [\hat{\pi}(x), \hat{\pi}(y)] = 0, \tag{2.105}$$

where $\hat{F}$ is some operator functional of the canonical variables, ϕ and π. The Hamiltonian operator is given as,

$$\hat{H}[\phi, \pi] = \frac{1}{2}\int \mathrm{d}x \left(\hat{\pi}^2 + (\partial_x\hat{\phi})^2\right). \tag{2.106}$$

From this Hamiltonian and using the commutation relations above, we find the operator form of Hamilton's equations,

$$\partial_t\hat{\phi} = \hat{\pi} \quad \text{and} \quad \partial_t\hat{\pi} = \partial_x^2\hat{\phi}. \tag{2.107}$$

Towards solving these equations, the story is the same as in the classical field case. So I simply write down the solution, in terms of the complex mode function $u_k(x,t) = N_k \exp[-\mathrm{i}(\omega_k t - kx)]$,

$$\hat{\phi}(x,t) = \int \mathrm{d}k \left(\hat{a}_k u_k(x,t) + \hat{a}_k^\dagger u_k^*(x,t)\right) \tag{2.108}$$

$$\hat{\pi}(x,t) = -\mathrm{i}\int \mathrm{d}k\, \omega_k \left(\hat{a}_k u_k(x,t) - \hat{a}_k^\dagger u_k^*(x,t)\right) \tag{2.109}$$

where $\hat{a}$ and $\hat{a}^\dagger$ are the annihilation and creation operators, respectively. We can extract these operators from the field via the Klein-Gordon inner product per usual, but first a redefinition,

$$(f,g)_{\mathrm{KG}} \overset{\mathrm{def}}{=} \frac{\mathrm{i}}{\hbar}\int \mathrm{d}x \left(f^* p_g - g p_f^*\right), \tag{2.110}$$

where f and g are classical solutions to the equations of motion and $p_f = \partial_t f$ (and similarly for g). This differs from the original, equation (2.86), only by a factor of $\hbar$. The Klein-Gordon inner product between the mode functions still hold with this re-scaling, as such

only changes the normalization factor to $N_k = \sqrt{\hbar/(4\pi\omega_k)}$. From this definition and the field operator, equation (2.108), we have,

$$\hat{a}_k = (u_k, \hat{\phi})_{\mathrm{KG}} \quad \text{and} \quad \hat{a}_k^\dagger = -(u_k^*, \hat{\phi})_{\mathrm{KG}}. \tag{2.111}$$

Using this relation and the canonical commutation relations, one can prove that,

$$[\hat{a}_k, \hat{a}_l^\dagger] = \delta(k-l) \tag{2.112}$$

$$[\hat{a}_k, \hat{a}_l] = [\hat{a}_k^\dagger, \hat{a}_l^\dagger] = 0. \tag{2.113}$$

With all this in hand, we re-write the Hamiltonian operator in terms of the creation and annihilation operators. After some algebra, a few integrals, and an application of the commutator (2.112), one finds,

$$\hat{H} = \int \mathrm{d}k\, \hbar\omega_k \hat{a}_k^\dagger \hat{a}_k + \delta(0) \int \mathrm{d}k\, \hbar\omega_k/2 \tag{2.114}$$

where $\delta(0)$ is the Dirac-delta distribution evaluated at the origin of its argument. The second term is the vacuum energy and is formally divergent, independently of the Dirac-delta distribution! This is because we are summing over an infinite number of oscillators, with the vacuum state for each mode, k, contributing a factor $\hbar\omega_k/2$ to the sum. The divergent vacuum energy is unavoidable once we transition to fields. In the end, it could be so that the field is just a continuum approximation for, e.g., a large but finite set of coupled oscillators, in which case the vacuum energy reduces to a finite sum (a large term, perhaps, but finite), or it could be so that our field theory is only appropriate up to some high energy scale (up to an upper value of ω), at which point a more sound theory steps in and saves the day. In any case, we will not think too much into it. Instead, we will do what any respectable physicist does and simply sweep this infinity under the rug. It will not bother us anyway.

We have thus solved the equations of motion and found a generic expression for the field operator, but as was the case with the quantum harmonic oscillator, we are not yet done, as we must now describe the quantum states of the system. We will take a similar approach as before, i.e. construct the Fock space (the space of states) by successive applications of the creation operator on the vacuum, however, we must be a bit gentle here. The reason being that we are dealing with an infinite set of oscillators, and we are working in a continuum (the former is the main issue), which will present some difficulties if we continue blindly. We will bypass these difficulties however by introducing wave-packets and reducing the infinite set oscillators to a finite set. Such a reduction is permissible as the dynamics of physically interesting situations is typically restricted to a handful of modes.

First, we build a Fock space, with suitably normalized basis states, by restricting to a single-mode wave-packet. We will generalize this to M modes later. Consider a wave-packet, f, which is a solution to the equations of motion satisfies,

$$(f, f)_{\mathrm{KG}} = 1. \tag{2.115}$$

Since $\{u_k\}$ form a basis of solutions to the equations of motion, we may expand f as,

$$f = \int \mathrm{d}k\, (\alpha_k u_k + \beta_k u_k^*)\,, \tag{2.116}$$

where, $\alpha_k = (u_k, f)_{\text{KG}}$ and $\beta_k = -(u_k^*, f)_{\text{KG}}$. This is a generic expansion, but we will restrict ourselves to $\beta_k = 0 \; \forall \; k$ momentarily. Speaking generally for now, given that $(f, f)_{\text{KG}} = 1$ by definition, we have

$$(f, f)_{\text{KG}} = 1 \implies \int \mathrm{d}k \left(|\alpha_k|^2 - |\beta_k|^2 \right) = 1, \tag{2.117}$$

which follows by expanding f per equation (2.116) and using linearity of the Klein-Gordon inner product. We now define the annihilation operator, $\hat{a}_f$, for the wave-packet f as,

$$\hat{a}_f \stackrel{\text{def}}{=} (f, \hat{\phi})_{\text{KG}}. \tag{2.118}$$

From which it follows,

$$[\hat{a}_f, \hat{a}_f^\dagger] = (f, f)_{\text{KG}} = 1. \tag{2.119}$$

From equation (2.118) and the expansion of the field operator (2.108), we can expand $\hat{a}_f$ in terms of the mode operators, $\hat{a}_k$ and $\hat{a}_k^\dagger$,

$$\hat{a}_f = \int \mathrm{d}k \left(\alpha_k^* \hat{a}_k - \beta_k^* \hat{a}_k^\dagger \right). \tag{2.120}$$

Proof. We prove the preceding equation. Consider the following set of equalities:

$$\begin{aligned}
\hat{a}_f &= (f, \hat{\phi})_{\text{KG}} && (2.121)\\
&= \left(f, \int \mathrm{d}k \left(\hat{a}_k u_k + \hat{a}_k^\dagger u_k \right) \right)_{\text{KG}} && (2.122)\\
&= \int \mathrm{d}k \left(\hat{a}_k (f, u_k)_{\text{KG}} + \hat{a}_k^\dagger (f, u_k^*)_{\text{KG}} \right) && (2.123)\\
&= \int \mathrm{d}k \left(\hat{a}_k (u_k, f)_{\text{KG}}^* + \hat{a}_k^\dagger (u_k^*, f)_{\text{KG}}^* \right) && (2.124)\\
&= \int \mathrm{d}k \left(\alpha_k^* \hat{a}_k - \beta_k^* \hat{a}_k^\dagger \right). && (2.125)
\end{aligned}$$

For the second equality, we have expanded the field operator in terms of the mode functions and mode operators. For the third equality, we have used the linearity of the Klein-Gordon inner product. For the fourth equality, we have used the fact that $(f, g)_{\text{KG}}^* = (g, f)_{\text{KG}}$, and for the final equality, we have used the fact that $\alpha_k = (u_k, f)_{\text{KG}}$ and $\beta_k = -(u_k^*, f)_{\text{KG}}$. □

Now define the vacuum state, $|0\rangle$, to be the ground state of the Hamiltonian operator, equation (2.114), satisfying $\hat{a}_k |0\rangle = 0 \; \forall \; k$ *and* $\hat{a}_f |0\rangle = 0$. With this choice, it follows that $\beta_k = 0 \; \forall \; k$, $\int \mathrm{d}k \, |\alpha_k|^2 = 1$, and $\hat{a}_f = \int \mathrm{d}k \, \alpha_k^* \hat{a}_k$. Similar to before, we construct the Fock basis, $\{|n_f\rangle\}$, by repeated applications of the creation operator, $\hat{a}_f^\dagger$, to the vacuum. I list a few results which follow:

- The set of orthonormal basis vectors, $\{|n_f\rangle\}$, for $n \in \mathbb{N}$, define a basis for the single-mode Fock space, $\mathscr{F}_f$, satisfying

  $$\langle m_f | n_f \rangle = \delta_{mn}, \tag{2.126}$$

  where δ_{mn} is the Kronecker delta.

- The basis states (Fock states), $|n_f\rangle$, can be constructed from the vacuum by successive applications of the creation operator, such that,

$$|n_f\rangle = \frac{\hat{a}_f^{\dagger n}}{\sqrt{n!}}|0\rangle\,. \tag{2.127}$$

  From this construction, it follows that the Fock states are eigenstates of the number operator, $\hat{n}_f = \hat{a}_f^\dagger \hat{a}_f$ with eigenvalue n.

- The time dependent annihilation operator for the wave-packet is given as

$$\hat{a}_f(t) = \int \mathrm{d}k \alpha_k^* \hat{a}_k \mathrm{e}^{-\mathrm{i}\omega_k t}, \tag{2.128}$$

  from which all other dynamical quantities of interest can be found.

- By computing the matrix elements of the Hamiltonian in equation (2.114) in the single-mode Fock basis of f, it can be shown that,

$$\langle m_f|\hat{H}|n_f\rangle = \hbar\omega_f n\delta_{mn}, \tag{2.129}$$

  where

$$\omega_f = \int \mathrm{d}k\, \omega_k |\alpha_k|^2 \quad \text{and} \quad |\alpha_k|^2 = |(u_k, f)_{\mathrm{KG}}|^2, \tag{2.130}$$

  and the divergent vacuum energy has been discarded. Hence, although the state $|n_f\rangle$ is not an eigenstate of the Hamiltonian, its energy nevertheless takes on discrete values, with an average given by $\hbar\omega_f n$. For example, the state $|1_f\rangle$ corresponds to the quantum state of a single photon occupying the wave-packet f, which carries a quantum of energy $\hbar\omega_f$ on average (averaging over k). If f is sharply peaked around some mode k_0, then $\hbar\omega_f \approx \hbar\omega_{k_0}$, which is just the Einstein-Planck relation for the energy of a photon with frequency ω_{k_0}.

We now generalize the single-mode construction to an M-mode construction, by introducing a finite set of functions, $\{f_i\}_{i=1}^M$, which are orthonormal in the Klein-Gordon inner product, i.e. $(f_i, f_j)_{\mathrm{KG}} = \delta_{ij}$. The Fock space is then given as a tensor product over all M modes, $\mathscr{F}_{\{f\}} = \bigotimes_i \mathscr{F}_{f_i}$. Of physical interest is a set of wave-packets which are dynamically decoupled under free Hamiltonian evolution. For instance, let each f_i have support only over a finite sector in k-space, and let each of these sectors not overlap (there are thus M independent sectors). That is, if $f_i = \int \mathrm{d}k \alpha_{i,k} u_k$, then we suppose that $\mathrm{supp}(\alpha_{i,k})$ is non-trivial only in finite domain and that $\mathrm{supp}(\alpha_{i,k}\alpha_{j,k}) = \varnothing$ if $i \neq j$. Therefore, under this prescription and assuming free evolution generated by the Hamiltonian in equation (2.114), each mode-sector, i, is dynamically decoupled from any other sector, meaning that there is no mixing between different wave-packet modes, f_i; however, there is mixing between the k-modes contained within a given sector. One can think of the different degrees of mixing as "external" versus "internal" dynamics, where the external dynamics describes the interactions between the different sectors (between wave-packets) and the internal dynamics describes the interactions occurring within a given sector (an individual wave-packet). It is often the case that

the external dynamics are physically more relevant (think of scattering between M initially independent wave-packets), and one must simply take care that the internal dynamics are not affecting the external dynamics in an impactful manner.

Before we conclude this section, I would like to introduce the *quadrature operators* for the wave-packet f, and make some comments which will, hopefully, permit an easy transition into the formalism of the next section. Define the quadrature operators, $\hat{X}_f$ and $\hat{P}_f$, as,

$$\hat{X}_f \stackrel{\text{def}}{=} \sqrt{\frac{1}{2}} \left(\hat{a}_f + \hat{a}_f^\dagger \right) \tag{2.131}$$

$$\hat{P}_f \stackrel{\text{def}}{=} -\mathrm{i}\sqrt{\frac{1}{2}} \left(\hat{a}_f - \hat{a}_f^\dagger \right). \tag{2.132}$$

Observe that,

$$\frac{\hbar\omega_f}{2} \left(\hat{P}_f^2 + \hat{X}_f^2 \right) = \hbar\omega_f (\hat{a}_f^\dagger \hat{a}_f + 1/2), \tag{2.133}$$

which is reminiscent of the single, quantum-harmonic oscillator. See equation (2.41). These operators satisfy,

$$[\hat{X}_f, \hat{P}_f] = \mathrm{i}, \tag{2.134}$$

for all times and undergo time evolution via the Hamiltonian of equation (2.114), leading to,

$$\hat{X}_f(t) = \sqrt{\frac{1}{2\omega_f}} \left(\hat{a}_f(t) + \hat{a}_f^\dagger(t) \right) \tag{2.135}$$

$$\hat{P}_f(t) = -\mathrm{i}\sqrt{\frac{\omega_f}{2}} \left(\hat{a}_f(t) - \hat{a}_f^\dagger(t) \right), \tag{2.136}$$

with $\hat{a}_f(t)$ given by equation (2.128). By inspecting equations (2.108) and (2.109), we see that the quadrature operators, $\hat{X}$ and $\hat{P}$, are quite similar to the canonical operators, $\hat{\phi}$ and $\hat{\pi}$. Due to their close correspondence with the canonical operators, I will refer to $\hat{X}$ and $\hat{P}$ as the canonical operators themselves. In the forthcoming sections, I use this language without discretion.

2.2 Photon dynamics

Our discussion on photon dynamics will be restricted to quadratic interactions and symplectic transformations. For generic remarks regarding systems and states associated with such dynamics, see Serafini's monograph [24] (which I highly recommend). A large part of the literature in quantum optics focuses on precisely this subset of quadratic interactions. Hence, for an quantum-optical perspective, see e.g. [21, 22]. From here on, unless stated otherwise, I set $\hbar = 1$.

Some notation

Our analyses has to do with a finite set of interacting quantum oscillators (or modes). Hence, if we consider n modes, then we are dealing with a Fock space

$$\mathcal{F} = \bigotimes_{k=1}^{n} \mathcal{F}_{1_k},$$

where $\mathscr{F}_{1_k}$ is the single-mode Fock space (which we previously encountered) for the kth mode. The modes themselves are associated with a pair of canonical operators, $(\hat{x}_i, \hat{p}_i)$, where i labels which mode of n, which satisfy the canonical commutation relations

$$[\hat{x}_i, \hat{p}_j] = \mathrm{i}\delta_{ij} \tag{2.137}$$

$$[\hat{x}_i, \hat{x}_j] = [\hat{p}_i, \hat{p}_j] = 0, \tag{2.138}$$

where δ_{ij} is the Kronecker delta-function. They are related to the annihilation and creation operators, $\hat{a}$ and $\hat{a}^\dagger$, via

$$\hat{x} = \frac{1}{\sqrt{2}}\left(\hat{a} + \hat{a}^\dagger\right) \quad \text{and} \quad \hat{p} = -\frac{\mathrm{i}}{\sqrt{2}}\left(\hat{a} - \hat{a}^\dagger\right). \tag{2.139}$$

These canonical operators are actually the (dimensionless) quadrature operators of the field introduced in the preceding section, however, I will simply refer to them as the canonical operators.

It will be efficient to define a $2n \times 1$ *vector of canonical operators*,

$$\hat{\mathbf{r}} \overset{\text{def}}{=} (\hat{x}_1, \hat{p}_1, \ldots, \hat{x}_n, \hat{p}_n)^\intercal, \tag{2.140}$$

which compactly describes all the field modes and their canonical momenta.[5] From the canonical commutation relations above, one can express the commutation relations between all modes via,

$$[\hat{\mathbf{r}}_i, \hat{\mathbf{r}}_j] = \mathrm{i}\Omega_{ij}, \tag{2.141}$$

where Ω_{ij} are the matrix coefficients of the $2n \times 2n$ *symplectic form*,

$$\Omega = \mathbb{I}_n \otimes \Omega_1 \quad \text{where} \quad \Omega_1 = \begin{pmatrix} 0 & 1 \\ -1 & 0 \end{pmatrix}. \tag{2.142}$$

As an aside, one can relate the total number of excitations to the canonical vector operator via,

$$\hat{n} = \frac{1}{2}\hat{\mathbf{r}}^\intercal\hat{\mathbf{r}} - n/2, \tag{2.143}$$

where $\hat{n}_i = \hat{a}_i^\dagger\hat{a}_i$ is the number operator for the ith mode and $\hat{n} = \sum_i \hat{n}_i$. The extra c-number, $n/2$, is due, essentially, to the vacuum of each mode contributing a factor of $1/2$ to the energy of the field. A similar relation was found in equation (2.133).

[5] We borrow this notation from Serafini [24].

Quadratic Hamiltonians and symplectic transformations

For interactions between various modes, we will restrict ourselves to *quadratic Hamiltonians* – implying, e.g., that the equations of motion for the fields are linear in the field variables though generally coupled. In what follows, I will discuss dynamics in a highly simplistic manner, making no reference to the field variables themselves, and will restrict the discussion only to the transformations of the quadrature variables introduced above. I will not provide support for this approach immediately, but will return to this matter later.

Dynamics and the Bloch-Messiah decomposition

Consider a general, time-independent quadratic Hamiltonian,

$$\hat{H} = \frac{1}{2}\hat{\mathbf{r}}^{\intercal}\mathcal{H}\hat{\mathbf{r}} = \frac{1}{2}\mathcal{H}_{ij}\hat{\mathbf{r}}_i\hat{\mathbf{r}}_j, \tag{2.144}$$

where $\mathcal{H}$ is a $2n \times 2n$, real, symmetric, positive definite ($\mathcal{H} > 0$) matrix, called the *Hamiltonian matrix*.[6] Let τ represent time (or any continuous parameter) associated with the Hamiltonian (generator) $\hat{H}$. Then, the time-evolved canonical operators can be written generically as,

$$\hat{\mathbf{r}}_k(\tau) = (S_{\mathcal{H}})_{ki}\,\hat{\mathbf{r}}_i, \tag{2.145}$$

where the $2n \times 2n$ *symplectic matrix*,

$$S_{\mathcal{H}} \stackrel{\text{def}}{=} \exp\left(\Omega\mathcal{H}\tau\right), \tag{2.146}$$

has been defined. Here, Ω is the symplectic form and $\mathcal{H}$ is the Hamiltonian matrix. Equation (2.145) shows, quite compactly, that the canonical operators at time τ are just a linear combinations of the canonical operators at $\tau = 0$.

Proof. We prove the preceding equations. Recall the quantum version of Hamilton's equations [see, e.g., equation (2.55)]. Then, consider following set of equalities,

$$\begin{aligned}
\partial_\tau\hat{\mathbf{r}}_k &= \mathrm{i}\Big[\hat{H}, \hat{\mathbf{r}}_k\Big] \\
&= \frac{\mathrm{i}}{2}\mathcal{H}_{ij}[\hat{\mathbf{r}}_i\hat{\mathbf{r}}_j, \hat{\mathbf{r}}_k] \\
&= \frac{\mathrm{i}}{2}\mathcal{H}_{ij}\left(\hat{\mathbf{r}}_i[\hat{\mathbf{r}}_j, \hat{\mathbf{r}}_k] + [\hat{\mathbf{r}}_i, \hat{\mathbf{r}}_k]\hat{\mathbf{r}}_j\right) \\
&= \Omega_{ki}\mathcal{H}_{ij}\hat{\mathbf{r}}_j \\
&= \left(\Omega\mathcal{H}\hat{\mathbf{r}}\right)_k,
\end{aligned}$$

where, in the third equality, the canonical commutation relations were used, and in the fourth and fifth equalities, the symmetry of the Hamiltonian matrix and the anti-symmetry of the canonical form was used. This is a first order differential equation, with a solution given by equation (2.145) if $S_{\mathcal{H}} = \exp(\Omega\mathcal{H}\tau)$. □

[6] Note that I have restricted to purely quadratic Hamiltonians. This is a minor point, and I will come back to it.

Recall, from quantum theory, that Hamiltonian dynamics corresponds to evolving the system by a unitary operator, $\hat{U}_\tau = \exp(-\mathrm{i}\hat{H}\tau)$, such that $\hat{U}_\tau^\dagger \hat{\mathbf{r}} \hat{U}_\tau = \hat{\mathbf{r}}(\tau)$ (Heisenberg evolution). It thus follows that, if the Hamiltonian is quadratic, then

$$\hat{U}_\tau^\dagger \hat{\mathbf{r}} \hat{U}_\tau = S_{\mathcal{H}} \hat{\mathbf{r}}. \tag{2.147}$$

This correspondence between unitary evolution and symplectic transformations allows us to discard discussion of the former in favor of the latter, which effectively reduces evolution to simple matrix multiplication.

With this correspondence in hand, it is also useful to know what generally happens if, for example, we concatenate successive symplectic transformations. For example, first evolve, in the Heisenberg picture via a unitary $\hat{S}_1$, then $\hat{S}_2$ then $\hat{S}_3$ etc., such that $\prod_{n=1}^{N} \hat{S}_n$ gives the full unitary process. One can then show that this concatenation of unitary processes corresponds to the transformation,

$$\hat{S}_1^\dagger \dots \hat{S}_N^\dagger \hat{\mathbf{r}} \hat{S}_N \cdots \hat{S}_1 = \left(\prod_{n=1}^{N} S_n \right) \hat{\mathbf{r}}, \tag{2.148}$$

which is a concatenation rule for symplectic tranformations. Here, S_n is the symplectic transformation corresponding to the unitary $\hat{S}_n$. An astute reader may notice that: The Heisenberg evolution, in terms of unitary operators, is like "evolving backwards", where the last unitary in the concatenation acts first on the canonical operator and so on and so forth (first $\hat{S_N}$, then $\hat{S}_{N-1}$ etc.). However, at the level of symplectic matrices, $\{S_n\}$, the evolution follows the actual sequence of events, from 1 to N, similar to the Schrödinger evolution of quantum states.

Proof. We prove the preceding equation for a sequence of two unitary operators, $\hat{S}_1$ and $\hat{S}_2$. The full result follows by induction. Consider the unitary operator, $\hat{U} = \hat{S}_2 \hat{S}_1$, where the unitary operator $\hat{S}_l$ has a corresponding symplectic matrix, S_l, and consider the Heisenberg evolution of the canonical operator, $\hat{\mathbf{r}}_k$. Then, the following set of equalities hold,

$$\begin{aligned}
\hat{U}^\dagger \hat{\mathbf{r}}_k \hat{U} &= \hat{S}_1^\dagger \hat{S}_2^\dagger \hat{\mathbf{r}}_k \hat{S}_2 \hat{S}_1 \\
&= \hat{S}_1^\dagger \left(\hat{S}_2^\dagger \hat{\mathbf{r}}_k \hat{S}_2 \right) \hat{S}_1 \\
&= \hat{S}_1^\dagger \Big((S_2)_{kj} \hat{\mathbf{r}}_j \Big) \hat{S}_1 \\
&= (S_2)_{kj} \left(\hat{S}_1^\dagger \hat{\mathbf{r}}_j \hat{S}_1 \right) \\
&= (S_2)_{kj} \Big((S_1)_{ji} \hat{\mathbf{r}}_i \Big) \\
&= (S_2)_{kj} (S_1)_{ji} \hat{\mathbf{r}}_i \\
&= \left(S_2 S_1 \hat{r} \right)_k .
\end{aligned}$$

For the third and fourth equalities, we used the relation between Heisenberg evolution and symplectic transformations [equation (2.147)] and then moved the matrix coefficients of S_2 around freely. The remaining equalities were found by the same sort of shuffling. For the

final equality, we equated the sum over matrix elements to the product of the matrices with proper ordering.

The generalization to a concatenation of N unitary operators follows by induction. For, let $\hat{S}_{12} \stackrel{\text{def}}{=} \hat{S}_2\hat{S}_1$ with corresponding symplectic matrix $S_{12} \stackrel{\text{def}}{=} S_2S_1$ and introduce another unitary evolution $\hat{S}_3$, with corresponding symplectic matrix S_3, such that $\hat{U} = \hat{S}_3\hat{S}_{12}$. From above, it follows that the unitary evolution of the canonical operator, $\hat{\mathbf{r}}_k$, equates to the matrix product $(S_3S_{12}\hat{\mathbf{r}})_k = (S_3S_2S_1\hat{\mathbf{r}})_k$. A similar relation thus holds for N such transformations, by extension. □

The matrices S are called symplectic since they generally obey the relation,

$$S^\intercal \Omega S = \Omega, \tag{2.149}$$

which, e.g., must hold in order for Hamiltonian dynamics to preserve the canonical commutation relations (2.141). Matrices which obey this relation form the *symplectic group*. I will not delve into the mathematical particulars concerning this group, but I will point out one very important observation. That is, *any symplectic transformation, on a finite number of modes, may be decomposed as a product of single-mode squeezers, phase shifters, and two-mode beamsplitters* [25]. This is known as the *Bloch-Messiah decomposition*. To provide a short description: Single-mode squeezers are single-mode transformations which reduce the variance in one quadrature of the mode and increase the variance in the other quadrature of the mode, all while saturating the Heisenberg uncertainty relation (for vacuum inputs). This process also corresponds to particle creation in a single mode. On the other hand, beamsplitters correspond to "passive" scattering events between two modes, while phase shifts correspond to free evolution. At the level of symplectic transformations, beamsplitters and phase shifters induce orthogonal transformations (e.g. rotations) and form a subgroup of the symplectic group. Such transformations are passive, in the sense that they preserve excitation (photon) number. This can be quickly seen by examining the invariance of equation (2.143) when the canonical operators are subject to a symplectic transformation, O, obeying the orthogonality condition, $O^\intercal O = \mathbb{I}$.

Sketch of proof. The decomposition of any (real) symplectic matrix into passive transformations and single-mode squeezers can be made more precise. First, observe that any real matrix, S, admits a spectral decomposition of the form,

$$S = O_1 D O_2, \tag{2.150}$$

where D is a positive semi-definite, diagonal matrix, with the singular values of S along its diagonal, and $\{O_k\}$ are orthogonal matrices ($O_k^\intercal O_k = \mathbb{I}$). For S a symplectic matrix: (i) $\{O_k\}$ are orthogonal and symplectic[7], and (ii) $\det S = 1$, implying that the singular value matrix, D, is positive definite. Furthermore, one can show that,

$$D = \bigoplus_{k=1}^{n} \begin{pmatrix} d_k & 0 \\ 0 & d_k^{-1}, \end{pmatrix}$$

[7]The fact that they are orthogonal follows from the singular value decomposition. The fact that they are orthogonal and symplectic [and thus isomorphic to $U(n)$] must be shown, but it is just a consequence of S being symplectic. I take this fact for granted here, but see Appendix B of [24] for an extended proof.

with $d_k > 0$ from the singular value decomposition. For, consider that,

$$\begin{aligned} S\Omega S^\intercal &= (O_1 D O_2)\,\Omega\,(O_2^\intercal D O_1^\intercal) \\ &= (O_1 D)\,\Omega\,(D O_1^\intercal)\,, \end{aligned}$$

but $S\Omega S^\intercal = \Omega$, since S is symplectic. Thus, using the fact that O_k are symplectic and orthogonal, it must be so that

$$D\Omega D = \Omega.$$

Writing D as a direct sum of two dimensional blocks,

$$D = \bigoplus_{k=1}^{n} \begin{pmatrix} d_k & 0 \\ 0 & d_k' \end{pmatrix},$$

and substituting into the previous relation, we find

$$\begin{aligned} D\Omega D &= \bigoplus_{k=1}^{n} \begin{pmatrix} d_k & 0 \\ 0 & d_k' \end{pmatrix} \begin{pmatrix} 0 & 1 \\ -1 & 0 \end{pmatrix} \begin{pmatrix} d_k & 0 \\ 0 & d_k' \end{pmatrix} \\ &= \bigoplus_{k=1}^{n} \begin{pmatrix} 0 & d_k d_k' \\ -d_k d_k' & 0 \end{pmatrix} \\ &= \bigoplus_{k=1}^{n} \begin{pmatrix} 0 & 1 \\ -1 & 0 \end{pmatrix}, \end{aligned}$$

which implies $d_k' = 1/d_k$, as claimed. Observe that D is just a direct sum of single-mode squeezing transformations with, e.g., $d_k = \mathrm{e}^{r_k}$ corresponding to squeezing (anti-squeezing) in one quadrature of the mode k and $1/d_k = \mathrm{e}^{-r_k}$ corresponding to anti-squeezing (squeezing) in the other quadrature, where r_k is the squeezing strength.

Here, the orthogonal transformations, O_1 and O_2, are elements of the symplectic orthogonal group which is isomorphic to the unitary group, $U(n)$. Hence, one can directly interpret O_1 and O_2 as corresponding to some finite-dimensional unitary matrix. Furthermore, it can be shown that any finite-dimensional unitary matrix may be decomposed into a set of two mode beamsplitters and phase shifters via the so-called Reck-Zeilinger decomposition [26]. It thus follows that any symplectic transformation can be decomposed as a set of independent single-mode squeezers sandwiched between two linear-optical circuits. □

Now to return to the physics of the matter. One must question how well (or if at all) do the simplistic dynamics thus posed correspond to physical scenarios of interest? The answer is quite well if, for instance, we restrict ourselves to well-posed scattering problems, which is what we will limit ourselves to in this thesis. In this context, we imagine well-defined modes, and thus well-defined Fock spaces, "far away" from some interaction region (quotations because this applies to spatially and temporally localized interactions). These asymptotic regions, which I will call the in and out regions, are presumably described by simple Hamiltonians, which can be easily handled and which define the underlying mode structure as well as well-defined in/out Fock spaces. See Figure 2.1 for an illustration. We

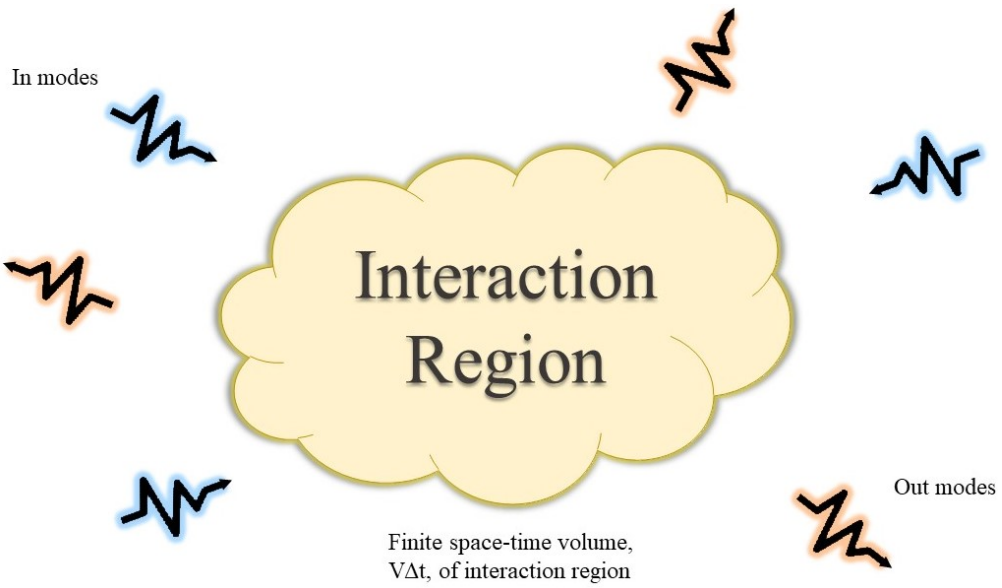

Figure 2.1: Scattering of the "in-modes" to the "out-modes". Asymptotically, far in the past/future and spatially far away, there exists a well-defined set of in/out modes. The in-modes scatter to the out-modes by impinging on an interaction region, which fills a finite space-time volume of size $V\Delta t$. Only quadratic interactions occur within this region, however the space-time dependence of these interactions is generically complex, thus permitting modes of different wavenumbers and/or frequencies to mix in a non-trivial way.

then formally view the dynamics – the scattering processes – as a mapping from the in-modes to the out-modes. That is, we assume there exists a bijective map, Φ, such that $\Phi : \mathscr{F}_{\text{in}} \to \mathscr{F}_{\text{out}}$, where $\mathscr{F}_{\text{in/out}}$ are the in/out Fock spaces just mentioned. At the level of quantum states, this corresponds to some unitary, $\hat{U}_{\text{in}\to\text{out}}$, that takes $|\psi\rangle_{\text{in}} \to |\psi\rangle_{\text{out}}$, where $|\psi\rangle_{\text{in}} \in \mathscr{F}_{\text{in}}$ and $|\psi\rangle_{\text{out}} \in \mathscr{F}_{\text{out}}$. What, then, could this unitary be? At the level of in/out canonical operators, which are well-defined by assumption, this unitary corresponds precisely to a symplectic transformation, which gives the output canonical operators as a linear combination of input canonical operators and vice versa (bijection). This must be so if the interactions are only quadratic; the equations of motion simply do not allow for any other possibility. Furthermore, since the scattering process must correspond to a symplectic transformation, it permits a decomposition into an array of linear-optical networks and squeezers. Therefore, to describe all physical processes of interest, at least the quadratic scattering-like interactions that we are restricting ourselves to, we need only provide an equivalent optical network, described by a set of appropriately tuned parameters – squeezing strengths, beamsplitter transmissivities, etc. This is the approach I take in this thesis to describe physical phenomena.

Before moving on, let me elaborate further on what I mean by "simple Hamiltonians" in the in/out regions. Simply put, I mean that the Hamiltonians are (locally) time-independent and also (but not necessarily) not-too-complicated in their spatial dependence, i.e. it is easy to diagonalize such Hamiltonians and construct Fock spaces from well-defined vacuum states in these regions. This amounts to finding the so-called *normal modes* of the Hamiltonian,

which provides a natural decomposition of the Hamiltonian into a set of independent harmonic oscillators in the in/out regions; i.e.,

$$\hat{H} = \sum_{k=1}^{n} \omega_k \left(\hat{X}_k^2 + \hat{P}_k^2 \right), \tag{2.151}$$

with $\{\omega_k\}$ being the set of natural frequencies for the modes. The corresponding Fock spaces can then be built with respect to this set of modes, which again, provide an unambiguous notion of ground state (or vacuum) asymptotically. The notion that such a decomposition exists is interesting, and it holds quite generically for time-independent quadratic interactions, as the following sketch shows.

Proof. We sketch the existence of the above decomposition for time-independent quadratic Hamiltonians. It relies on the so-called normal mode decomposition (or "Williamson's theorem") for any positive-definite, real matrix, which we apply here without justification or proof of the theorem. Consider a quadratic, stable (i.e. there exists a ground state) Hamiltonian, which can be written as

$$\hat{H} = \mathcal{H}_{ij} \hat{\mathbf{r}}_i \hat{\mathbf{r}}_j / 2,$$

per equation (2.144), where $\hat{\mathbf{r}}$ is an arbitrary but well-defined vector of canonical (quadrature) operators. Now, by assumption of stability, the Hamiltonian matrix, $\mathcal{H}$, is a positive-definite, real matrix, and thus admits a normal-mode decomposition by Williamson's theorem, such that,

$$\mathcal{H} = S^\intercal D_{\mathcal{H}} S \quad \text{with} \quad D_{\mathcal{H}} = \bigoplus_{k=1}^{n} \omega_k \mathbb{I}_2,$$

and S being symplectic. Here, $\{\omega_k\}$ are the symplectic eigenvalues of the Hamiltonian matrix, $\mathcal{H}$. Now, define a new set of canonical operators,

$$\hat{\mathbf{R}} \stackrel{\text{def}}{=} S \hat{\mathbf{r}}, \tag{2.152}$$

such that, e.g., $\hat{\mathbf{R}} = (\hat{X}_1, \hat{P}_1, \dots)^\intercal$. Since symplectic transformations preserve the canonical commutation relations, these new operators are well-defined canonical operators. Furthermore, in these new variables, the Hamiltonian decouples and takes on the form,

$$\begin{aligned} \hat{H} &= (D_{\mathcal{H}})_{ij} \hat{\mathbf{R}}_i \hat{\mathbf{R}}_j / 2 \\ &= \sum_{k=1}^{n} \omega_k \left(\hat{X}_k^2 + \hat{P}_k^2 \right), \end{aligned}$$

which was to be shown. Hence, any time-independent quadratic Hamiltonian can be decomposed into a set of independent quantum harmonic oscillators (normal modes), which vibrate at the natural frequencies $\{\omega_k\}$. □

Weyl operators

I made a brief footnote regarding the restriction to purely quadratic Hamiltonians in equation (2.144). Obviously, one can generalize such by introducing a pure c-number, which is trivial, but one can also introduce a linear piece $\boldsymbol{\lambda}^\intercal \hat{\mathbf{r}}$, where $\boldsymbol{\lambda}$ is some $2n$ column vector (not a vector operator). However, one can show that inclusion of the latter is equivalent to taking the purely quadratic Hamiltonian of (2.144) and transforming via a unitary operator known as the *Weyl* (or *displacement*) operator. The Weyl operator is defined as

$$\hat{D}_{\mathbf{R}} = \exp\left(\mathrm{i}\mathbf{R}^\intercal \Omega \hat{\mathbf{r}}\right) = \bigotimes_{k=1}^{n} \hat{D}_{\mathbf{R}_k}, \tag{2.153}$$

with,

$$\mathbf{R} = \bigoplus_{k=1}^{n} \mathbf{R}_k \in \mathbb{R}^{2n}$$

and $\mathbf{R}_k$ being a 2-dimensional displacement vector, associated with the kth mode, and I have made it explicit that a Weyl operator over all the modes is equivalent to a tensor product of local Weyl operators. Displacements are local operations which correspond to simple shifts, i.e.

$$\hat{D}_{\mathbf{R}} \hat{\mathbf{r}} \hat{D}_{\mathbf{R}}^\dagger = \hat{\mathbf{r}} + \mathbf{R}. \tag{2.154}$$

Physically, displacements can be thought as a semi-classical case of a purely quadratic Hamiltonian, where one replaces a subset of the canonical operators in a purely quadratic Hamiltonian with c-numbers. This scenario then corresponds to e.g. a set of quantum harmonic oscillators coupled to a set of classical oscillators.

As an aside, the Weyl operators obey the composition rule,

$$\hat{D}_{\mathbf{R}_2} \hat{D}_{\mathbf{R}_1} = \hat{D}_{\mathbf{R}_1 + \mathbf{R}_2} \mathrm{e}^{-\mathrm{i}\mathbf{R}_1^\intercal \Omega \mathbf{R}_2}, \tag{2.155}$$

which follows from a trivial use of the canonical commutation relations. Further, one can also provide a generic form for the composition of a unitary $\hat{S}$ – corresponding to a symplectic transformation, S – and a Weyl operator,

$$\hat{S}^\dagger \hat{D}_{\mathbf{R}} = \left(\hat{S}^\dagger \hat{D}_{\mathbf{R}} \hat{S}\right) \hat{S}^\dagger = \hat{D}_{S\mathbf{R}} \hat{S}. \tag{2.156}$$

Examples of symplectic transformations

For quick reference and for pedagogical purposes, I give a few worked-out examples of popular and useful symplectic transformations corresponding to, e.g., two-mode squeezing and two-mode beamsplitter transformations.

Example 2.2.1 (Beamsplitter)**.** *Consider the following two-mode Hamiltonian operator,*

$$\hat{H}_{BS} = \frac{1}{2}\theta \left(\hat{a}_1^\dagger \hat{a}_2 + \hat{a}_1 \hat{a}_2^\dagger\right), \tag{2.157}$$

where θ is the continuous parameter associated with the generator $\hat{H}_{BS}$ and $\{\hat{a}_i\}$ are the annihilation operators for the two modes. We wish to decompose this into the form, $\mathcal{H}_{ij}\hat{\mathbf{r}}_i\hat{\mathbf{r}}_j/2$,

thereby obtaining the Hamiltonian matrix elements. This will allow us to define a symplectic matrix associated with the unitary evolution of this Hamiltonian. Rewriting the above in terms of the canonical operators, $\hat{x}$ and $\hat{p}$, we find,

$$\begin{aligned}\hat{H}_{BS} &= \frac{1}{2}\theta\left(\hat{x}_1\hat{x}_2 + \hat{p}_1\hat{p}_2\right) \\ &\stackrel{def}{=} \frac{1}{2}(\mathcal{H}_{BS})_{ij}\hat{\mathbf{r}}_i\hat{\mathbf{r}}_j,\end{aligned} \tag{2.158}$$

where $\hat{\mathbf{r}} = (\hat{x}_1, \hat{p}_1, \hat{x}_2, \hat{p}_2)$. By matching coefficients, we find the 4×4 beamsplitter Hamiltonian matrix,

$$\mathcal{H}_{BS} = \theta\begin{pmatrix}0 & \mathbb{I}_2 \\ \mathbb{I}_2 & 0\end{pmatrix} = \theta\sigma_x \otimes \mathbb{I}_2, \tag{2.159}$$

where $\mathbb{I}_2$ is the 2×2 identity matrix and σ_x is the Pauli x-matrix. Multiplying by the 4×4 symplectic form,

$$\Omega = \mathbb{I}_2 \otimes \Omega_1,$$

we quickly obtain,

$$\Omega\mathcal{H}_{BS} = \theta\sigma_x \otimes \Omega_1. \tag{2.160}$$

To get the corresponding symplectic matrix, we exponentiate the previous matrix [recall equation (2.146)],

$$O_{BS} = \exp\left(\Omega\mathcal{H}_{BS}\right) = \exp\left(\theta\sigma_x \otimes \Omega_1\right). \tag{2.161}$$

Expanding this exponential in a power series and using basic facts about products of Pauli operators and about products of the symplectic form, one finally obtains,

$$S_{BS} = \begin{pmatrix}\cos\theta\mathbb{I}_2 & \sin\theta\Omega_1 \\ \sin\theta\Omega_1 & \cos\theta\mathbb{I}_2.\end{pmatrix} \tag{2.162}$$

In terms of creation and annihilation operators, I note that this corresponds to the following transformation,

$$\hat{a}_1 \to \cos\theta\hat{a}_1 - i\sin\theta\hat{a}_2 \tag{2.163}$$

$$\hat{a}_2 \to \cos\theta\hat{a}_2 - i\sin\theta\hat{a}_1. \tag{2.164}$$

We may actually rid ourselves of the pesky i by introducing a phase in our original beamsplitter Hamiltonian. I leave it as an exercise for the reader to show that,

$$\hat{H}_{BS} = \frac{i}{2}\theta\left(\hat{a}_1^\dagger\hat{a}_2 - \hat{a}_1\hat{a}_2^\dagger\right) \implies O_{BS} = \begin{pmatrix}\cos\theta\mathbb{I}_2 & \sin\theta\mathbb{I}_2 \\ -\sin\theta\mathbb{I}_2 & \cos\theta\mathbb{I}_2\end{pmatrix}, \tag{2.165}$$

which, for instance, corresponds to the following mode transformations,

$$\hat{a}_1 \to \cos\theta\hat{a}_1 + \sin\theta\hat{a}_2 \tag{2.166}$$

$$\hat{a}_2 \to \cos\theta\hat{a}_2 - \sin\theta\hat{a}_1. \tag{2.167}$$

As discussed previously, beamsplitter transformations are passive and thus orthogonal (i.e. $O_{BS}^\intercal O_{BS} = \mathbb{I}_4$), as one can easily check from these equations.

Example 2.2.2 (Two-mode squeezing)**.** *Consider the Hamiltonian operator for two-mode squeezing,*

$$\hat{H}_{SQ} \overset{def}{=} \frac{1}{2i} r \left(\hat{a}_1 \hat{a}_2 e^{i\phi} - \hat{a}_1^\dagger \hat{a}_2^\dagger e^{-i\phi} \right), \tag{2.168}$$

with r being the squeezing parameter/strength and ϕ being the squeezing angle. This can be rewritten in terms of the canonical operators as,

$$\hat{H}_{SQ} = \frac{1}{2} r \Big(\cos\phi(\hat{x}_1 \hat{p}_2 + \hat{p}_1 \hat{x}_2) + \sin\phi(\hat{x}_1 \hat{x}_2 - \hat{p}_1 \hat{p}_2) \Big). \tag{2.169}$$

Going through the same procedure as before, we find the Hamiltonian matrix,

$$\mathcal{H}_{SQ} = r\sigma_x \otimes \left(R_\phi \sigma_x R_\phi^\intercal \right), \tag{2.170}$$

where,

$$R_\phi \overset{def}{=} \begin{pmatrix} \cos\phi/2 & \sin\phi/2 \\ -\sin\phi/2 & \cos\phi/2 \end{pmatrix} \tag{2.171}$$

is a 2×2 rotation matrix. Then, multiplying by the symplectic form, $\Omega = \mathbb{I}_2 \otimes \Omega_1$, we find,

$$\begin{aligned} \Omega\mathcal{H}_{SQ} &= r\sigma_x \otimes \left(\Omega_1 R_\phi \sigma_x R_\phi^\intercal \right) \\ &= r\sigma_x \otimes \left(R_\phi \Omega_1 \sigma_x R_\phi^\intercal \right) \\ &= r\sigma_x \otimes \left(R_\phi \sigma_z R_\phi^\intercal \right), \end{aligned} \tag{2.172}$$

where σ_z is the Pauli z-matrix, I used the fact that R_ϕ preserves the symplectic form (since R_ϕ is a symplectic transformation on the single-mode space), and used $\Omega_1 \sigma_x = \sigma_z$. From this, one finds the symplectic transformation for a generic two-mode squeezer,

$$S_{SQ} = \exp\left(\Omega\mathcal{H}_{SQ}\right) = \begin{pmatrix} \cosh r\mathbb{I}_2 & \sinh r \left(R_\phi \sigma_z R_\phi^\intercal \right) \\ \sinh r \left(R_\phi \sigma_z R_\phi^\intercal \right) & \cosh r\mathbb{I}_2 \end{pmatrix}. \tag{2.173}$$

As example, observe that, for $\phi = 0$, we have the mode transformations,

$$\hat{a}_1 \to \cosh r \hat{a}_1 + \sinh r \hat{a}_2^\dagger \tag{2.174}$$

$$\hat{a}_2 \to \cosh r \hat{a}_2 + \sinh r \hat{a}_1^\dagger. \tag{2.175}$$

Gaussian systems

This section is only pertinent for the analogue gravity application discussed in Chapter 4. I thus streamline the presentation and highlight key definitions and tools which are useful for handling Gaussian systems. I also rely more on heuristic arguments to validate some statements, which would otherwise take us off route for some time if elaborated further.

Gaussian states

We will restrict ourselves to a particular set of quantum systems/states, so-called *Gaussian states*. Physically, we will think of Gaussian states in the following way: Consider a quadratic Hamiltonian, $\hat{H}$, which admits a normal-mode decomposition as,

$$\hat{H} = \sum_{k=1}^{n} \omega_k \left(\hat{x}_k^2 + \hat{p}_k^2 \right), \tag{2.176}$$

where $\{\omega_k\}$ are the natural frequencies of the system and $\{(\hat{x}_k, \hat{p}_k)\}$ are the canonical pairs which naturally decouple the Hamiltonian. And define the (uniform temperature) thermal state for the system, Θ_β, as

$$\Theta_\beta = \frac{\bigotimes_{k=1}^{n} \exp\left(-\beta \hat{H}_{\omega_j}\right)}{\prod_{k=1}^{n} \mathrm{Tr}\left\{ \exp\left(-\beta \hat{H}_{\omega_j}\right) \right\}}, \tag{2.177}$$

where $\{\hat{H}_{\omega_j}\}$ are the set of free oscillator Hamiltonians with corresponding eigenfrequencies $\{\omega_j\}$ and $\beta > 0$ is, effectively, the inverse temperature. In the zero temperature limit ($\beta \to \infty$), this state approaches the ground (vacuum) state for the normal modes; i.e. $\lim_{\beta\to\infty} \Theta_\beta = |0\rangle\langle 0|$, where $|0\rangle\langle 0|$ is the ground state.

We now define *Gaussian states* to be the set of the quantum states which are unitarily related to the above thermal state, by local displacements and symplectic transformations. That is, let ρ_G denote a Gaussian state, then it can be written as

$$\rho_G \stackrel{\text{def}}{=} \left(\hat{D}_{-\boldsymbol{\mu}} \hat{S} \right) \Theta_\beta \left(\hat{S}^\dagger \hat{D}_{-\boldsymbol{\mu}}^\dagger \right), \tag{2.178}$$

with $\hat{D}_{\boldsymbol{\mu}}$ corresponding to a displacement by an amount $\boldsymbol{\mu}$ and $\hat{S}$ corresponding to some symplectic transformation, S. Pure Gaussian states are approached in the zero-temperature limit $\beta \to \infty$.[8]

First and second moments

The moniker of "Gaussian" is usually restricted to systems which can be completely characterized by the first and second moments (means and covariances). This is indeed the case for the Gaussian states defined above, as we will argue in the following. First, consider the decomposition of the thermal state in the Fock space spanned by the normal modes; it is easy to show that,

$$\Theta_\beta = \bigotimes_{k=1}^{n} \left(\left(1 - \mathrm{e}^{-\beta\omega_k}\right) \sum_{m_k=0}^{\infty} \mathrm{e}^{-\beta\omega_k m_k} \left| m \right\rangle\!\left\langle m \right|_k \right), \tag{2.179}$$

[8]Note that the zero-temperature limit leads to $\lim_{\beta\to\infty} \rho_G = \hat{D}_{\boldsymbol{\mu}} \hat{S} \left|0\right\rangle\!\left\langle 0\right| \hat{S}^\dagger \hat{D}_{\boldsymbol{\mu}}^\dagger$; i.e., all pure Gaussian states are generated from the vacuum by local displacements and unitary operations corresponding to symplectic transformations.

where, e.g., $|m\rangle_k$ is the Fock state for the kth mode carrying m quanta. Now consider the vector of canonical operators for the normal modes as $\hat{\mathbf{r}} = (\hat{x}_1, \hat{p}_1, \dots)^\intercal$. It then follows that,

$$\mathrm{Tr}\{\hat{\mathbf{r}}\Theta_\beta\} = 0. \tag{2.180}$$

This observation will be useful in what follows.

The *vector of first moments* of a quantum state, ρ, is generally defined as the expectation value, $\mathrm{Tr}\{\hat{\mathbf{r}}\rho\}$. For a generic Gaussian state, ρ_G, given by equation (2.178), we find,

$$\boldsymbol{\mu} = \mathrm{Tr}\{\hat{\mathbf{r}}\rho_G\}. \tag{2.181}$$

Observe that the first moments completely encode the displacement operator part of ρ_G in equation (2.178).

Proof. We prove the preceding equation. Consider the following set of equalities:

$$\begin{aligned}
\mathrm{Tr}\{\hat{\mathbf{r}}\rho_G\} &= \mathrm{Tr}\Big\{\hat{\mathbf{r}}\left(\hat{D}_{-\boldsymbol{\mu}}\hat{S}\right)\Theta_\beta\left(\hat{S}^\dagger\hat{D}^\dagger_{-\boldsymbol{\mu}}\right)\Big\} \\
&= \mathrm{Tr}\Big\{\left(\hat{S}^\dagger\hat{D}^\dagger_{-\boldsymbol{\mu}}\right)\hat{\mathbf{r}}\left(\hat{D}_{-\boldsymbol{\mu}}\hat{S}\right)\Theta_\beta\Big\} \\
&= \mathrm{Tr}\Big\{\left(\hat{S}^\dagger\hat{D}_{\boldsymbol{\mu}}\right)\hat{\mathbf{r}}\left(\hat{D}^\dagger_{\boldsymbol{\mu}}\hat{S}\right)\Theta_\beta\Big\} \\
&= \mathrm{Tr}\Big\{\hat{S}^\dagger\left(\hat{\mathbf{r}} + \boldsymbol{\mu}\right)\hat{S}\Theta_\beta\Big\} \\
&= \mathrm{Tr}\Big\{\hat{S}^\dagger\hat{\mathbf{r}}\hat{S}\Theta_\beta\Big\} + \mathrm{Tr}\{\boldsymbol{\mu}\Theta_\beta\} \\
&= \mathrm{Tr}\{S\hat{\mathbf{r}}\Theta_\beta\} + \boldsymbol{\mu}\,\mathrm{Tr}\{\Theta_\beta\} \\
&= S\,\mathrm{Tr}\{\hat{\mathbf{r}}\Theta_\beta\} + \boldsymbol{\mu} \\
&= \boldsymbol{\mu}.
\end{aligned}$$

In the first equality, we expanded ρ_G via equation (2.178). In the fourth equality, we used relation (2.154). In the fifth equality, we used linearity of the trace and the fact that $\hat{S}$ is unitary. For final four equalities, we used the symplectic transformation of a canonical operator [equation (2.147)] to pull the symplectic matrix, S, outside of the trace, used the fact that the first moment for a thermal state (or any state diagonal in the Fock basis) is zero, and use the fact that $\mathrm{Tr}\,\Theta_\beta = 1$. □

The second moments of a Gaussian state can likewise be found. Compactly, we encode them into the *covariance matrix*, σ, defined as the following symmetric matrix,

$$\sigma_{ij} \stackrel{\mathrm{def}}{=} \mathrm{Tr}\left(\left\{\hat{\mathbf{r}}_i - \boldsymbol{\mu}_i, \hat{\mathbf{r}}_j - \boldsymbol{\mu}_j\right\}\rho\right), \tag{2.182}$$

where the anti-commutator $\{A, B\} = AB - BA$ was used, and we have subtracted off the first moments. The covariance matrix for a Gaussian state, ρ_G, given by equation (2.178), takes on the generic form,

$$\sigma = S\sigma_\beta S^\intercal. \tag{2.183}$$

Here, σ_β is the covariance matrix for the thermal state, Θ_β, which satisfies,

$$\sigma_\beta = \bigoplus_{k=1}^{n} \nu_k \mathbb{I}_2 \quad \text{with} \quad \nu_k = \frac{1 + \exp(-\beta\omega_k)}{1 - \exp(-\beta\omega_k)} \geq 1. \tag{2.184}$$

Sketch of proof. We outline the computation leading to the above equation. Consider a Gaussian state defined by equation (2.178) and consider the following set of equalities:

$$\begin{aligned}
\sigma_{ij} &= \mathrm{Tr}\left(\left\{\hat{\mathbf{r}}_i - \boldsymbol{\mu}_i, \hat{\mathbf{r}}_j - \boldsymbol{\mu}_j\right\}\rho_G\right) \\
&= \mathrm{Tr}\left(\left\{\hat{\mathbf{r}}_i - \boldsymbol{\mu}_i, \hat{\mathbf{r}}_j - \boldsymbol{\mu}_j\right\}\left(\hat{D}_{-\boldsymbol{\mu}}\hat{S}\right)\Theta_\beta\left(\hat{S}^\dagger\hat{D}^\dagger_{-\boldsymbol{\mu}}\right)\right) \\
&= \mathrm{Tr}\left(\hat{S}^\dagger\{\hat{\mathbf{r}}_i, \hat{\mathbf{r}}_j\}\hat{S}\Theta_\beta\right) \\
&= \mathrm{Tr}\left(\hat{S}^\dagger\left(\hat{\mathbf{r}}_i\hat{\mathbf{r}}_j + \hat{\mathbf{r}}_j\hat{\mathbf{r}}_i\right)\hat{S}\Theta_\beta\right) \\
&= \mathrm{Tr}\left(S_{ik}S_{jl}\left(\hat{\mathbf{r}}_k\hat{\mathbf{r}}_l + \hat{\mathbf{r}}_l\hat{\mathbf{r}}_k\right)\Theta_\beta\right) \\
&= S_{ik}\,\mathrm{Tr}\left(\left(\hat{\mathbf{r}}_k\hat{\mathbf{r}}_l + \hat{\mathbf{r}}_l\hat{\mathbf{r}}_k\right)\Theta_\beta\right)(S^\intercal)_{lj} \\
&= S_{ik}(\sigma_\beta)_{kl}S^\intercal{}_{lj}.
\end{aligned}$$

The jump from the second to third equalities uses the computation for the first moments of the Gaussian state. The remaining equalities use relations for symplectic transformations and a shuffling around of matrices. And for the final equality, the thermal covariance matrix,

$$(\sigma_\beta)_{kl} \overset{\text{def}}{=} \mathrm{Tr}\left(\left(\hat{\mathbf{r}}_k\hat{\mathbf{r}}_l + \hat{\mathbf{r}}_l\hat{\mathbf{r}}_k\right)\Theta_\beta\right), \tag{2.185}$$

was implicitly defined. Thus, $\sigma = S\sigma_\beta S^\intercal$. It now remains to find an explicit expression for σ_β which equates to the one provided in equation (2.184). The remaining details can be found in reference [24]. □

The preceding set of results are significant. Recall the equation for a generic Gaussian state, equation (2.178). This state is determined by (i) a displacement by an amount $\boldsymbol{\mu}$, (ii) a unitary, $\hat{S}$, corresponding to the symplectic transformation, S, and (iii) the thermal state for the normal modes, Θ_β, which is characterized by the inverse temperature, β, and the set of n natural frequencies, $\{\omega_k\}$. What we have effectively shown is that all of these parameters, which define the state ρ_G, are entirely encoded in the vector of first moments (the mean), $\boldsymbol{\mu}$, and the covariance matrix, σ. This is the defining characteristic of a Gaussian state.

A useful identity, which I point out here for reference, is a relationship between the covariance matrix, the first moments, and the average number of particles within the system. From the definition of the covariance matrix, equation (2.182), it follows that

$$\sigma_{ii} = 2\left(\langle\hat{\mathbf{r}}_i^2\rangle - \boldsymbol{\mu}_i^2\right), \tag{2.186}$$

where $\langle\cdot\rangle$ is the expectation value with respect to the quantum state of the system. Relating this equation to equation (2.143), it is easy to show that, for a n-mode quantum state,

$$\langle\hat{n}\rangle = \frac{1}{4}\,\mathrm{Tr}\{\sigma\} + \boldsymbol{\mu}^2 - \frac{1}{2}n. \tag{2.187}$$

Taking a coherent state as an example, we have $\sigma = \mathbb{I}_{2n}$, thus $\mathrm{Tr}\{\sigma\} = 2n$, and $\langle\hat{n}\rangle = \boldsymbol{\mu}^2$, as expected.

As a final note, let me comment on the input-output dynamics for Gaussian systems, which should seem natural at this point. Consider an input Gaussian state, $\rho^{(\text{in})}$, with first and second moments $(\boldsymbol{\mu}^{(\text{in})}, \sigma^{(\text{in})})$ – undergoing unitary evolution under the operator $\hat{S}$, corresponding to a symplectic transformation matrix, S. The corresponding output state is then a Gaussian state given by $\rho^{(\text{out})} = \hat{S}\rho^{(\text{in})}\hat{S}^{\dagger}$ with first and second moments $(\boldsymbol{\mu}^{(\text{out})}, \sigma^{(\text{out})})$, completely determined via the following transformations on the input moments

$$\boldsymbol{\mu}^{(\text{out})} = S\boldsymbol{\mu}^{(\text{in})} \tag{2.188}$$

$$\sigma^{(\text{out})} = S\sigma^{(\text{in})}S^{\intercal}. \tag{2.189}$$

Something similar can be found for displacements, but this just corresponds to shifting the mean of the input (no change to the covariance matrix), i.e., $\boldsymbol{\mu}^{(\text{in})} \to \boldsymbol{\mu}^{(\text{in})} + \mathbf{R}$, where $\mathbf{R}$ is the corresponding displacement vector.

2.3 Photons as information carriers

We take a very brief foray into quantum information science, which has to do with the transmission and processing of information, when that information is encoded in the quantum mechanical degrees of freedom of a system (like e.g. the polarization of single photons). We do not need to know much about the quantum information sciences to understand this thesis, only a few basic elements, such as:

- the basic unit of quantum information is the quantum bit (qubit), which is a generalization of the classical bit,
- one can encode a qubit into the degrees of freedom of a photon,
- and that quantum entanglement is a resource which is useful for a host of tasks, like e.g. quantum teleportation.

We expand upon these notions in the succeeding subsections. In the latter part of this section, we also discuss a measure for quantum entanglement (the logarithmic negativity), which I utilize in Chapter 4 to analyze quantum correlations generated by multi-mode scattering events in the context of analogue gravity.

For generic considerations and thorough discussions about quantum information theory, see Wilde's book on the subject [27] (which I highly recommend). For more focus on quantum-optics and its place in quantum-informatino processing, see Kok and Lovett's book [22].

Flying qubits

The quantum bit, or qubit, is the basic unit of quantum information and is generalization of the classical bit. Whereas the classical bit takes on a determined binary value, either 0 or 1, a qubit can be in a *superposition* of binary values. This is an abstract notion of the basic unit of quantum information, but in reality, to transmit and process this information, one must encode it into some physical, quantum-mechanical system. For quantum communication

tasks, photons are the most natural couriers. Perhaps the most common encoding for photon-mediated quantum-communication is the Fock space spanned by the polarization modes of a single-photon, which is known to be robust against noise in various scenarios. We focus on this encoding here.

As usual, quantum states are defined via the creation and annihilation operators, $\hat{a}^\dagger$ and $\hat{a}$, of the electromagnetic field, which satisfy the commutation relations

$$[\hat{a}_j, \hat{a}_k^\dagger] = \hat{\mathbb{I}}\delta_{jk}, \tag{2.190}$$

where the indices j, k are binary numbers which represent orthogonal polarization modes of the elctromagnetic field, e.g. horizontal H and vertical V. Generally one uses these operators to construct the polarization Fock space spanned by states of the form

$$\frac{(\hat{a}_j^\dagger)^n(\hat{a}_k^\dagger)^m}{\sqrt{n!m!}}\left|0_j, 0_k\right\rangle \stackrel{\text{def}}{=} \left|n_j, m_k\right\rangle, \tag{2.191}$$

where $|0_j\rangle$ is the vacuum state for the jth subspace and $|n_j\rangle$ the n-photon Fock state for the jth subspace, e.g. $|n_j\rangle$ corresponds to n photons with polarization j. Now, label the creation operators for the horizontal and vertical polarization modes as $\hat{a}_H^\dagger$ and $\hat{a}_V^\dagger$. We then define the *qubit space* as the single-photon subspace of the polarization Fock space. A basis for this space is given by the orthonormal single-photon states,

$$|H\rangle \stackrel{\text{def}}{=} |1_H, 0_V\rangle \tag{2.192}$$

$$|V\rangle \stackrel{\text{def}}{=} |0_H, 1_V\rangle, \tag{2.193}$$

which serve as the logical 0 and 1. Any qubit in this space can then be written as

$$|\psi\rangle = \alpha|H\rangle + \beta|V\rangle, \tag{2.194}$$

with $\alpha, \beta \in \mathbb{C}$ and $|\alpha|^2 + |\beta|^2 = 1$. Hence, when we discuss qubits in this thesis, we are physically referring to a single-photon in a superposition of horizontal and vertical polarization modes.

The erasure channel

Quantum communication has to do not only with the encoding of information into quantum mechanical degrees of freedom of a system but also with the transmission of that information through possibly noisy or lossy *quantum channels*. We do not need to know the formal details surrounding the definition of a quantum channel, as it suffices to say that a quantum channel is a generalization of unitary evolution which, for instance, can generally map pure states to mixed states (convex combination of pure states). This is something that does not occur in unitary evolution.

For quantum communication using photons and polarization encoding, the most prevalent form of noise is in the form of pure loss, i.e. a photon either makes it to the receiving end or does not. At the single-photon level, this type of evolution is equivalent to evolution through an *erasure channel*. That is, given an arbitrary qudit (generalization of a qubit to d

dimensions) state, ρ, the evolution of ρ through an erasure channel, $\mathcal{E}_\eta$, is given generically by

$$\mathcal{E}_\eta(\rho) = \eta\rho + (1-\eta)\,|e\rangle\langle e| \tag{2.195}$$

where η is the transmittance of the channel (i.e. the probability that the qubit gets transmitted) and $|e\rangle\langle e|$ is the erasure state, which is some state orthogonal to the basis states of the subspace in which ρ is contained. This evolution can be obtained using the so-called Kraus decomposition of the erasure channel

$$\mathcal{E}_\eta(\rho) = K_1\rho{K_1}^\dagger + \sum_{j=0}^{d-1} K_{1,j}\rho K_{1,j}^\dagger \tag{2.196}$$

with

$$K_1 = \sqrt{\eta}\sum_{j=0}^{d-1}|j\rangle\langle j| \tag{2.197a}$$

$$K_{1,j} = \sqrt{1-\eta}\,|e\rangle\langle j| \tag{2.197b}$$

the Kraus operators of the channel and $\{|j\rangle\}_{j=0}^{d-1}$ the states spanning the qudit subspace in which ρ is contained.

This type of evolution can be put into the previous language of symplectic transformations. Indeed, consider a photon-encoding for the qudit state. Then, the erasure channel physically corresponds to interacting the photon with the vacuum on a beamsplitter, which has a transmittance η, and tracing over the environment modes.

Proof by example. Consider the single-photon qubit state,

$$|\psi\rangle_a = \left(\alpha\hat{a}_H^\dagger + \beta\hat{a}_V^\dagger\right)|0\rangle_a \stackrel{\text{def}}{=} \hat{a}^\dagger\,|0\rangle_a\,,$$

where I have written out the state explicitly in terms of creation operators and have implicitly defined the single-photon annihilation operator, $\hat{a} \stackrel{\text{def}}{=} \alpha^*\hat{a}_H + \beta^*\hat{a}_V\ \forall\ (\alpha,\beta)\in\mathbb{C}$ which satisfy $|\alpha|^2 + |\beta|^2 = 1$. In what follows, we will assume that the erasure channel acts identically on each polarization mode, which justifies this definition. Now let e represent the "environment modes" which interact with the single photon via a beamsplitter interaction which takes,

$$\hat{a} \to \sqrt{\eta}\hat{a} + \sqrt{1-\eta}\hat{e},$$

where η is the probability to transmit through the beamsplitter (i.e. the transmittance) and $\hat{e} \stackrel{\text{def}}{=} \alpha^*\hat{e}_H + \beta^*\hat{e}_V$. Then, taking the initial, pure quantum state as, $|\psi\rangle_a \otimes |0\rangle_e$, with $|0\rangle_e$ the vacuum on the environment, it is easy to show that the quantum state after the beamsplitter is given by,

$$|\psi\rangle_a \otimes |0\rangle_e \to |\Psi\rangle_{ae} = \sqrt{\eta}\,|\psi\rangle_a \otimes |0\rangle_e + \sqrt{1-\eta}\,|0\rangle_a \otimes |\psi\rangle_e\,.$$

Tracing over the environment modes then gives us the output density matrix for the a modes,

$$\mathcal{E}_\eta(|\psi\rangle\langle\psi|) \stackrel{\text{def}}{=} \mathrm{Tr}_e\,|\Psi\rangle\langle\Psi|_{ae} = \eta\,|\psi\rangle\langle\psi|_a + (1-\eta)\,|0\rangle\langle 0|_a\,,$$

which is equivalent to evolution through the erasure channel, with the erasure state given by the vacuum state for the modes. □

One important property about erasure channels is that when you concatenate erasure channels, say $\mathcal{E}_1$ and $\mathcal{E}_2$ with transmittance parameters η_1 and η_2, then one can show that the evolution of a quantum state ρ through the concatenated channel is given by

$$(\mathcal{E}_1 \circ \mathcal{E}_2)(\rho) = \eta_1\eta_2\rho + (1 - \eta_1\eta_2)\,|e\rangle\langle e|\,. \tag{2.198}$$

In which case, one could prescribe the transmittance $\eta_{12} = \eta_1\eta_2$ to the single erasure channel $\mathcal{E}_{12} = \mathcal{E}_1 \circ \mathcal{E}_2$. That is, the concatenation of erasure channels is again an erasure channel, with transmittance given by the product of the transmittances of the concatenated channels. This is useful to know, and I will implicitly use it in Chapter 3.

Another important property to know is what happens when one sends a bipartite (i.e. a two-qudit) state ρ_{AB} through two erasure channels $\mathcal{E}_A$ and $\mathcal{E}_A$, with individual transmittance values η_A and η_B, acting independently on qudit subsystems A and B. Using the Kraus representation for the independent channels, it is straightforward to show that,

$$\begin{aligned}\mathcal{E}_A \otimes \mathcal{E}_B(\rho) = \eta_A\eta_B\rho_{AB} + \eta_A(1-\eta_B)\sigma_A \otimes |e\rangle\langle e|_B \\ + (1-\eta_A)\eta_B\,|e\rangle\langle e|_A \otimes \tau_B + (1-\eta_A)(1-\eta_B)\,|e\rangle\langle e|_A \otimes |e\rangle\langle e|_B\end{aligned} \tag{2.199}$$

where $\sigma_A = \mathrm{Tr}_A(\rho_{AB})$ is the reduced state for subsystem A (and likewise for τ_B).

A physical interpretation of the bipartite channel evolution follows. Let ρ represent a two-photon entangled state [see e.g. equation (2.201)] and A and B correspond to receiving parties Alice and Bob. With probability $\eta_A\eta_B$, the entangled photon-pair is successfully transmitted to Alice and Bob. With probability $\eta_A(1-\eta_B)$, Alice receives a photon in the quantum state σ, but Bob's was lost in transmission and only vacuum remains (and vice versa for τ). Finally with probability $(1-\eta_A)(1-\eta_B)$, Alice and Bob receive nothing, as the photon pair was lost to the environment.

Quantum entanglement

Quantum entanglement is a tricky business, which, on the one hand, has induced heated philosophical debates about its place in our physical reality, yet, on the other hand, has led to intriguing operational interpretations and meaningful uses. For instance, pre-shared, high-fidelity quantum entanglement is crucial for many quantum communication tasks, e.g. quantum teleportation, and forms the "backbone" of futuristic quantum networks. Thus, understanding and unambiguously quantifying entanglement, and distinguishing it from classical resources, is important. Here, I provide brief discussions on quantum entanglement in order to gain some minimal understanding of entanglement and to provide only what is necessary to understand the part it plays in the applications of Chapters 3 and 4.

Refresher on separability and entanglement

Recall the definition of entanglement, which is often stated in the following contrary manner: Consider a quantum state, Ψ_{AB}, with subsystems A and B. The state, Ψ_{AB}, is separable across this partition if it can be written as a convex combination of tensor-product states, i.e.

$$\Psi_{AB} = \sum_n p_n \rho_A^{(n)} \otimes \tau_B^{(n)}, \tag{2.200}$$

where p_n is some probability distribution for the random variable n, and ρ and τ are genuine density matrices on the subsystems A and B. Entangled states are then quantum states which cannot be written in this fashion.

The general assumption of "convex combination of tensor-product states" simply states that we allow for probabilistic mixtures of separable states. Physically, one may think that a referee sends Alice and Bob a separable state $\rho_A^{(n)} \otimes \tau_B^{(n)}$ according to some underlying probability distribution p_n that only the referee knows. This generic prescription still allows for *classical* correlations. For, if Alice "measures her state" to be $\rho^{(N)}$, where N is a realization of the random variable n, then it is immediate that Bob has the state $\tau^{(N)}$, irrespective of any further measurements or communication that Alice or Bob may do. The correlations between Alice's and Bob's states are, however, "hidden" within the underlying probability distribution, p_n. Quantum entanglement is something intrinsically different. I dare tread further.

Bell states

The simplest example of a quantum entangled system is an entangled pair of qubits. In terms of photons, this corresponds to a pair of single photons, which share correlations in e.g. their polarization degree of freedom. The best example in this context is one of the *Bell states*, such as

$$\left|\Phi^+\right\rangle_{AB} = \frac{1}{\sqrt{2}} \left(|H,H\rangle + |V,V\rangle\right)_{AB}, \tag{2.201}$$

where the subscripts, A and B, distinguish the different photons. We see that if one of the photons, say A, is measured with horizontal polarization, then the partner photon, B, will be measured with horizontal polarization with certainty and vice versa. The same occurs when the measurement outcome is vertical polarization. However, the state of the photons, whether they have horizontal or vertical polarization, is altogether indeterminate. Furthermore, one can show that this state is not separable (but is entangled) in the sense of equation (2.200). Indeed, all of the Bell states, $\{\Phi^\pm, \Psi^\pm\}$ (which, by the way, serve as a basis for the two-qubit space), share this property. For completeness, I write out the Bell states here,

$$\begin{aligned}
\left|\Phi^\pm\right\rangle &= \frac{1}{\sqrt{2}} \left(|H,H\rangle \pm |V,V\rangle\right) \\
\left|\Psi^\pm\right\rangle &= \frac{1}{\sqrt{2}} \left(|H,V\rangle \pm |V,H\rangle\right).
\end{aligned}$$

The Bell states, and quantum entanglement in general, plays a pivotal role in many quantum communication and quantum computational tasks; so much so, that there exists a basic unit of entanglement, the entangled bit, or ebit. One Bell pair (any one of them) is then equivalent to one ebit.

PPT criterion

We discuss a popular criterion, the PPT (or Peres-Horodecki) criterion, which is a necessary criterion that a generic separable state must satisfy (see, e.g., [28] for details). This criterion

allows one to unambiguously distinguish separable (classical) states from quantum entangled states, at least in certain cases.

Let us first recall the properties that a bona fide density operator must satisfy:

1. $\mathrm{Tr}\,\rho = 1$ (unit trace)
2. $\rho^\dagger = \rho$ (Hermitian)
3. $\langle\varphi|\rho|\varphi\rangle \geq 0 \;\; \forall\, \varphi$ (non-negative)

Observe that the property of non-negativity is a statement about the non-negativity of the eigenvalues of the density matrix, ρ. The PPT criterion exploits this property in the following way. It states that: if a quantum state ρ is separable across a bipartition (A, B), then the partially transposed state, $\rho_{AB}^{\intercal_B}$ (the partial transposition could be done on the either subsystem, A or B), has non-negative eigenvalues and thus satisfies property 3 above. This condition is *necessary* for separability, which is easy to show.

Proof. We argue that satisfaction of the PPT criterion is necessary for separability. Consider that a quantum state is separable, and can thus be written as in equation (2.200). Then, the partial transposition with respect to the system B gives,

$$\tilde{\Psi}_{AB} \stackrel{\text{def}}{=} \Psi_{AB}^{\intercal_B} = \sum_n p_n \rho_A^{(n)} \otimes (\tau_B^{(n)})^\intercal, \tag{2.202}$$

where $(\cdot)^\intercal$ denotes the full transposition. Note, however, that the full transposition of a quantum state gives back a bona fide (though generally different) quantum state, satisfying the three properties above. Thus, the partially transposed matrix, $\tilde{\Psi}$, is a bona fide quantum state and is thus non-negative. □

It follows that violation of the PPT criterion is sufficient for entanglement. Bear in mind, however, that violation of the PPT is only necessary and sufficient in particular cases. As example, for Gaussian systems, violation of the PPT criterion is necessary and sufficient for entanglement given that the partial transposition is taken across a 1 vs. n mode bipartition of a (n+1)-mode system.

Logarithmic negativity

The logarithmic negativity (or *log-negativity* for short) is an easily computable entanglement measure, which quantifies the violation of the PPT criterion. It as an entanglement monotone, which is to say that it does not increase under local operations and classical communications [29, 30]. Physically, the log-negativity is an upper bound to the amount of ebits which can be extracted from a quantum state via some distillation process (though, this bound is not tight; see [31]). It is defined by the following: Let ρ be a genuine density matrix, and let us take the partial transpose with respect to some subsystem B. The log-negativity is then given as,

$$E_{\mathcal{N}}(\rho) \stackrel{\text{def}}{=} \log_2 \|\rho^{\intercal_B}\|_1, \tag{2.203}$$

where $\|A\|_1 = \mathrm{Tr}\left(\sqrt{AA^\dagger}\right)$ is the trace norm of the operator A and is, effectively, the sum of the absolute eigenvalues of A.

To justify that this measure is related to PPT, recall that the non-negative property of a quantum state (property 3) is contingent on the positivity of its eigenvalues, and that the PPT criterion is contingent on this as well (violation of the PPT criterion is equivalent to violation of property 3). Also note that the trace of a partially transposed density matrix, which is just the sum of its eigenvalues, is one, as partial transposition does not change the trace of an operator. Therefore, the violation of the PPT criterion, which implies that at least one of the eigenvalues of the partially transposed density matrix is negative, also implies that the sum of the absolute values of its eigenvalues (i.e. its trace norm) is greater than one. Thus, the log-negativity of a quantum state which violates the PPT criterion is necessarily greater than zero. We therefore see that a non-zero value of the log-negativity is in one-to-one correspondence with the violation of the PPT criterion.

As an example, it is easy to show that the Bell states, $\{\Phi^\pm, \Psi^\pm\}$, all have $E_\mathcal{N} = 1$ (i.e. 1 entangled bit can be distilled from them). An interesting extension of this example is the Werner state,

$$\rho_W(\Phi^+) = \frac{4}{3}(F - 1/4)\Phi^+ + \frac{4}{3}(1 - F)\pi \otimes \pi, \tag{2.204}$$

where Φ^+ is the target state, $\pi = \mathbb{I}/2$ is the maximally mixed state, and $F = \langle\Phi^+|\rho_W|\Phi^+\rangle$ is the fidelity of the Werner state with respect to the target. The physical interpretation here is that ρ_W is approximately a Bell-state but with some inherent "white noise" ($\pi \otimes \pi$) coming from, e.g., background photons etc. One can show that the log-negativity of the Werner state is non-zero if and only if the fidelity, F, is above $1/2$. This fidelity bound plays a practical role in quantum communication and quantum networks, in the form of entanglement purification [32, 33].

Log-negativity for Gaussian states: Recall that, Gaussian states are completely determined by their covariance matrix σ. One may then ask: how does the partial transposition of a Gaussian state translate to its covariance matrix? The answer is quite simple. One can show that (see Chapter 7 of [24]) partial transposition of a (n+m)-mode Gaussian state, ρ_G, with covariance matrix, σ, corresponds to the following transformation on the covariance matrix,

$$\begin{gathered} \sigma \quad \longrightarrow \quad \tilde{\sigma} = T\sigma T, \\ \text{where} \quad T = \mathbb{I}_{2n} \oplus \Sigma_m \quad \text{and} \quad \Sigma_m = \mathbb{I}_m \otimes \sigma_z, \end{gathered} \tag{2.205}$$

with σ_z being the Pauli-z matrix and the partial transposition has been done on the last m modes. Furthermore, one can compute the log-negativity for a generic Gaussian state, which goes as (see Chapter 7 of [24] for details)

$$E_\mathcal{N}(\rho_G) = \sum_{j=1}^{n+m} \max\left(0, -\log_2 \tilde{\nu}_j\right), \tag{2.206}$$

where $\{\tilde{\nu}_j\}$ are the symplectic eigenvalues of the partially transposed covariance matrix, $\tilde{\sigma}$. Recall the generic condition that the symplectic eigenvalues for a bona fide Gaussian state

must obey, $\nu_k \geq 1$ (again, consult [24]). Thus, violation of the PPT criterion, i.e. having a non-zero value for the log-negativity, corresponds to having at least one $\tilde{\nu}_j < 1$. For a two-mode Gaussian state, there exists only two distinct symplectic eigenvalues, $\nu_\pm$, where $\nu_- \leq \nu_+$. Thus, for two-mode Gaussian states, equation (2.206) reduces to,

$$E_{\mathcal{N}}(\rho_G) = \max\left(0, -\log_2 \tilde{\nu}_-\right), \tag{2.207}$$

where $\tilde{\nu}_-$ is the smallest symplectic eigenvalue of the partially transposed, two-mode covariance matrix, $\tilde{\sigma}$.

CHAPTER 3. AN APPLICATION: SPACE-BASED ENTANGLEMENT DISTRIBUTION

This chapter is based off the work in [1][1] and follows that presentation closely, with only minor changes made for the purpose of increased coherency. The following analyses corresponds to a real-world application of quantum-optical technologies and principles of quantum information theory, at a not-too-sophisticated theoretical level. To comprehend this chapter, it suffices to have a minimal understanding of the basic elements presented in Section 2.3 (as well as some Newtonian mechanics).

3.1 Introduction

One of the most remarkable applications of quantum mechanics is the ability to perform secure communication via quantum-key distribution (QKD) [34, 35, 36, 37]. While current global communication systems rely on computational security and are breakable with a quantum computer [38, 39, 40], QKD offers, in principle, unconditional (information-theoretic) security even against adversaries with a quantum computer. With several metropolitan-scale QKD systems already in place [41, 42, 43, 44, 45, 46, 47, 48], and with the development of quantum computers proceeding at a steady pace [49, 50, 51], the time is right to begin transitioning to a global quantum communications network before full-scale quantum computers render current communication systems defenseless [52, 53, 54]. In addition to QKD, a global quantum communications network, or quantum internet [15, 55, 56, 57, 16], would allow for the execution of other quantum-information-processing tasks, such as quantum teleportation [58, 59], quantum clock synchronization [60, 61, 62], distributed quantum computation [63], and distributed quantum metrology and sensing [64, 65, 66].

Building the quantum internet is a major experimental challenge. All of the aforementioned tasks make use of shared entanglement between distant locations on the earth, which is typically distributed using single-photonic qubits sent through either the atmosphere or optical fibers. These schemes require reliable single-photon sources, quantum memories with high coherence times, and quantum gate operations with low error. It is well known that optical signals transmitted through either the atmosphere or optical fibers undergo an exponential decrease in the transmission success probability with distance [67, 68]. Quantum repeaters [69, 70, 71] have been proposed to overcome this exponential loss by dividing the transmission line into smaller segments along which errors and loss can be corrected using entanglement swapping [58, 72] and entanglement purification [73, 74, 75]. Several theoretical proposals for quantum repeater schemes have been made (see Refs. [71, 76, 77] and references therein); however, many of these proposals have resource requirements that are currently unattainable. Furthermore, experimental demonstrations performed so far have been limited [78, 79, 80] and do not scale to the distances needed to realize a global-scale quantum internet.

Satellites have been recognized as one of the best methods for achieving global-scale quantum communication with current or near-term resources [86, 87, 88, 55, 89, 90]. Using

[1]Reference [1] is publicly available through the journal *npj Quantum Information* under a creative commons license.

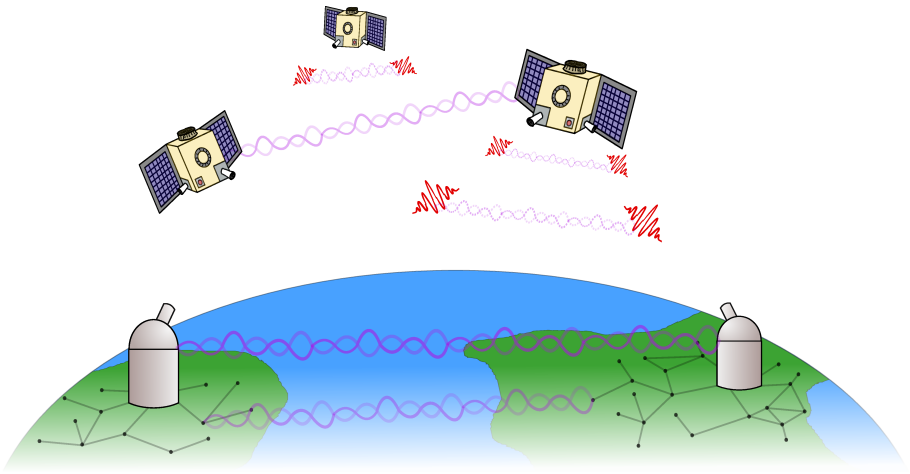

Figure 3.1: A hybrid global quantum communications network. A satellite constellation distributes entangled photon pairs (red wave packets; entanglement depicted by wavy lines) to distant ground stations (observatories) that host multimode quantum memories for storage [81, 82, 83]. These stations act as hubs that connect to local nodes (black dots) via fiber-optic or atmospheric links. Using these nearest-neighbor entangled links, via entanglement swapping, two distant nodes can share entanglement. Note that this architecture can support inter-satellite entanglement links as well, which is useful for exploring fundamental physics [84], and for forming an international time standard [85].

satellites is advantageous due to the fact that the majority of the optical path traversed by an entangled photon pair is in free space, resulting in lower loss compared to ground-based entanglement distribution over atmospheric or fiber-optic links. Satellites can also be used to implement long-distance QKD with untrusted nodes, which is missing from most current implementations of long-distance QKD due to the lack of a quantum repeater. A satellite-based approach also allows for the possibility to use quantum strategies for tasks such as establishing a robust and secure international time scale via a quantum network of clocks [85], extending the baseline of telescopes for improved astronomical imaging [91, 92, 93], and exploring fundamental physics [94, 84].

Several proposals for satellite-based quantum networks have been made that use satellite-to-ground transmission, ground-to-satellite transmission, or both [86, 95, 96, 97, 98, 99, 100, 89, 90, 101, 102, 103]. Recent experiments [99, 104, 14, 105, 106, 107, 13, 108] (see also Ref. [109] for a review) between a handful of nodes opens up the possibility of building a global-scale quantum internet using satellites. As shown in Fig. 3.1, this means having a constellation of orbiting satellites that transmit either bipartite or multipartite entanglement to ground stations. These ground stations can act as hubs that then distribute entanglement to neighboring ground stations via short ground-based links. In order to successfully implement such a global-scale satellite-based quantum internet, many factors must be taken into account, such as economics, current technology, resource availability, and performance requirements. Ideally, the satellite network should have continuous global coverage and provide entanglement on demand at a reasonably high rate between any two distant points on earth. Given this performance requirement, important questions related to economics and

resources arise, such as: How many satellites are needed for continuous global coverage? At what altitude should the satellites be placed? What entanglement-distribution rates are possible between any points on earth, and how do these rates compare to those that can be achieved using ground-based quantum repeater setups?

In this work, we address these questions by analyzing a global-scale quantum internet architecture in which satellites arranged in a constellation of polar orbits (see Fig. 3.2) act as entanglement sources that distribute entangled photon pairs to ground stations. The nearest-neighbor entangled links can then be extended via entanglement swapping to obtain shared entanglement over longer distances. We start by determining the required number of satellites for such a network to have continuous global coverage. Since satellites are a costly resource, continuous global coverage should be achieved with as few satellites as possible. To that end, our first contribution is to define a figure of merit that allows us to investigate the trade-off between the number of satellites, their altitude, the average loss over a 24-hour period, and the average entanglement-distribution rates. By running simulations in order to optimize our figure of merit, we obtain one of our main results, which is the optimal number of satellites needed for continuous global coverage, as well as the optimal altitude at which the satellites should be placed such that the average loss is below a certain threshold. We then compare the resulting entanglement-distribution rates to those obtained via a ground-based entanglement distribution scheme assisted by quantum repeaters. This leads to another key result of our work, which is that the satellite-based scheme (without quantum repeaters) can outperform ground-based quantum repeater schemes in certain cases. We also consider entanglement distribution to major global cities over intercontinental distances. The key result here is that, with a constellation of 400 satellites, entanglement distribution at a reasonably high rate is not possible beyond approximately 7500 km.

We remark that our approach is similar to the approach taken in Ref. [98], in which ground stations are placed only on the equator and there is a single ring of satellites in an equatorial orbit around the earth. Our work goes beyond this by considering a genuine network scenario in which multiple ground stations are placed arbitrarily on the earth and there is a constellation of satellites in polar rather than equatorial orbits, as shown in Fig. 3.2. Furthermore, while prior work has considered satellite constellations for entanglement distribution [103, 110], to our knowledge, the type of dynamic quantum network simulation with satellite constellations that we consider, along with optimization over different constellation configurations, has not been previously studied.

We expect the results of this work to serve as a guide for building a global-scale quantum internet, both in terms of the number of satellites needed as well as the expected performance of the network. In particular, our results comparing satellite-based entanglement distribution to ground-based repeater-assisted entanglement distribution suggest that, at least in the near term, satellites are indeed the most viable approach to obtaining a global-scale quantum internet.

3.2 Network architecture

Our proposed satellite network architecture is illustrated in Fig. 3.2. We consider N_R equally spaced rings of satellites in polar orbits. We allow for N_S equally-spaced satellites in each ring, so that there are $N_R N_S$ satellites in total, all of which are at the same altitude h. This

Figure 3.2: Our proposed satellite-based quantum network. We allow for N_R equally-spaced rings of satellites. Within each ring, we allow for N_S satellites in polar orbits.

type of satellite constellation falls into the general class of Walker star constellations [111], and we consider it mainly for its simplicity, but also because this constellation is similar to the Iridium communications-satellite constellation [112, 113]. Prior works have examined various other types of satellite constellations for the purpose of continuous global coverage [114, 111, 115, 116]. The recent Starlink constellation [117] is also being used to provide a global satellite-based internet service. Investigations of these other satellite constellation types, and comparisons between them in the context of a global quantum internet, is an interesting direction for future work.

The satellites act as source stations that transmit pairs of entangled photons to line-of-sight ground stations for the purpose of establishing elementary entanglement links. The ground stations can act as quantum repeaters in this scheme—performing entanglement purification and entanglement swapping once the elementary links have been established. In this way, we execute long-distance entanglement distribution between ground stations. Note that we could alternatively use the satellites as quantum repeaters [118, 119], which would require uplinks. It has been shown in, e.g., Ref. [97], that uplinks are more lossy and lead to lower key rates for QKD. For this reason, we consider downlinks only. The photon sources on the satellites produce polarization-entangled photon pairs. State-of-the-art sources of entangled photons are capable of producing polarization-entangled photons on a chip with a fidelity up to 0.97 [120, 121, 122, 123].

3.3 Overview of simulations

We obtain our results by running several entanglement distribution simulations using the satellite network architecture illustrated in Fig. 3.2. We consider as our baseline requirement

that a satellite network should provide continuous coverage to two ground stations located on the equator. We thus start by running a 24-hour simulation with two ground stations at the equator separated by distances d between 100 km and 5000 km, and satellite configurations ranging from 20 to 400 satellites at altitudes between 500 km and 10000 km. We choose ground distances starting from 100 km because 100 km is roughly the longest distance at which ground-based entanglement distribution can be successfully performed at a reasonable rate without quantum repeaters; see, e.g., Refs. [124, 125, 126, 127]. Our choice of satellite altitudes encompasses both low earth orbits and medium earth orbits, which are the orbits currently being used for most satellite communications systems [113, 117].

A satellite configuration is given by the number N_R of satellite rings, the number N_S of satellites per ring, and the altitude h of the satellites. Our requirement of continuous coverage means that both ground stations must be simultaneously in view of a satellite at all times. We also impose an additional requirement that, even when in view of both ground stations, the total transmission loss between a satellite and the ground station pair should not exceed 90 dB, in order to keep ebit rates above 1 Hz. Note that, based on the satellite constellations that we consider here, two ground stations at the equator is the worst-case scenario, in the sense that two ground stations at higher or lower latitudes will always have less satellite-to-ground loss on average (we show this in Fig. 3.6 below).

For all of our simulations, we take into account attenuation due to the atmosphere (see subsection just below). However, we assume clear skies, hence no rain, haze, or cloud coverage in any area. Including these extra elements would introduce extra attenuation factors (see, e.g., Ref. [68, Section 2.1.1.4] and Refs. [128, 129]), which would increase the overall satellite-to-ground transmission loss. See Refs. [110, 130] for an analysis of satellite-to-ground quantum key distribution in a localized area that incorporates local weather conditions. We also point out that, especially in the daytime, background photons (e.g., from the sun) can reduce the fidelity of the distributed entangled pairs, because the receiver will collect those background photons in addition to the signal photons from the entanglement source. This source of background photons is perhaps the most difficult obstacle to continuous global coverage. Timing information, as well as information about the spectral and spatial profile of the signal, can help reduce the noise via filtering, but only to a certain extent (see, e.g., Refs. [104, 131]). Furthermore, because the probability to transmit single photons from satellite to ground is quite low, the communicating parties must ensure that the probability to collect background photons is even lower in order to ensure a high signal-to-noise ratio (SNR), and thus a high fidelity for the received quantum state. In Appendix A, we show how the fidelity of the transmitted states is affected by spurious background photons.

Loss model

In the absence of spurious background photons, the transmission of photons from satellites to ground stations is modeled well by a bosonic pure-loss channel with transmittance η_{sg} [24]. For single-photon polarization qubits, transmission through the pure-loss channel corresponds to an erasure channel (see Section 2.3 and reference [132]). That is, given a single-photon polarization density matrix ρ, the evolution of ρ is given as

$$\rho \mapsto \eta_{\text{sg}}\rho + (1-\eta_{\text{sg}})\,|\text{vac}\rangle\langle\text{vac}| \tag{3.1}$$

Table 3.1: Parameters used in the modeling of loss from satellites to ground stations.

Parameter	Definition	Value
r	Receiving aperture radius	0.75 m
w_0	Initial beam waist	2.5 cm
λ	Wavelength of satellite-to-ground signals	810 nm
$\eta_{\text{atm}}^{\text{zen}}$	Atmospheric transmittance at zenith	0.5 at 810 nm [97]

where $|\text{vac}\rangle\langle\text{vac}|$ is the vacuum state. Hence, with probability η_{sg}, the qubit is successfully transmitted and with probability $1-\eta_{\text{sg}}$ the qubit is lost. For the transmission of an entangled photon-pair, let $\eta_{\text{sg}}^{(1)}$ and $\eta_{\text{sg}}^{(2)}$ be the transmittances of the two pure-loss channels. Then, with probability $\eta_{\text{sg}}^{(1)}\eta_{\text{sg}}^{(2)}$, both qubits are successfully transmitted and with probability $1-\eta_{\text{sg}}^{(1)}\eta_{\text{sg}}^{(2)}$ at least one of the qubits is lost [133].

The transmittance η_{sg} generally depends on atmospheric conditions (such as turbulence and weather conditions) and on orbital parameters (such as altitude and zenith angle) [128, 134, 129]. In general, we can decompose η_{sg} as

$$\eta_{\text{sg}} = \eta_{\text{fs}}\eta_{\text{atm}} \tag{3.2}$$

where η_{fs} is the free-space transmittance and η_{atm} is the atmospheric transmittance. Free-space loss occurs due to diffraction (i.e., beam broadening) over the channel and due to the use of finite-sized apertures at the receiving end. These effects cause η_{fs} to scale as the inverse-distance squared in the far-field regime. Atmospheric loss occurs due to absorption and scattering in the atmosphere and scales exponentially with distance as a result of the Beer-Lambert law [135, 136, 68]. However, since atmospheric absorption is relevant only in a layer of thickness 10-20 km above the earth's surface [68], free-space diffraction is the main source of loss in space-based quantum communication. In order to characterize the free-space and atmospheric transmittances with simple analytic expressions, we ignore turbulence-induced effects in the lower atmosphere, such as beam profile distortion, beam broadening (prominent for uplink communication [68, 97]), and beam wandering (see, e.g., Ref. [134]). Note that turbulence effects can be corrected using classical adaptive optics [68]. We also ignore the inhomogeneous density profile of the atmosphere, which can lead to path elongation effects at large zenith angles. A comprehensive analysis of loss can be found in Refs. [136, 134].

Consider the lowest-order Gaussian spatial mode for an optical beam traveling a distance L between the sender and receiver, with a circular receiving aperture of radius r. Then, the

free-space transmittance η_{fs} is given by [67]

$$\eta_{\text{fs}}(L) = 1 - \exp\left(-\frac{2r^2}{w(L)^2}\right). \tag{3.3}$$

where

$$w(L) \stackrel{\text{def}}{=} w_0\sqrt{1 + \left(\frac{L}{L_R}\right)^2} \tag{3.4}$$

is the beam waist at a distance L from the focal region ($L = 0$), $L_R \stackrel{\text{def}}{=} \pi w_0^2 \lambda^{-1}$ is the Rayleigh range, λ is the wavelength of the optical mode, and w_0 is the initial beam-waist radius.

We model the atmosphere as a homogeneous absorptive layer of finite thickness in order to characterize η_{atm}. Uniformity of the atmospheric layer then implies uniform absorption (at a given wavelength), such that η_{atm} depends only on the optical path traversed through the atmosphere. Under these assumptions, and using the Beer-Lambert law [135], for small zenith angles we have that

$$\eta_{\text{atm}}(L, h) = \begin{cases} (\eta_{\text{atm}}^{\text{zen}})^{\sec\zeta}, & \text{if } -\frac{\pi}{2} < \zeta < \frac{\pi}{2}, \\ 0, & \text{if } |\zeta| \geq \frac{\pi}{2}, \end{cases} \tag{3.5}$$

with $\eta_{\text{atm}}^{\text{zen}}$ the transmittance at zenith ($\zeta = 0$). For $|\zeta| > \frac{\pi}{2}$, we set $\eta_{\text{atm}} = 0$, because the satellite is over the horizon and thus out of sight. The zenith angle ζ is given by

$$\cos\zeta = \frac{h}{L} - \frac{1}{2}\frac{L^2 - h^2}{R_E L} \tag{3.6}$$

for a circular orbit of altitude h, with $R_E \approx 6378$ km being the earth's radius.

Note that the model of atmospheric transmittance given by Eq. (3.5) and Eq. (3.6) is quite accurate for small zenith angles [68]. However, for space-based quantum communication at or near the horizon (i.e., for $\zeta = \pm\pi/2$), more exact methods relying on the standard atmospheric model must be used [134]. In practice, it makes sense to set $\eta_{\text{atm}} = 0$ at large zenith angles, effectively severing the quantum channel, because the loss will typically be too high for the link to be practically useful.

To summarize, the following parameters characterize the total loss $\eta_{\text{sg}} = \eta_{\text{fs}}\eta_{\text{atm}}$: the initial beam waist w_0, the receiving aperture radius r, the wavelength λ of the satellite-to-ground signals, and the atmospheric transmittance $\eta_{\text{atm}}^{\text{zen}}$ at zenith. See Table 3.1 for the values that we take for these parameters in our simulations.

Using the values in Table 3.1, we plot in Fig. 3.3 (bottom) the total transmittance as a function of the ground distance d between two ground stations with a satellite at the midpoint; see Fig. 3.3 (top). We observe that for larger ground separations the total transmittance η_{sg}^2 is actually larger for a higher altitude than for a lower altitude; for example, beyond approximately $d = 1600$ km the transmittance for $h = 1000$ km is larger than for $h = 500$ km. We also observe that there are altitudes at which the transmittance is maximal. Intuitively, beyond the maximum point, the atmospheric contribution to the loss is less dominant, while below the maximum (i.e., for lower altitudes) the atmosphere is the dominant source of loss. This feature is unique for point-to-multipoint optical transmission from satellite to ground.

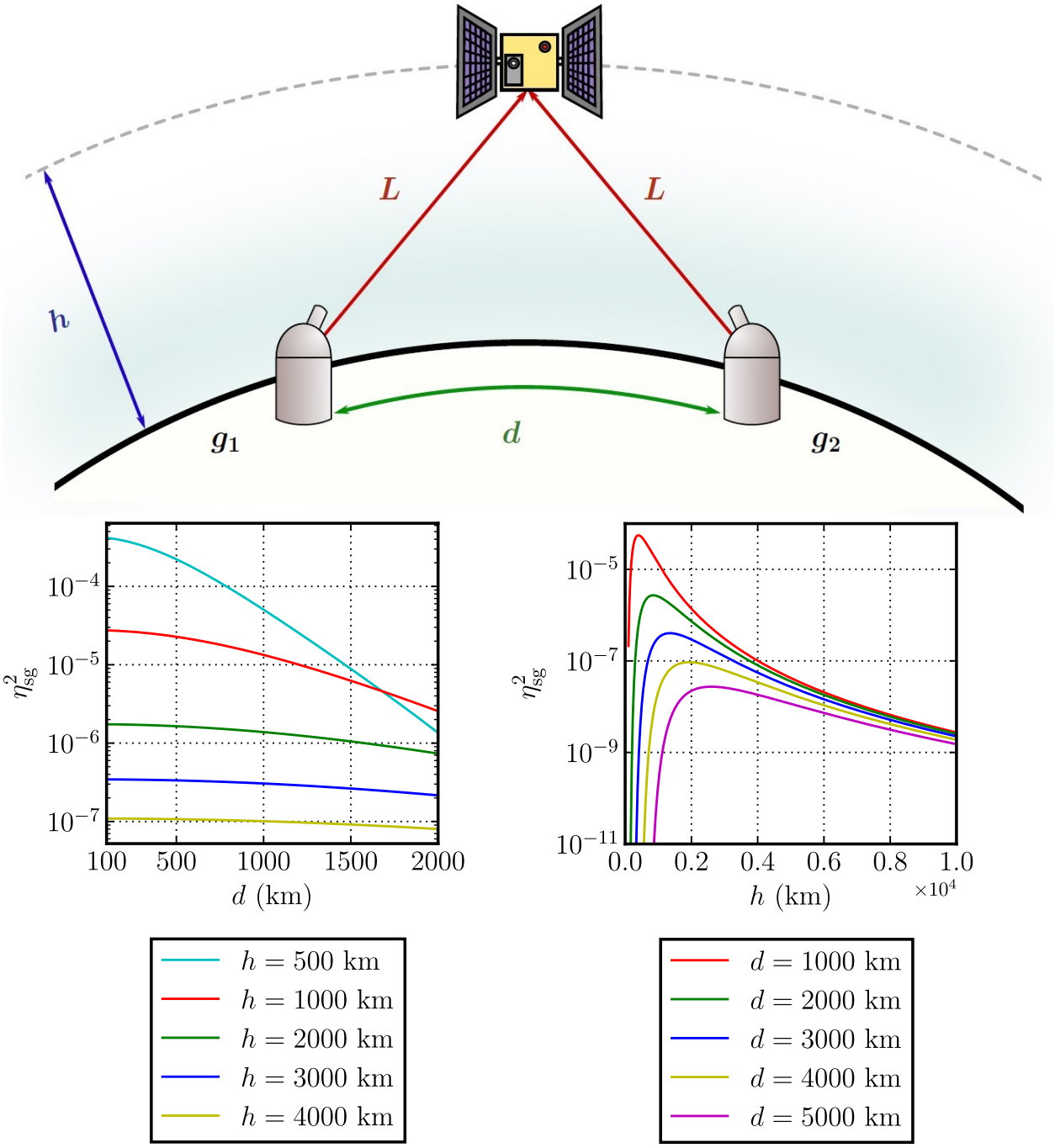

Figure 3.3: Optical satellite-to-ground transmission. The total transmittance is given by $\eta_{\text{sg}} = \eta_{\text{fs}}\eta_{\text{atm}}$, where the free-space transmittance η_{fs} given by Eq. (3.3), and the atmospheric transmittance η_{atm} is given by Eq. (3.5). (Top) Two ground stations g_1 and g_2 are separated by a distance d with a satellite at altitude h at the midpoint. Both ground stations are the same distance L away from the satellite, so that the total transmittance for two-qubit entanglement transmission (one qubit to each ground station) is η_{sg}^2. (Bottom) Plots of the transmittance η_{sg}^2 as a function of d and h.

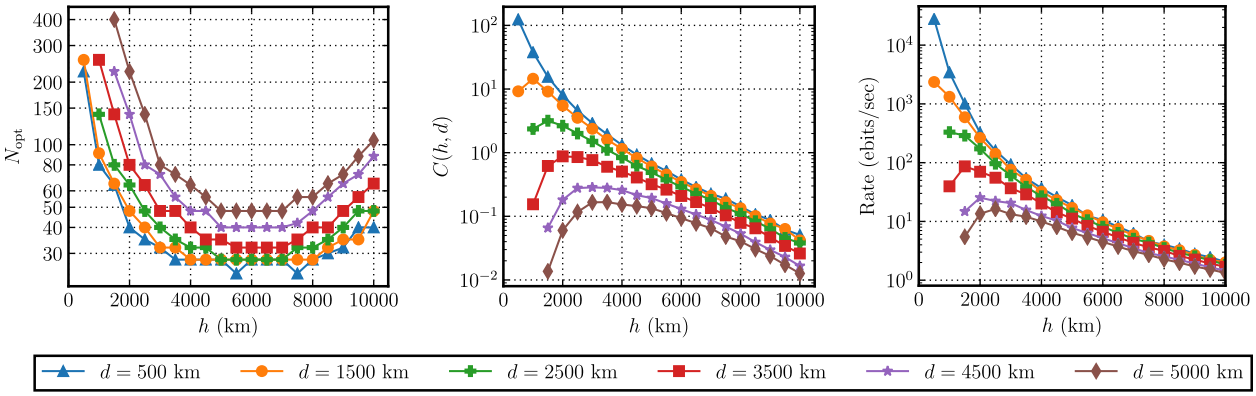

Figure 3.4: Simulation results for two ground stations at the equator separated by a distance d. (Left) Optimal number $N_{\text{opt}}(h, d)$ of satellites for continuous 24-hour coverage. (Center) Figure of merit in Eq. (3.10) in units of ebits per second per satellite. Satellite configurations corresponding to the maxima of the curves are shown in Table 3.2. (Right) Entanglement-distribution rates corresponding to the points in the plot in the central panel. We assume a source rate of $R_{\text{source}} = 10^9$ ebits per second [137].

We introduce dynamics into the situation by parameterizing the link distance, L, as a function of time, using standard Newtonian mechanics. An example of the time parameterized loss channel is shown in Figure 3.5.

Optimal network configurations for global coverage

Given two ground stations separated by a distance d and situated at the equator, along with a particular satellite constellation defined by (N_R, N_S, h), as described above, how do we evaluate the performance of the given satellite constellation? Since satellites are currently an expensive resource, we would like to have as few satellites as possible in the network while still maintaining complete and continuous coverage. We could therefore take as our figure of merit the total number of satellites in the network. Specifically, given an altitude h of the satellites and distance d between the two ground stations, we define $N_{\text{opt}}(h, d)$ to be the minimum total number of satellites needed to have continuous 24-hour coverage for the two ground stations. We could then minimize $N_{\text{opt}}(h, d)$ with respect to altitudes. On the other hand, we also want high entanglement distribution rates. We let $\overline{R}(N_R, N_S, h, d)$ denote the average entanglement-distribution rate over 24 hours for the satellite configuration given by (N_R, N_S, h) and two ground stations at the equator separated by a distance d. The rate is calculated in a simple scenario without multimode transmission from the satellites and without multimode quantum memories at the ground stations. We could then take the quantity

$$\overline{R}^{\text{opt}}(h, d) \stackrel{\text{def}}{=} \max_{N_R, N_S} \overline{R}(N_R, N_S, h, d) \tag{3.7}$$

as our figure or merit, which is the average rate (in ebits per second) over a 24-hour period for a given altitude h and a given distance d, where the optimization is over satellite configurations with a fixed h such that there is continuous coverage for 24 hours and the loss at any time is less than 90 dB. Now, as one might expect, with fewer satellites the average loss

d (km)	$h^\star$ (km)	$N_R^\star$	$N_S^\star$	$\overline{\eta}_{\text{dB}}$	$\overline{R}$ (ebits/sec)
1500	1000	7	13	62.80	1321.32
2500	1500	7	13	66.86	289.07
3500	2000	8	10	72.93	70.02
4500	3000	8	9	77.64	20.52
5000	3500	8	9	79.75	12.03

Table 3.2: Satellite configurations $(N_R^\star, N_S^\star, h^\star)$, as defined in Eq. (3.9), corresponding to the maxima of the curves for the figure of merit $C(h,d)$ plotted in the central panel of Fig. 3.4. Also shown are the average loss $\overline{\eta}_{\text{dB}} \equiv \overline{\eta}_{\text{dB}}(N_R^\star, N_S^\star, h^\star, d)$ and average rate $\overline{R} \equiv \overline{R}(N_R^\star, N_S^\star, h^\star, d)$ over 24 hours for the optimal satellite configuration.

would increase, thus decreasing entanglement-distribution rates, while increasing the number of satellites would decrease the loss, hence increasing the average entanglement-distribution rate. In order to balance our two competing goals—minimizing the total number of satellites and also maximizing the average rate—we take as our figure of merit the ratio of the average entanglement-distribution rate to the total number of satellites:

$$c(N_R, N_S, h, d) \stackrel{\text{def}}{=} \frac{\overline{R}(N_R, N_S, h, d)}{N_R N_S}, \tag{3.8}$$

which has units of ebits per second per satellite. Then, the goal is to take the satellite configuration that maximizes this figure of merit. In other words, our goal is to find

$$(N_R^\star(d), N_S^\star(d), h^\star(d)) \stackrel{\text{def}}{=} \arg\max_{N_R, N_S, h} c(N_R, N_S, h, d) \tag{3.9}$$

for any given distance d between the two ground stations, where the optimization is constrained such that there is continuous coverage to the two ground stations for 24 hours and the transmission loss at any given time is less than 90 dB. We suppress the dependence of the functions $N_R^\star$, $N_S^\star$, and $h^\star$ on the distance d when it is understood from the context. We let

$$C(h,d) \stackrel{\text{def}}{=} \max_{N_R, N_S} c(N_R, N_S, h, d) \tag{3.10}$$

be the figure of merit c optimized over N_R and N_S, with the constraint that both ground stations have continuous coverage over 24 hours and that the transmission loss at any time is less than 90 dB.

The results of our simulations are shown in Fig. 3.4. The complete set of results for all ground distances and satellite configurations considered is contained in the data files accompanying the paper. We first consider the quantity $N_{\text{opt}}(h,d)$ as a function of altitude h for fixed ground-station separations d (left panel of Fig. 3.4). In terms of the satellite configurations, we find that at higher altitudes more satellites per ring are required in general, while at lower altitudes generally more rings are required. In terms of the total number of satellites, we find that as the altitude increases the total number of satellites decreases. Interestingly, however, as we continue to increase the altitude we find that there are altitudes

(between 5000 km and 6000 km) at which the total number of satellites reaches a minimum. Beyond this range of altitudes, the required number of satellites *increases*. The presence of this minimum point gives us an indication of the altitudes at which satellites should be placed in order to minimize the total number of satellites. However, for these altitudes, the average entanglement-distribution rates are generally quite low, on the order of 10 ebits per second.

Next, we consider the figure of merit $C(h, d)$ defined in Eq. (3.10). We plot this quantity for various values of the altitude h and distance d in the central panel of Fig. 3.4. In the right panel of Fig. 3.4, we plot the corresponding average entanglement-distribution rate over 24 hours. For all distances d, except for $d = 500$ km, we find that there is an altitude h at which $C(h, d)$ is maximal. These optimal altitudes, along with the values of N_R and N_S achieving the value of $C(h, d)$ and the corresponding average loss and average entanglement-distribution rate over 24 hours, are shown in Table 3.2. Given a desired distance between the ground stations, these optimal parameters can be used to decide on the number of satellites to put in the network and the altitude at which to put them so that there is continuous coverage, which then leads to particular values for the average loss and the average entanglement-distribution rate. Conversely, given a particular performance requirement (in terms of the entanglement-distribution rate), we can use our results to determine both the required satellite configuration and the required distance between the ground stations in order to achieve the desired rate. For example, using the plot on the right panel of Fig. 3.4, in order to achieve a rate greater than 10^3 ebits per second on average in 24 hours, the satellite constellation altitude should be less than 2000 km (among the constellations considered), and the distance d between the ground stations has to be roughly less than 1500 km.

In Fig. 3.5, we plot the entanglement-distribution rate to two ground stations at the equator separated by a distance $d = 1000$ km with a satellite constellation given by $N_R = 9$ satellite rings, $N_S = 10$ satellites per ring, and altitude $h = 1500$ km. We also plot the distances of the ground stations to a satellite. We find that the rate exhibits a distinct oscillatory behavior with periodic bumps. In each bump, the rate increases as a satellite gets closer to the ground stations and decreases as the satellite passes by. All of the bumps in the rate have slightly different duration and slightly different peaks due to the fact that, at each time, the ground station pair is generally in view of multiple satellites, and we pick the satellite with the lowest transmission loss to the ground station pair. In general, therefore, each bump corresponds to a different satellite distributing entanglement to the two ground stations.

Let us now consider optimal entanglement-distribution rates to the two ground stations, i.e., let us consider the quantity $\overline{R}^{\text{opt}}(h, d)$ defined in Eq. (3.7). The results are shown in the top panel of Fig. 3.6. We assume that the satellites transmit entangled photon pairs at a rate of $R_{\text{source}} = 10^9$ ebits per second [137]. Unsurprisingly, for every pair (h, d) of altitudes h and distances d, the quantity $\overline{R}^{\text{opt}}(h, d)$ is attained by the satellite configuration that we considered that has the highest number of satellites, namely $N_R = 20$ rings and $N_S = 20$ satellites per ring. However, despite the sharp increase in the number of satellites, the rates are not much higher than those in the right panel of Fig. 3.4, which are obtained by optimizing our main figure of merit $C(h, d)$. The highest rate among all distances is around 4.6×10^4 ebits per second, which is attained for a distance of 500 km and altitude of 500 km.

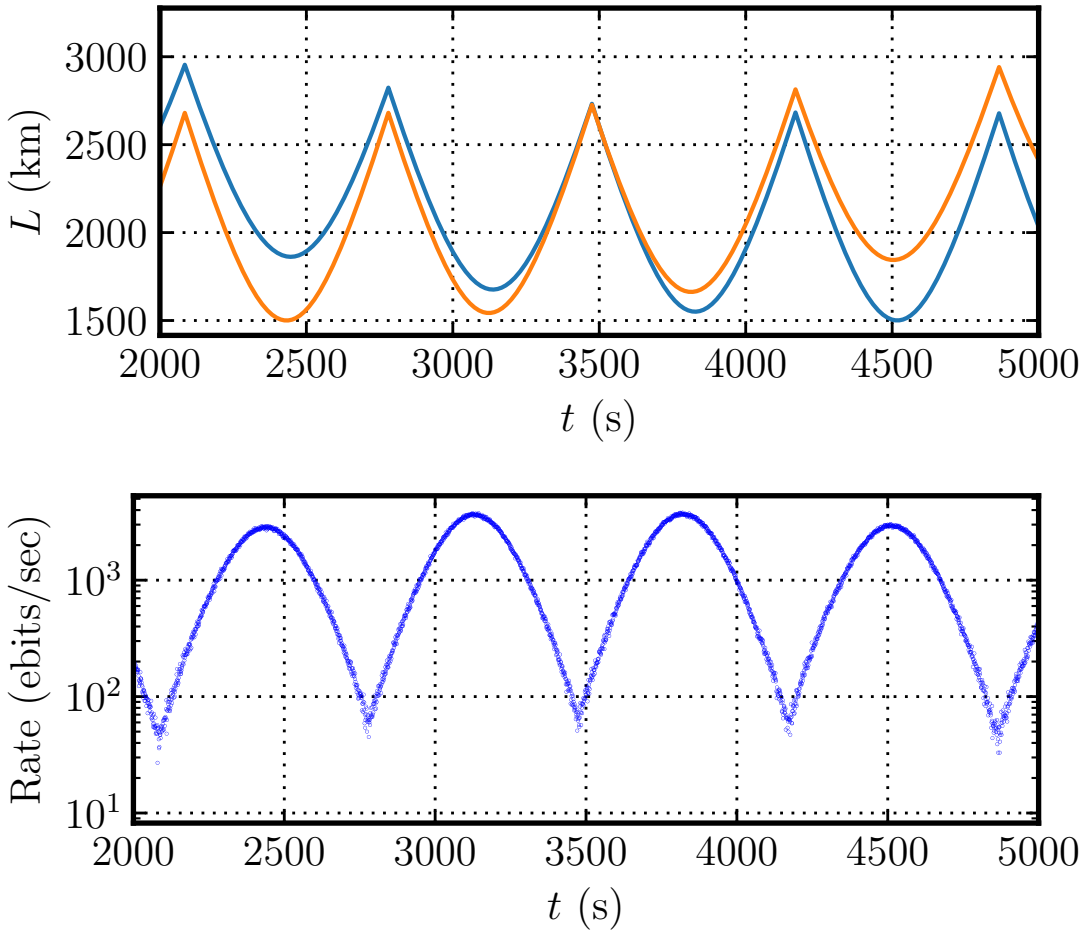

Figure 3.5: Entanglement distribution as a function of time to two ground stations at the equator. The ground stations are separated by $d = 1000$ km with a satellite constellation given by $N_R = 9$ satellite rings, $N_S = 10$ satellites per ring, and altitude $h = 1500$ km. We show a snapshot from 2000 s to 5000 s of our 24-hour simulation. (Top) The distance L of each ground station to the satellite with the least total transmission loss. (Bottom) The corresponding entanglement-distribution rate as a function of time, assuming a source rate of $R_{\text{source}} = 10^9$ ebits per second [137].

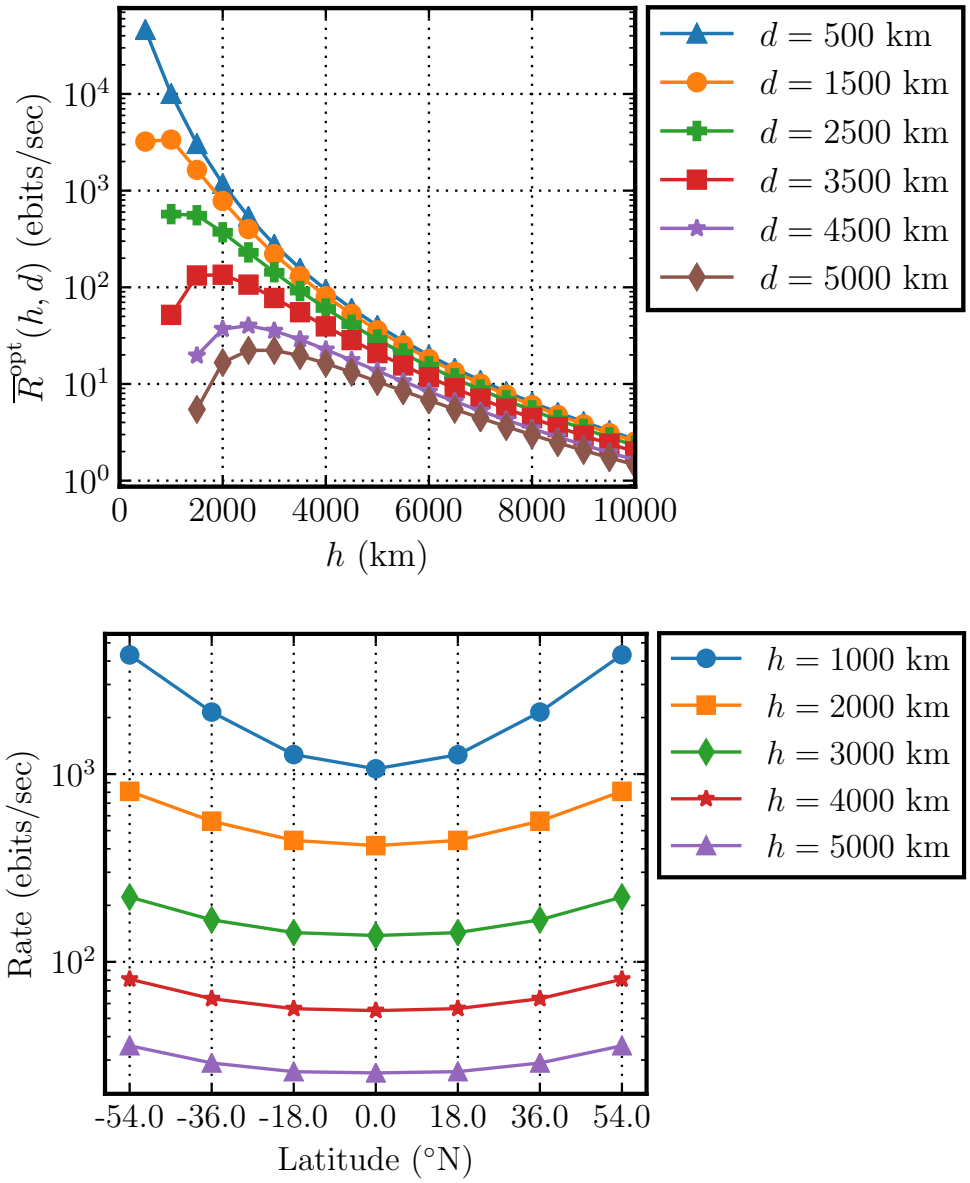

Figure 3.6: Average entanglement distribution rates (over 24 hours) for two ground stations for various satellite constellations. In all cases, we assume that the satellites transmit entangled photon pairs at a rate of $R_{\text{source}} = 10^9$ ebits per second [137]. (Top) Optimal rate (as defined in Eq. (3.7)) among all satellite configurations considered for two ground stations at the equator separated by a distance d. Each point in the plot corresponds to $N_R = 20$ satellite rings and $N_S = 20$ satellites per ring, because we find that this configuration achieves the maximum in Eq. (3.7). (Bottom) Both ground stations at various latitudes. The ground stations are separated by approximately 18° in longitude. The satellite constellation consists of $N_R = 15$ satellite rings with $N_S = 15$ satellites per ring.

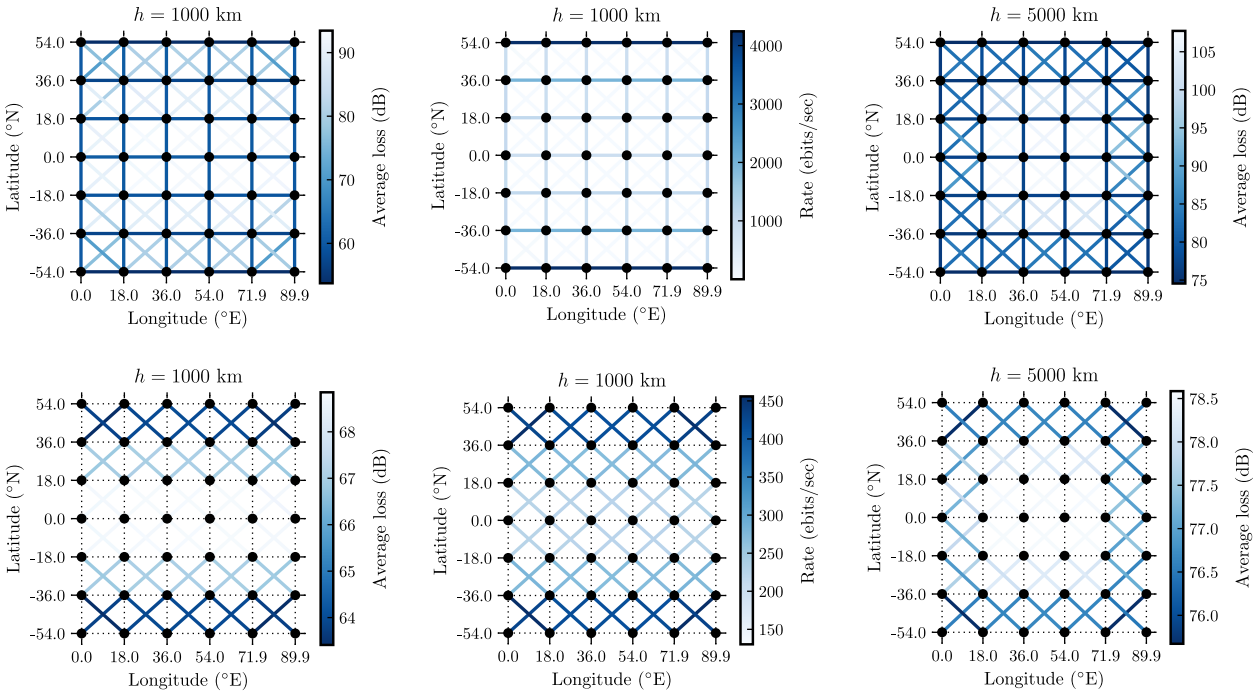

Figure 3.7: Average loss and rate (over 24 hours) for pairwise entanglement distribution for a collection of ground stations in a grid-like configuration. The nearest neighbors are separated by approximately 18° in latitude and longitude. The satellite constellation consists of $N_R = 15$ rings and $N_S = 15$ satellites per ring, for a total of 225 satellites. Average rates in the central panel are calculated in a simple scenario without multimode transmission from the satellites and without multimode quantum memories at the ground stations. We assume that the satellites transmit entangled photon pairs at a rate of $R_{\text{source}} = 10^9$ ebits per second [137]. (Top) Entanglement distribution to all possible nearest-neighbor pairs. (Bottom) Entanglement distribution only to diagonal nearest-neighbor pairs.

In the bottom panel of Fig. 3.6, we display the results of our entanglement distribution simulations when both ground stations are at a different latitude, with $N_R = N_S = 15$. Due to the fact that the satellites follow polar orbits in our network architecture, meaning that they congregate at the poles, the entanglement-distribution rates are higher for latitudes closer to the north and south poles than for the equator. This result also confirms that placing two ground stations at the equator is the worst-case scenario in terms of average loss (and thus average rate).

Before continuing, let us remark that our technique for obtaining optimal satellite configurations for continuous global coverage, via optimization of the quantities defined in Eq. (3.8) and Eq. (3.10), can be straightforwardly extended to an optimization procedure that consists of more than two ground stations (see reference [1] section for details).

Multiple ground stations

We now present the results of an entanglement distribution simulation consisting of multiple ground stations. We place 42 ground stations in a grid-like arrangement, with horizontal

separation (i.e., separation in longitude) of approximately 18° and vertical separation (i.e., separation in latitude) of approximately 18°. We use a satellite constellation of $N_R = 15$ rings and $N_S = 15$ satellites per ring, for a total of 225 satellites. In Fig. 3.7, we display the average loss for nearest neighbor pairs over a simulation time of 24 hours.

In the top plots of Fig. 3.7, we consider all possible nearest-neighbor pairs in the simulation. As expected, the loss is lowest away from the equator (latitude 0°), because neighboring ground stations are closer to each other away from the equator, due to the curvature of the earth, and because of the nature of our satellite constellation (satellites congregate at the poles). We also find that diagonal nearest-neighbor pairs have higher losses compared to pairs that are horizontally or vertically separated. This can be explained by the fact that diagonally-separated ground stations are farther away from each other than horizontally- or vertically-separated ground-station pairs. Our strategy for assigning a satellite to a ground-station pair thus favors pairs that are horizontally or vertically separated. We also find that the maximum loss for a satellite altitude of $h = 1000$ km is around 90 dB and the minimum loss is around 50 dB. For $h = 5000$ km, the maximum loss is around 105 dB and the minimum loss is around 75 dB.

In the bottom plots of Fig. 3.7, we simulate a network such that the satellites can only distribute entanglement to diagonally-separated nearest-neighbor pairs. Now, since we do not allow entanglement distribution between horizontally- and vertically-separated pairs, we find that the maximum average loss decreases and the minimum average loss increases. We still find that ground-station pairs at latitudes farther away from the equator have lower loss.

In the central panels of Fig. 3.7, we plot average entanglement-distribution rates in a simple scenario without multimode transmission from the satellites and without multimode quantum memories at the ground stations. We assume that the satellites transmit entangled photon pairs at a rate of $R_{\text{source}} = 10^9$ ebits per second [137]. In the case of entanglement distribution to all nearest-neighbor pairs (top part of the central panel of Fig. 3.7), the maximum average rate is around 4000 ebits per second, and this occurs for horizontally separated ground stations at latitudes of 54°N and −54°N. For entanglement distribution only to diagonally-separated nearest-neighbor pairs (bottom part of the central panel of Fig. 3.7), the maximum average rate is around 450 ebits per second. It is possible to compensate for the loss by having multimode signal transmission from the satellites and by including multimode quantum memories at the ground stations, which would increase the average rates.

Entanglement distribution between major global cities

Although the ultimate goal of a satellite-based quantum internet is to have satellites distribute entanglement between any collection of nodes on the ground, an example of which we considered above, satellite-based quantum communication networks will likely have a hybrid form in the near term. In a hybrid network, the satellites distribute entanglement to major global cities, which act as hubs that then distribute entanglement to smaller nearby cities using ground-based links (see Fig. 3.1). With this in mind, we now consider entanglement distribution between pairs of major global cities. We run a 24-hour simulation with a satellite constellation of 400 satellites, with $N_R = N_S = 20$, at altitudes of $h = 500$ km,

City pairs	Distance (km)	Average loss (dB)					
		500 km	1000 km	2000 km	3000 km	4000 km	5000 km
Toronto – New York City	551	45.1	52.0	60.9	66.7	71.1	74.6
Lijiang – Delingha	1200	50.6	52.9	60.5	66.3	70.7	74.3
Houston – Washington DC	1922	75.1	66.9	73.7	78.3	81.1	83.1
Sydney – Auckland	2156	65.5	59.3	62.9	67.6	71.6	74.9
New York City – London	5569	> 90	> 90	82.6	79.1	79.7	81.1
Singapore – Sydney	6306	> 90	> 90	> 90	83.3	82.5	83.2
London – Mumbai	7191	> 90	> 90	> 90	> 90	89.0	88.3

Table 3.3: Average loss over a 24-hour period between select pairs of major global cities for a constellation of 400 satellites ($N_R = N_S = 20$) at various altitudes. The following cities are included in the simulation: Toronto, New York City, London, Singapore, Sydney, Auckland, Rio de Janeiro, Baton Rouge, Mumbai, Johannesburg, Washington DC, Lijiang, Ngari, Delingha, Nanshan, Xinglong, and Houston.

1000 km, 2000 km, 3000 km, 4000 km, and 5000 km. We include the following cities in the simulation: Toronto, New York City, London, Singapore, Sydney, Auckland, Rio de Janeiro, Baton Rouge, Mumbai, Johannesburg, Washington DC, Lijiang, Ngari, Delingha, Nanshan, Xinglong, and Houston. The Lijiang-Delingha pair is chosen for comparison to a recent experiment [14]. The simulation results are shown in Table 3.3.

From Table 3.3, we see that at around a distance of 6300 km, which is the distance between Singapore and Sydney, we can only obtain an average loss less than 90 dB for altitudes greater than 2000 km. Similarly, entanglement distribution between London and Mumbai (which are 7200 km apart) at an average loss less than 90 dB is possible only for an altitude greater than 3000 km. These results suggest that, using our constellation of 400 satellites, a distance of around 7500 km is the highest for which entanglement distribution at a loss less than 90 dB can be achieved. Indeed, for Houston and London (which are 7800 km apart), we find that the average loss is greater than 90 dB for all of the satellite altitudes that we consider.

3.4 Comparison to ground-based entanglement distribution

Let us now compare the entanglement-distribution rates obtained with satellites to the rates that can be obtained via ground-based photon transmission through optical fiber with the assistance of quantum repeaters. In particular, we compare the rates in the top panel of Fig. 3.6 for two ground stations at the equator separated by a distance d between 100 km and 2000 km to ground-based repeater chains with endpoints the same distance d apart. For the latter, we suppose that the distance d between the endpoints is split into M elementary links by $(M-1)$ equally-spaced quantum repeaters. We place a source at the center of each elementary link that transmits entangled photon pairs to the nodes at the ends of the elementary link. We assume that the probability of establishing an elementary link is $p = \mathrm{e}^{-\alpha \frac{d}{M}}$, where $\alpha = \frac{1}{22 \text{ km}}$ [133], and we also assume that all repeater nodes are equipped

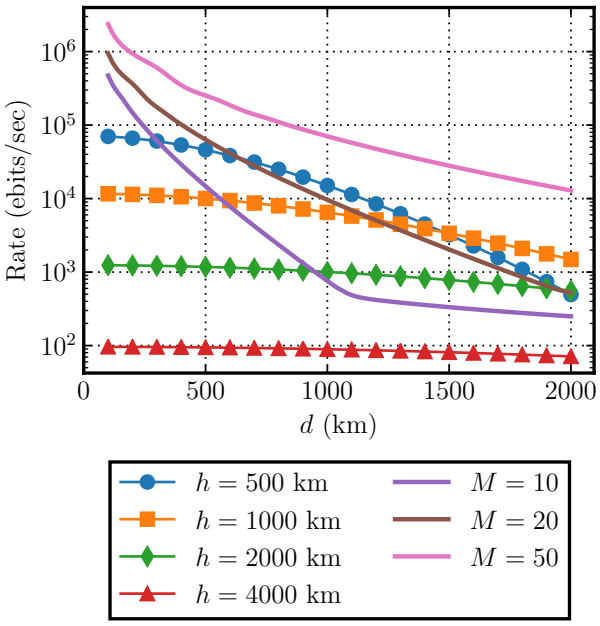

Figure 3.8: Comparison of satellite-based entanglement distribution to ground-based repeater-assisted entanglement distribution. We consider two ground stations at the equator separated by a distance d, with $N_R = 20$ satellite rings and $N_S = 20$ satellites per ring. We compare to a ground-based repeater chain of the same distance d consisting of M elementary links of equal length and $N_{\text{mem}} = 50$ quantum memories per elementary link. The rate is given by Eq. (3.11).

with N_{mem} quantum memories facing each of its nearest neighbors. Under these conditions, the rate $R_{M,N_{\text{mem}}}$ (in ebits per second) of entanglement distribution between the endpoints is

$$R_{M,N_{\text{mem}}} = \frac{cN_{\text{mem}}}{2(d/M)} \frac{1}{W_{M,N_{\text{mem}}}}, \tag{3.11}$$

where c is the speed of light and

$$W_{M,N_{\text{mem}}} = \sum_{n=1}^{\infty} \left(1 - \left(1 - (1-p)^{n-1}\right)^{M}\right)^{N_{\text{mem}}}. \tag{3.12}$$

(See Appendix A for details.) Note that our assumption that $p = \mathrm{e}^{-\alpha \frac{d}{M}}$ is the best-case scenario in which the sources fire perfect Bell pairs (so that no entanglement purification is required) and the Bell measurements for entanglement swapping are deterministic. Furthermore, the formula in Eq. (3.11) holds in the case that the quantum repeaters have perfect read-write efficiency and have infinite coherence time.

In Fig. 3.8, we compare the rate in Eq. (3.11) with $N_{\text{mem}} = 50$ to the rates shown in the top panel of Fig. 3.6. For an altitude of 500 km, we find that the quantum repeater scheme with $M = 50$ elementary links outperforms the satellite-based scheme for all distances up to 2000 km. However, for $M = 10$ and $M = 20$ elementary links, we find that there are critical distances beyond which satellites can outperform the ground-based repeater schemes. For example, for an altitude of 500 km, the satellite-based scheme outperforms the $M = 20$ quantum repeater scheme beyond approximately 600 km and the $M = 10$ scheme beyond approximately 300 km. For an altitude of 1000 km, the satellite-based scheme outperforms the $M = 20$ repeater scheme beyond approximately 1200 km. Similarly, for an altitude of 2000 km, the satellite-based scheme outperforms the quantum repeater scheme beyond approximately 900 km. For an altitude of 4000 km, the satellite-based rates are lower than the quantum repeater rates for all values of M considered.

Currently, satellite-based schemes are arguably more viable, because high-coherence-time quantum memories (which are not widely available) are not required. However, the monetary cost of the satellites, along with other overhead monetary costs (e.g., launch costs), can make implementing a satellite-based entanglement-distribution network challenging. Furthermore, local weather conditions and background photons during the daytime make it difficult to achieve the continuous coverage assumed here, which ultimately results in lower entanglement-distribution rates. On the other hand, ground-based quantum repeater schemes can achieve higher rates than satellite-based schemes, but this occurs only when the number of repeater nodes is quite high, the number of quantum memories per repeater node is high, and the coherence times of the memories is high. In addition, quantum memories currently exist mostly in a laboratory environment and are not at the stage of development that they can be widely deployed in the field, and they certainly do not have high enough coherence times to achieve the rates presented here.

3.5 Summary and future work

In this paper, we explored the possibility of using satellites for a global-scale quantum communications network. Our network architecture consists of a constellation of satellites in

polar orbits around the earth that transmit entangled photon pairs to ground stations (see Fig. 3.2). By defining a figure of merit that takes into account both the number of satellites as well as satellite-to-ground entanglement-distribution rates, we provided estimates on the number of satellites needed to maintain full 24-hour coverage at a high rate based on the maximum value of the figure of merit. Using our figure of merit to decide the number of satellites in the network, we estimated the transmission loss and entanglement-distribution rates that can be achieved for two ground stations placed at various latitudes, for multiple ground stations at various locations in a grid-like arrangement, and for multiple major global cities in a hybrid satellite- and ground-based network in which the cities can act as hubs that receive entanglement from satellites and disperse it to surrounding locations via ground-based links. Finally, we compared the achievable entanglement-distribution rates for two ground stations using satellites to achievable entanglement-distribution rates using ground-based links with quantum repeaters. With a large enough number of repeater nodes, along with a high enough number of high-coherence-time quantum memories at each node, it is possible to obtain entanglement-distribution rates that surpass those obtained with satellites. However, satellite-based schemes operating without quantum repeaters can, in certain cases, outperform quantum repeater schemes, with drawbacks being that a relatively high number of satellites is required and that adverse weather conditions can prevent continuous operations and thus reduce the rate. These drawbacks appear to be less prohibitive in the near term than the major drawback of ground-based, repeater-assisted entanglement distribution, which is that quantum memories with very high coherence times are simply not widely available. Therefore, it appears that a satellite-based scheme will remain the preferred option over ground-based repeater schemes into the near term, especially with the improving miniaturization and increasing fidelity of entanglement sources [122, 99] and the decreasing cost and miniaturization of satellites [87, 89, 90].

Our analysis of a global, satellite-based quantum internet opens the door to plenty of further study. For example, our simulations can be refined by taking into account local weather conditions. Our optimization procedure can also be extended to include more than two ground stations. It would also be interesting to compare other types of satellite constellations, much like those studied in Refs. [115, 116]. Finally, to have a genuine quantum network requires efficient routing algorithms. It would be interesting to explore entanglement routing in a satellite network along the lines of, e.g., Refs. [138, 139, 117] in the classical setting.

In summary, the broad-scope vision is to have a quantum-connected world, similar to today's internet, where users across the globe can share quantum information for any desirable task. In our view, the backbone of such a network is built on local and global quantum entanglement, in which intercontinentally-separated ground stations located in major cities act as entanglement hubs connecting the local network users of one city to those of another (Fig. 3.1). Hybrid networks interfacing space-based quantum communication platforms with ground-based quantum repeaters will make this vision a real possibility. Though, even before such a globally connected network exists, there are a plethora of benefits at our hands now. For instance, the space-based entanglement distribution network that we introduced here can serve a dual-purpose almost immediately upon construction: allowing secure quantum-communications as well as providing a platform for secure clock synchronization around the globe (see e.g. [140, 141, 142]). The requirements for the latter application are almost iden-

tical to the requirements of former, up to e.g. an extra uplink quantum channel needed for cross-correlation measurements (via the method of reference [141]). Thorough analyses in this domain is duly wanting and is something we are currently pursuing. The application space for near-term, space-based, global quantum-communications is currently blossoming and is a fruitful arena for potentially useful and creative ideas.

CHAPTER 4. ANOTHER APPLICATION: OPTICAL ANALOGUE-GRAVITY

We now discuss the Hawking effect in (optical) analogue-gravity systems. Though the physics underlying this effect in this context is quite rich, I will, more or less, sweep this richness under the rug, in favor of describing things with both simplicity and sufficient breadth. In this sense, I will reduce all physical mechanisms under study to elementary elements, which correspond to a set of simple symplectic transformations. However, I will make reference to physical setups along the way, providing references to the literature when needed for support or further reading. To understand the bulk of this chapter, it is sufficient to understand the discussion on symplectic transformations and Gaussian systems in Section 2.2 as well as some parts of Section 2.3, especially the part on entanglement and logarithmic negativity for Gaussian states.

The results presented here are part of a project which is currently under development, though nearing its end. This section thus represents on-going research.

4.1 Introduction

In the mid-1970's, Stephen Hawking discovered the surprising result that astrophysical black holes, formed by the complete gravitational collapse of an astronomical body, are not completely black but instead are black-bodies. That is, black holes emit radiation (Hawking radiation) according to a Planckian distribution, with a characteristic temperature (the Hawking temperature) given, in natural units, by $T_H = \kappa/(2\pi) \propto 1/M$, where κ is the surface gravity of the event horizon of the black hole and M is the mass of the collapsed body [143, 144]. Interestingly, the Hawking temperature is independent of any particular characteristics of the collapsed body and of the details of the collapse. This result was theoretically found by analyzing a free quantum field theory on the classical background of a dynamical space-time described by a massive body undergoing complete gravitational collapse. What is intriguing is that the emission process is a spontaneous effect! I.e. given an initial vacuum for the quantum field, an asymptotic observer, exterior to the black hole, will be bombarded by a constant flux of blackbody radiation, in accordance with the description above. Thus the formation of black hole, in and of itself, is unstable, and the black hole will (plausibly) decay away, leaving behind only a soup of blackbody radiation.[1]

Perhaps more surprising than this is the fact that the Hawking effect seems to be a universal phenomena, appearing generically when a causal barrier (e.g. an event horizon) forms, and not just in extreme astrophysical contexts [146]. This is readily seen by pointing to the plethora of scenarios and systems which support a Hawking-like effect, in the absence of any gravitational interactions, like for accelerated observers in flat space-time [147, 148]

[1] This interpretation of a decaying black-hole assumes that Hawking's calculation holds good through the entire process, which has been criticized and contended over the past fifty-odd years and which has led to the so-called information-loss paradox. Though much research into this area has been done over the last half-century, the paradox stands firm. It is not my intention to discuss the paradox here, only to remark on its theoretical significance in this brief footnote. For the interested reader, see e.g. [145] and references therein.

and analogue-gravity systems [149, 150, 151]. Of particular significance are analogue-gravity systems, as such systems provide a way to actually observe and detect the Hawking effect, in contrast to the astrophysical context. There are many physical systems which support the Hawking effect – fluid analogues [152, 153], Bose-Einstein condensates [154, 155, 156, 157], fiber-optical setups [158, 159, 160], etc. (see [161] and references therein, for a recent review of the myriad of analogue-gravity platforms). I will base our discussions mainly around (fiber-)optical analogues (see references e.g. [158, 159, 160] and Figure 4.1). Though much of which to be said applies to other systems as well, due to the apparent universality of the Hawking effect.

In optical setups, a strong pump-pulse propagating in a dielectric medium can locally change the refractive index of the medium via the optical Kerr effect[2], forming a causal barrier (an analogue event horizon) in the vicinity of the pulse, for a range of weak probe-modes propagating atop this background structure. See Figure 4.1 for an illustration and further explanation. If the weak probe-modes are reduced to vacuum fluctuations, one expects the classical background, i.e. the strong pump-pulse, to spontaneously emit radiation in pairs, in accordance with the Hawking effect. There have been numerous numerical studies [162, 163, 164] and experiments [158, 159] indicating that this is indeed the case, though further validation and support is wanting.

Due to the complications of dealing with non-linear optical effects analytically in phenomenological terms (i.e. at the level of Maxwell's equations, susceptibility tensors, etc.), many authors have turned towards micro-physical models to gain a firmer analytical-handle on the Hawking effect in the optical context (see, for instance, references [165, 166, 167, 168]). There, one treats the medium directly by providing a detailed model for the medium itself as well as the coupling between the constituents of the medium and background electromagnetic fields. For instance, in reference [167], the authors take the dielectric medium as being composed of a large set of identical harmonic oscillators, which couple linearly to weak electromagnatic fields propagating within the medium. The effect of a strong pump-field is to locally change the characteristic frequencies of the oscillators, leading to changes in the local refractive index. Importantly, this is a linear theory which, under suitable approximations, can be quantized and solved exactly. Linder et al [167] (and others, e.g., [165, 166, 168]) have demonstrated that, in this micro-physical model, a dielectric medium can indeed support the Hawking effect through the formation of an analogue event horizon. The authors computed the Hawking spectrum outright and showed that it follows a Planckian distribution, with a characteristic temperature which can be related to the surface gravity found from an effective space-time metric for the medium, in agreement with the Hawking process. See Section VII of reference [167] for more on this last statement.

In this work, I extend the results of Linder et al [167] by providing a plausible, full unitary description of the scattering processes (Section 4.2) as well as an in-depth mode-correlation study in the face of deleterious environmental effects and with various initial quantum states (Sections 4.3 and 4.4). The plausibility of the unitary description I provide draws motivation and support from the Bloch-Messiah reduction [25], which generally applies to linear theories. The Bloch-Messiah reduction allows one to decompose any symplectic (linear) transforma-

[2]This is a non-linear optical effect where, for weak probe modes, the local change in the refractive index is proportional to the intensity of the strong pump-field.

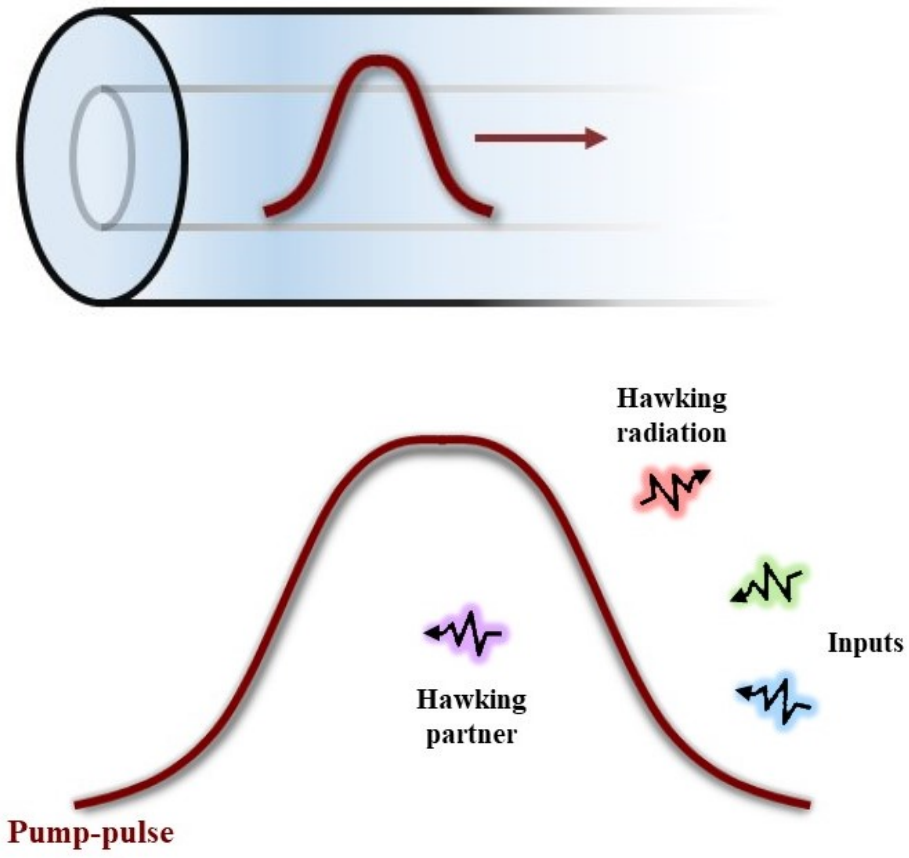

Figure 4.1: Illustration of a pump-pulse induced analogue event-horizon in an optical fiber. Top: A strong, pump-pulse propagates in a dielectric medium (e.g. an optical fiber), locally changes the refractive index of the medium via the Kerr effect. If the pump-pulse intensity is strong enough, i.e. the local change of the refractive index is great enough, then the pulse acts as a causal barrier, restricting the flows of weak probe-modes. Bottom: The situation in the reference frame of the pulse. The leading edge (the right side) of the pulse acts as an analogue black-hole event-horizon. The interior of the pump-pulse is correspondingly the interior of the analogue black-hole. Any modes which fall into the interior cannot propagate back out to the right – i.e. the interior flow is strictly leftward for all relevant modes. The formation of the event horizon induces the creation of particle-pairs, á la the Hawking effect, which are condensed from the (classical) pump-pulse. Generally, there exists a black-hole/white-hole pair, with the white-hole event-horizon corresponding to the trailing edge (the left side) of the pulse. See references [158, 159] and the discussion in Section 4.5 for more on this.

tion into a discrete set of elementary operations. This greatly simplifies conceptual issues surrounding the Hawking process, in general, by allowing one to draw intuitive diagrams which have a one-to-one correspondence with the actual physical process via this reduction. Under this extraordinary simplification and using techniques from Gaussian quantum information theory [169], I examine the quantum aspects of the stimulated Hawking effect, with regards to the quantum correlations within the system, showing explicitly the detrimental repercussions of a non-negligible background temperature and backscattering effects, as well as discussing the benefits of stimulating the process with single-mode, non-classical resources. Though much of the discussion is phrased in terms of optical-analogue event horizons, the methods used and the results so obtained apply just as well to a variety of other systems supporting the Hawking effect. Furthermore, the Bloch-Messiah reduction allows one to easily extend the discussions to more exotic scenarios like, for instance, a white-hole–black-hole pair pair (Section 4.5). The physics of these exotic systems is quite rich due to the increased complexity of the relevant dynamics. I give only a taste here of the richness contained in these systems, leaving a more detailed study for future work.

4.2 The model and basic formalism

Motivation from a micro-physical model

We focus here on a particular micro-physical model for the Hawking effect in an optical-analogue gravity system, following reference [167]. The purpose of this section is primarily to motivate succeeding sections, gain some familiarity with a physical system, and establish the mode structure and notation. Thus, much of the discussion is qualitative, with many details left to the references (mainly reference [167]; though, see e.g. [165, 166] as well).

The model that we shall have in mind for an optical-analogue system is, effectively, a continuum version of the Lorentz oscillator model of an isotropic optical-medium far from resonance (see e.g. Chapter 2 of [170] for more on the Lorentz oscillator model with regards to dielectric media). That is, we will suppose that the medium to be described quite well by a large set of decoupled and identical quantum harmonic-oscillators, which, in the continuum limit, can be described by a scalar field $\psi(x,t)$ with characteristic frequency Ω_0.[3] We also assume the medium to be isotropic and work only in one scalar dimension, x, which is taken to lie along the optical axis for electromagnetic-field modes propagating in the medium (i.e. the x-axis is parallel to the Poynting vector of the electromagnetic fields). We describe the (weak) electromagnetic field by the vector-potential, $A(x,t)$, such that the electric field goes as, $E(x,t) = \partial_t A$ in the temporal gauge, and the vector potential and electric field are taken to lie in the yz-plane, perpendicular to the optical axis. We assume a dipole-like coupling between the medium oscillators and weak fields. In the absence of non-linear effects induced by a strong, background pump-pulse, the Lagrangian density for the system is given by (in natural units),

$$\mathcal{L}_{\text{lab}} = \frac{1}{2}\underbrace{\left((\partial_t A)^2 - (\partial_x A)^2\right)}_{\text{Free EM field}} + \frac{1}{2}\underbrace{\left((\partial_t \psi)^2 - \Omega_0^2 \psi^2\right)}_{\text{Medium oscillators}} + \underbrace{g\psi(\partial_t A)}_{\text{Dipole coupling}} \tag{4.1}$$

[3] The continuum limit holds good whenever wavelengths of the electromagnetic field are large compared to the inter-molecular spacing of the media. We assume this to be the case.

where g is a coupling constant. I note that this is taken in the rest frame of oscillators. From here, one can find the Euler-Lagrange equations for the system, from which one can derive a Sellmeier relation for the (lab) frequency-modes, $\omega_{\rm lab}$, of the fields (see [167] for details),

$$n(\omega_{\rm lab})^2 = 1 + \frac{g^2}{\Omega_0^2 - \omega_{\rm lab}^2}, \tag{4.2}$$

where $n(\omega)$ is the refractive index of the medium. It should be clear that the physical model holds good near, but not too near, a single medium resonance (i.e. $\omega_{\rm lab} \ll \Omega_0$, but not so much so that another resonant frequency is met). This establishes the asymptotic mode structure for the field theory in the lab frame.

Now to introduce non-linear effects. We shall assume that the effect of a strong, background pump-pulse is to only change the medium resonance of the oscillators, i.e. $\Omega_0 \to \Omega(x,t)$, where $\Omega(x,t)$ now depends on the intensity of the pump-pulse as well as its spatio-temporal profile. Furthermore, we will assume that the pulse does not change drastically as it propagates through the medium (e.g. a solitonic approximation) such that $\Omega(x - vt)$, where v is the group velocity of the pulse. This establishes a preferred reference frame, (τ, χ), which is related to the lab frame, (t, x), by a Lorentz boost,

$$\tau = \gamma(t - vx) \tag{4.3}$$

$$\chi = \gamma(x - vt), \tag{4.4}$$

where $\gamma = 1/\sqrt{1 - v^2}$ is the Lorentz-boost factor. In this reference frame, $\Omega(\chi)$ is τ independent and thus $\partial_\tau \Omega = 0$. We shall further assume that the effects of the pump are localized, e.g. $\Omega(\chi \to \pm\infty) =$ constant, so that we have asymptotically well-defined normal-modes in these coordinates. We shall take $\chi \approx 0$ to indicate the position of the pump, and thus the position of the analogue-horizon; $\chi < 0$ is the black hole interior ($\chi \to -\infty$ is deep within the interior), and $\chi \to \infty$ is taken far in the exterior region of the pump, where e.g. $\Omega = \Omega_0$. Moreover, I assume that $\Omega(\chi < 0) < \Omega_0$, i.e. the pump reduces the resonance frequency of the medium, thereby increasing the refractive index of the medium, in line with the Kerr effect. As a consequence, if the non-linear effects are strong enough, the interior region ($\chi < 0$) only supports modes with negative group velocities (the flow strictly points towards decreasing χ), as I discuss below, thus indicating the presence of a causal barrier.

The Lagrangian, in the presence of the pulse and in the pulse reference-frame, is

$$\mathcal{L}_{\rm pulse} = \frac{1}{2}\big((\partial_t A)^2 - (\partial_x A)^2\big) + \frac{1}{2}\left(\big((\partial_t - v\partial_\chi)\psi\big)^2 - \Omega^2\psi^2\right) + \gamma g \psi(\partial_t - v\partial_\chi)A. \tag{4.5}$$

One can find the Euler-Lagrange equations from this and, in turn, determine the asymptotic mode structure far away from the pump. Let translations in τ be associated with the co-moving frequency, ω, which by the way is conserved here since Ω is τ independent, and let translations in χ be associated with the co-moving wave-vector, k. Then, one may find a transcendental equation for the dispersion relation, $\omega(k)$, in the pulse frame [167]

$$\underbrace{\gamma(\omega + vk)}_{\omega_{\rm lab}} = \pm \underbrace{\Omega\sqrt{1 + \frac{g^2}{\omega^2 - k^2 - g^2}}}_{F(k)}, \tag{4.6}$$

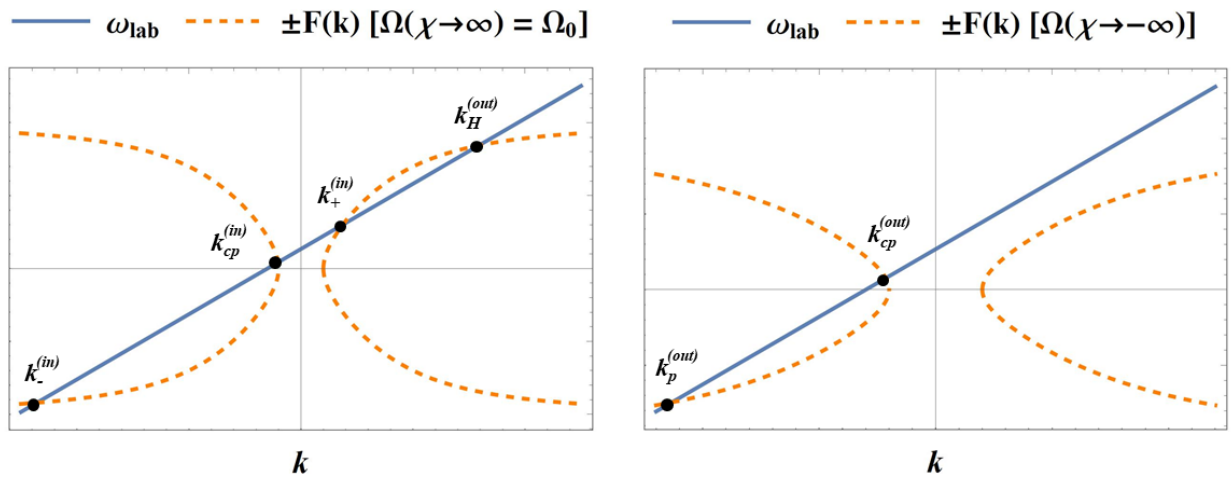

Figure 4.2: Dispersion relation in the asymptotic regions. Left: The mode structure far away in the exterior of the black hole. For a given range of co-moving frequencies, this region supports four modes, $k_+^{(\text{in})}$, $k_-^{(\text{in})}$, $k_{cp}^{(\text{in})}$, and $k_H^{(\text{out})}$. The first three have negative group velocities and thus propagate towards the event horizon (towards the pulse). The last mode, the Hawking mode, $k_H^{(\text{out})}$, has positive group velocity, and thus propagates away from the event horizon. Right: The mode structure far into the interior of the black hole. Observe that this region does not support any modes with positive group velocity; i.e. all modes which fall into the interior only plunge further in.

where it is understood that this derivation is only sensible far away from the pump. Plotting these functions then gives the set of allowable wave-vector modes, k, for a given co-moving frequency, ω. See Figure 4.2. This set of wave-vectors determines the (asymptotic) normal modes, and thus defines the in/out Fock spaces for the fields upon quantization.

From Figure 4.2, one finds the in/out-modes in the asymptotic regions $\chi \to \pm\infty$. The distinction of "in" and "out" is determined by the group velocity of the mode. As discussed in reference [167], there exists only one mode with positive group velocity – i.e. propagating away from the black hole. This is the k_H mode, the outgoing Hawking mode, which has support only in the exterior of the black hole ($\chi \to \infty$). All other modes have negative group velocity and thus propagate towards the black hole (from $\chi = \infty$) or deeper into the black hole (towards $\chi = -\infty$). Thus, for a given ω, we have the informal mapping between in and out modes,

$$(k_+^{(\text{in})}, k_-^{(\text{in})}, k_{cp}^{(\text{in})}) \to (k_H^{(\text{out})}, k_p^{(\text{out})}, k_{cp}^{(\text{out})}), \tag{4.7}$$

induced by the presence of an analogue event-horizon. Here, $k_p^{(\text{out})}$ is the Hawking-partner mode, which is entangled with the Hawking mode and which falls deep into the interior of the black hole; $k_{cp}^{(\text{in})}$ is the counter-propagating mode, which can scatter into the out-going Hawking mode via a classical scattering process. This classical scattering process is the source of a greybody factor in the out-going Hawking spectrum. See Figure 4.3 and the next subsection for more on this, and see reference [167] for more details.

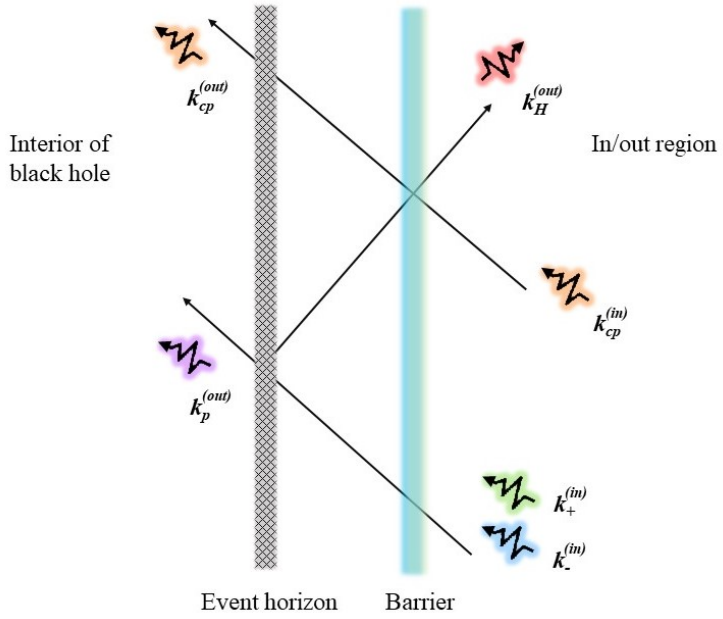

Figure 4.3: The Hawking process. The in-modes, $(k_+^{(\mathrm{in})}, k_-^{(\mathrm{in})}, k_{cp}^{(\mathrm{in})})$, are converted into an outgoing Hawking mode, $k_H^{(\mathrm{out})}$, and two other modes, $(k_p^{(\mathrm{out})}, k_{cp}^{(\mathrm{out})})$, which fall into the interior of the black hole. Scattering occurs in two steps: (1) the in-modes $(k_+^{(\mathrm{in})}, k_-^{(\mathrm{in})})$ pass through an effective potential barrier unscathed and are subsequently converted into Hawking pairs – a Hawking mode and its infalling partner, $k_p^{(\mathrm{out})}$ – near the event horizon; (2) the outgoing Hawking mode then interacts with a counter-propagating mode, $k_{cp}^{(\mathrm{out})}$, via a passive scattering process at the barrier. The former process creates quanta and generates quantum correlations between the Hawking pairs, while the passive scattering process merely shifts some of these generated quanta and quantum correlations from the outgoing Hawking mode to the infalling counter-propagating mode, $k_{cp}^{(\mathrm{out})}$. Passive scattering also leads to a greybody factor in the outgoing Hawking spectrum for the $k_H^{(\mathrm{out})}$ mode and induces classical correlations between this mode and the infalling counter-propagating mode, $k_{cp}^{(\mathrm{out})}$.

Symplectic equivalence: The symplectic Hawking matrix

We focus now on the quantitative relations between modes, leaning on the results of Linder et al [167], for the scenario qualitatively discussed in the previous subsection and in Figure 4.3. The situation is as follows. A Hawking pair is generated near an (optical) event horizon and the outgoing Hawking mode undergoes classical scattering at an effective potential barrier. Explicitly, Linder et al found that the relation between in-going modes and the out-going Hawking mode – i.e. the mapping $(k_+^{(\mathrm{in})}, k_-^{(\mathrm{in})}, k_{cp}^{(\mathrm{in})}) \to k_H^{(\mathrm{out})}$ – is given by,

$$\hat{a}_{k_H}^{(\mathrm{out})} = \alpha \hat{a}_{k_+}^{(\mathrm{in})} + \beta \hat{a}_{k_-}^{(\mathrm{in})} + \eta \hat{a}_{k_{cp}}^{(\mathrm{in})}, \tag{4.8}$$

with the unitarity relation, $|\alpha|^2-|\beta|^2+|\eta|^2=1$, holding. Further, the usual *Hawking relation* was found to hold, i.e.,

$$\frac{|\alpha|^2}{|\beta|^2}=\exp\left(\omega/T_H\right), \tag{4.9}$$

where ω is the co-moving frequency of the modes and T_H is (the frequency independent) Hawking temperature. From this and the unitarity relation, the number of spontaneously generated quanta in the out-going Hawking mode can be found,

$$|\beta|^2=\frac{1-|\eta|^2}{\exp\left(\omega/T_H\right)-1}=\frac{\Gamma}{\exp\left(\omega/T_H\right)-1}, \tag{4.10}$$

where $0\leq\Gamma=1-|\eta|^2\leq 1$ is the greybody factor. The authors thus showed that, in this micro-physical model for a dielectric medium perturbed by a space-time dependent background pulse, Hawking radiation is spontaneously generated and follows a (grey-body corrected) Planckian distribution, with characteristic temperature given by the Hawking temperature, T_H.[4]

I now go about extending these results by providing an ansatz for the unitary (and corresponding symplectic transformation) of the above dynamics. All of what follows are, more or less, new results. Also, I begin to slowly depart from the optical-analogue thus described and start to speak in more general terms. Though, it may be beneficial for the reader to keep a particular physical system in mind when digesting the forthcoming discussions.

Importantly, equation (4.8) is a linear relationship between the in-modes and one out-mode and formally corresponds to a symplectic projection (a 6×2 rectangular matrix which maps 3 modes to 1) onto a smaller mode space, however this projection can be enlarged to a full symplectic transformation (6×6) which maps 3 in-modes to 3-out modes.[5] From this, we can envision and then construct (via the Bloch-Messiah decomposition) a set of squeezers and beamsplitters which exactly provide this mapping. Indeed, one can show that a properly placed two-mode squeezing transformation followed by an orthogonal beamsplitter transformation does the trick, provided that the complex coefficients of the two-mode squeezer obey the Hawking relation [equation (4.9)] and that the transmission probability of the beamsplitter equals the greybody factor.

Proof. Consider a two-mode squeezing operator, $\hat{S}$, such that,

$$\hat{S}^\dagger\hat{a}^{(\text{in})}_{k_+}\hat{S}=\mu\hat{a}^{(\text{in})}_{k_+}+\nu\hat{a}^{(\text{in})\dagger}_{k_-}, \tag{4.11}$$

with the complex coefficients, (μ,ν), satisfying $|\mu|^2-|\nu|^2=1$. Also, consider a two-mode beamsplitter transformation, $\hat{O}$, such that,

$$\hat{O}^\dagger\hat{a}^{(\text{in})}_{k_+}\hat{O}=t\hat{a}^{(\text{in})}_{k_+}+r\hat{a}^{(\text{in})}_{k_{cp}}, \tag{4.12}$$

[4]They give an explicit expression for the Hawking temperature, T_H, and the greybody factor, Γ, in terms of their model-parameters, as well as a relation between the temperature to the surface gravity of an effective space-time metric. I will not delve deeper into these details, as providing further discussion would take us too far astray.

[5]This is analogous to providing a Stinespring dilation (or unitary extension) of the map.

with the transmission and reflection coefficients, (t, r), satisfying the orthogonality relation $|t|^2 + |r|^2 = 1$. Then, construct the unitary operator, $\hat{U} \overset{\text{def}}{=} \hat{O}\hat{S}$, which in the Heisenberg picture acts as

$$\begin{aligned}
\hat{U}^\dagger \hat{a}^{(\text{in})}_{k_+} \hat{U} &= \hat{S}^\dagger \hat{O}^\dagger \hat{a}^{(\text{in})}_{k_+} \hat{O}\hat{S} \\
&= \hat{S}^\dagger \left(t\hat{a}^{(\text{in})}_{k_+} + r\hat{a}^{(\text{in})}_{k_{cp}} \right) \hat{S} \\
&= \mu t \hat{a}^{(\text{in})}_{k_+} + \nu t \hat{a}^{(\text{in})\dagger}_{k_-} + r\hat{a}^{(\text{in})}_{k_{cp}} \\
&\overset{\text{def}}{=} \alpha \hat{a}^{(\text{in})}_{k_+} + \beta \hat{a}^{(\text{in})\dagger}_{k_-} + \eta \hat{a}^{(\text{in})}_{k_{cp}}.
\end{aligned}$$

Whence,

$$\frac{|\alpha|^2}{|\beta|^2} \overset{\text{def}}{=} \exp\left(\omega/T_H\right) \implies \frac{|\mu|^2}{|\nu|^2} = \exp\left(\omega/T_H\right).$$

The equivalence of the greybody factor to the transmission probability, i.e. $\Gamma = |t|^2$, completes the correspondence. □

Observe that $\hat{U}^\dagger \hat{a}^{(\text{in})}_{k_+} \hat{U}$ is just the outgoing Hawking mode, $\hat{a}^{(\text{out})}_{k_H}$. Hence, $\hat{U}$ (and $\hat{U}^\dagger$) gives us the mapping we want, but it actually provides more, since[6]

$$\hat{U}^\dagger : \ (k^{(\text{in})}_+, k^{(\text{in})}_-, k^{(\text{in})}_{cp}) \to (k^{(\text{out})}_H, k^{(\text{out})}_p, k^{(\text{out})}_{cp}). \tag{4.13}$$

The question is: is this the fully correct transformation for the physical dynamics that we are considering? The authors of reference [167] do not provide the full scattering computation for all modes nor have I in this thesis, but one can argue that the unitary extension given above is certainly plausible. Firstly, any additional transformations which may be missing in our unitary should not change the mode transformation (4.8). This limits the potential, missing dynamics to unitaries acting strictly on the subspace of out-modes $(k^{(\text{out})}_p, k^{(\text{out})}_{cp})$, which are deep in the interior of the black hole. As one expects most scattering events to happen at or near the event horizon, i.e. where the background profile changes most abruptly, it seems plausible that the modes $(k^{(\text{out})}_p, k^{(\text{out})}_{cp})$ decouple deep in the interior and thus do not mix (or negligibly so). The above decomposition is also the simplest that one can provide and makes a direct connection with the Hawking process in other systems as well – in the astrophysical context and in analogue fluid-systems (cf. to results in Section 3.4 of [171] for the astrophysical case and the transformations derived in references [172, 173, 174]); thus being in line with the apparent universality of the Hawking effect in systems which support the appropriate causal structure (i.e. systems with event horizons; see reference [146]). I therefore focus on this transformation/interpretation, due to its simplicity and its generality.[7]

With the correspondence between the Hawking process and the decomposition into squeezers and beamsplitters made explicit, I now put everything in the Gaussian formalism and find the *symplectic Hawking matrix* corresponding to the physical process described

[6] One should think of this as a unitary map from the in Hilbert space to the out Hilbert space.

[7] To gain further support, we are also investigating the completeness of this unitary-extension numerically, for this particular model. This will appear in future work.

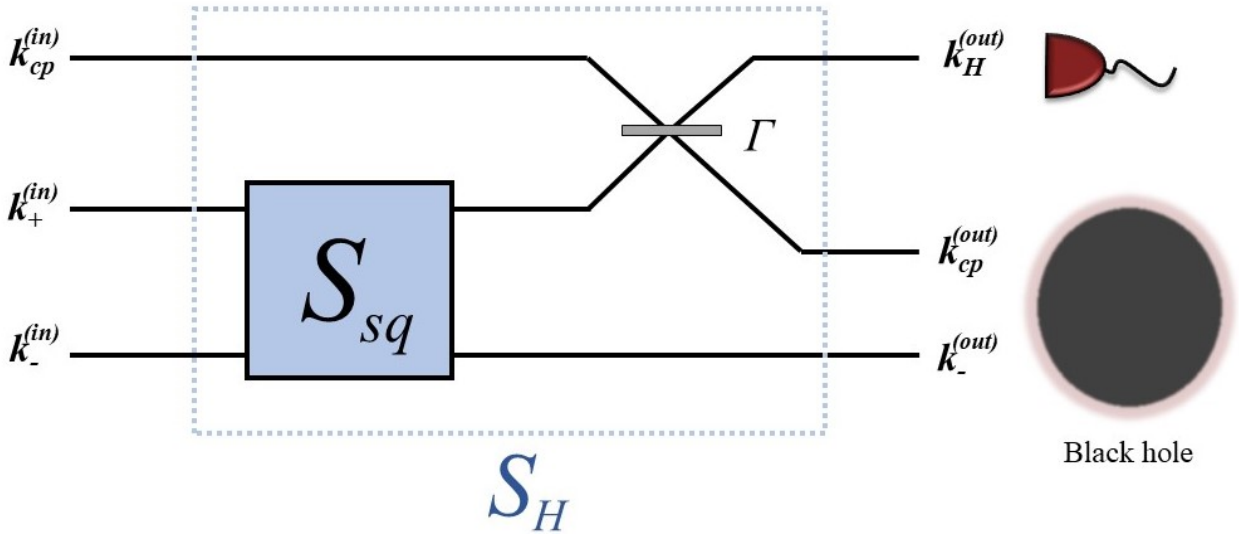

Figure 4.4: Circuit-equivalent of the Hawking process. The dashed boxed region corresponds to the symplectic Hawking matrix, S_H, which we represent here by an equivalent optical ciruit consisting of a two-mode squeezer, S_{sq}, followed by a beamsplitter with transmission probability Γ. The formal equivalence between the above circuit and the Hawking process follows from the Bloch-Messiah decomposition for symplectic transformations. Observe that this circuit is also in one-to-one correspondence with the intuitive picture of the process, drawn in Figure 4.3.

above. Let us first introduce a certain ordering and relabeling for the in/out canonical operators,

$$\hat{\mathbf{r}}^{(\text{in})} = \left(\hat{\mathbf{r}}^{(\text{in})}_{k_+}, \hat{\mathbf{r}}^{(\text{in})}_{k_-}, \hat{\mathbf{r}}^{(\text{in})}_{k_{cp}}\right)^{\intercal} \stackrel{\text{def}}{=} \left(\hat{\mathbf{r}}^{(\text{in})}_{1}, \hat{\mathbf{r}}^{(\text{in})}_{2}, \hat{\mathbf{r}}^{(\text{in})}_{3}\right)^{\intercal} \tag{4.14}$$

$$\hat{\mathbf{r}}^{(\text{out})} = \left(\hat{\mathbf{r}}^{(\text{out})}_{k_H}, \hat{\mathbf{r}}^{(\text{out})}_{k_p}, \hat{\mathbf{r}}^{(\text{out})}_{k_{cp}}\right)^{\intercal} \stackrel{\text{def}}{=} \left(\hat{\mathbf{r}}^{(\text{out})}_{1}, \hat{\mathbf{r}}^{(\text{out})}_{2}, \hat{\mathbf{r}}^{(\text{out})}_{3}\right)^{\intercal}, \tag{4.15}$$

For instance, in this new labeling, $(k_1^{(\text{out})}, k_2^{(\text{out})})$ denotes the generated Hawking pair, where $k_1^{(\text{out})}$ is the out-going Hawking mode and $k_2^{(\text{out})}$ its in-falling partner. Observe that this choice of ordering follows the transmission paths of the modes in the circuit diagram of Figure 4.4. Since the Hawking process is a linear process, the in and out canonical operators are connected by a symplectic matrix – the symplectic Hawking matrix, S_H – such that,

$$\hat{\mathbf{r}}^{(\text{out})} = S_H \hat{\mathbf{r}}^{(\text{in})}. \tag{4.16}$$

The Hawking matrix is in one-to-one correspondence with the unitary operator $\hat{U}_{\text{in}\to\text{out}}$, which maps the in-modes to the out-modes, and is likewise decomposed into a product of a two-mode squeezing matrix, S_{sq}, and an orthogonal beamsplitter matrix, O, such that,

$$S_H = O S_{sq} \tag{4.17}$$

I now encode the Bogoliuobov coefficients, (α, β, η), into these symplectic matrices. For simplicity, let us assume all of the Bogoliuobov coefficients are real (e.g. ignorning squeezing

angles), and let us parameterize them by two quantities: (1) $|\beta_H|^2$, which is the number of Hawking pairs generated in the squeezing process and is equivalent to $|\beta|^2$ when backscattering is absent,[8] and (2) Γ, the greybody factor. Then,

$$\alpha \stackrel{\text{def}}{=} \sqrt{\Gamma(|\beta_H|^2+1)} \tag{4.18}$$

$$\beta \stackrel{\text{def}}{=} \sqrt{|\beta_H|^2\Gamma} \tag{4.19}$$

$$\eta \stackrel{\text{def}}{=} \sqrt{1-\Gamma}. \tag{4.20}$$

The orthogonal matrix, O, and squeezing matrix, S_{sq}, can be written with this parameterization,

$$O = \begin{pmatrix} \sqrt{\Gamma}\mathbb{I}_2 & 0 & \sqrt{1-\Gamma}\mathbb{I}_2 \\ 0 & \mathbb{I}_2 & 0 \\ -\sqrt{1-\Gamma}\mathbb{I}_2 & 0 & \sqrt{\Gamma}\mathbb{I}_2 \end{pmatrix}, \quad S_{sq} = \begin{pmatrix} \sqrt{1+|\beta_H|^2}\mathbb{I}_2 & \sqrt{|\beta_H|^2}\sigma_z & 0 \\ \sqrt{|\beta_H|^2}\sigma_z & \sqrt{1+|\beta_H|^2}\mathbb{I}_2 & 0 \\ 0 & 0 & \mathbb{I}_2 \end{pmatrix}. \tag{4.21}$$

Observe that, e.g., the squeezing matrix only has non-trivial elements in the first and second rows/columns, in line with our operator ordering of equation (4.15) and the fact that the Hawking pair is the only mode-pair relevant to the squeezing process. From here, the symplectic Hawking matrix is found,

$$S_H = OS_{sq} = \begin{pmatrix} \sqrt{\Gamma(1+|\beta_H|^2)}\mathbb{I}_2 & \sqrt{\Gamma|\beta_H|^2}\sigma_z & \sqrt{1-\Gamma}\mathbb{I}_2 \\ \sqrt{|\beta_H|^2}\sigma_z & \sqrt{1+|\beta_H|^2}\mathbb{I}_2 & 0 \\ -\sqrt{(1-\Gamma)(1+|\beta_H|^2)}\mathbb{I}_2 & -\sqrt{(1-\Gamma)|\beta_H|^2}\sigma_z & \sqrt{\Gamma}\mathbb{I}_2 \end{pmatrix}. \tag{4.22}$$

One can check that this prescription leads to the mode transformation (4.8) by using the input-output relation between the canonical operators, equation (4.16), using the relation between canonical operators and annihilation/creation operators, equation (2.139), and accounting for the parameterization given in equations (4.18)-(4.20). Observe that the Hawking matrix reduces to two-mode squeezing for the Hawking pair and a trivial identity transformation on the counter-propagating mode whenever backscattering is negligible ($\Gamma \approx 1$).

As suggested before, the transformation thus described is equivalent to those found in astrophysical black hole evaporation scenarios as well as other analogue systems. In this sense, the symplectic Hawking matrix, S_H, appears to be a fundamental ingredient, irrespective of the illusory distinctions in the physics underlying such systems.

4.3 In-out relations: a Gaussian analysis

Now that I have characterized the scattering dynamics for the analogue Hawking effect, I wish to analyze it under various environments – e.g. amid a uniform thermal background – and with various inputs. To do this with sufficient depth and efficiency, I will restrict the

[8] I.e., $|\beta_H|^2 = 1/(\mathrm{e}^{\omega/T_H}-1)$. See equation (4.10).

analysis to Gaussian quantum states, which include, for instance, displaced-thermal states, single-mode squeezed states, etc. This restriction allows one to efficiently analyze quantum-state transformations by reducing the description of the full quantum-state dynamics to the description of the dynamics of the mean and covariance of the state. See, for instance, equations (2.188).

Gaussian inputs and moment transformations

Let $(\boldsymbol{\mu}^{(\text{in})}, \sigma^{(\text{in})})$ be the first and second moments describing the in-modes to the Hawking process. The output moments are then completely determined by,

$$\boldsymbol{\mu}^{(\text{out})} = S_H \boldsymbol{\mu}^{(\text{in})} \tag{4.23}$$

$$\sigma^{(\text{out})} = S_H \sigma^{(\text{in})} S_H^{\intercal}, \tag{4.24}$$

which fully characterizes the output quantum state. Generically, I write the output covariance matrix as,

$$\sigma^{(\text{out})} \stackrel{\text{def}}{=} \begin{pmatrix} \sigma_1^{(\text{out})} & \sigma_{12}^{(\text{out})} & \sigma_{13}^{(\text{out})} \\ \sigma_{12}^{(\text{out})\intercal} & \sigma_2^{(\text{out})} & \sigma_{23}^{(\text{out})} \\ \sigma_{13}^{(\text{out})\intercal} & \sigma_{23}^{(\text{out})\intercal} & \sigma_3^{(\text{out})} \end{pmatrix}, \tag{4.25}$$

where $\sigma_k^{(\text{out})}$ is the single-mode covariance matrix for the kth out-mode and $\sigma_{kj}^{(\text{out})}$ is the correlation matrix between the kth and jth out-modes. I will further restrict the inputs to uncorrelated quantum states. Thus,

$$\boldsymbol{\mu}^{(\text{in})} \stackrel{\text{def}}{=} \left(\boldsymbol{\mu}_1^{(\text{in})}, \boldsymbol{\mu}_2^{(\text{in})}, \boldsymbol{\mu}_3^{(\text{in})}\right)^{\intercal} \tag{4.26}$$

$$\sigma^{(\text{in})} \stackrel{\text{def}}{=} \begin{pmatrix} \sigma_1^{(\text{in})} & 0 & 0 \\ 0 & \sigma_2^{(\text{in})} & 0 \\ 0 & 0 & \sigma_3^{(\text{in})} \end{pmatrix}, \tag{4.27}$$

where, e.g., $\sigma_1^{(\text{in})}$ is the single-mode covariance matrix for the k_1 in-mode etc. From here, I find generic expressions for the output covariance sub-matrices,

$$\begin{aligned}
\sigma_1^{(\text{out})} &= \sigma_3^{(\text{in})} + \Gamma\left(\sigma_1^{(\text{in})} - \sigma_3^{(\text{in})}\right) + \Gamma|\beta_H|^2\left(\sigma_1^{(\text{in})} + \sigma_z\sigma_2^{(\text{in})}\sigma_z\right) \\
\sigma_2^{(\text{out})} &= \sigma_2^{(\text{in})} + |\beta_H|^2\left(\sigma_2^{(\text{in})} + \sigma_z\sigma_1^{(\text{in})}\sigma_z\right) \\
\sigma_3^{(\text{out})} &= \Gamma\sigma_3^{(\text{in})} + (1-\Gamma)\left(\sigma_1^{(\text{in})} + |\beta_H|^2\left(\sigma_1^{(\text{in})} + \sigma_z\sigma_2^{(\text{in})}\sigma_z\right)\right) \\
\sigma_{12}^{(\text{out})} &= \sqrt{\Gamma|\beta_H|^2(|\beta_H|^2+1)}\left(\sigma_1^{(\text{in})}\sigma_z + \sigma_z\sigma_2^{(\text{in})}\right) \\
\sigma_{13}^{(\text{out})} &= -\sqrt{\Gamma(1-\Gamma)}\left(\left(|\beta_H|^2+1\right)\sigma_1^{(\text{in})} + |\beta_H|^2\sigma_z\sigma_2^{(\text{in})}\sigma_z - \sigma_3^{(\text{in})}\right) \\
\sigma_{23}^{(\text{out})} &= -\sqrt{(1-\Gamma)|\beta_H|^2(|\beta_H|^2+1)}\left(\sigma_z\sigma_1^{(\text{in})} + \sigma_2^{(\text{in})}\sigma_z\right).
\end{aligned} \tag{4.28}$$

Observe that the correlation matrix between the Hawking-partner mode and the infalling counter-propagating mode, $\sigma_{23}^{(\text{out})}$, is generally independent of the input counter-propagating

mode, $\sigma_3^{(\text{in})}$. This is because there is no direct interaction between these modes. Indeed, the source of these correlations is a shuffling around of the Hawking-pair correlations via a transfer of outgoing Hawking particles to the infalling counter-propagating mode, which is induced by backscattering (see Figures 4.3 and 4.4 for illustrations). This is seen explicitly in the equation for $\sigma_{23}^{(\text{out})}$ by considering the extreme cases of negligible backscattering ($\Gamma \approx 1$) and/or negligible particle creation ($|\beta_H|^2 \approx 1$), for which $\sigma_{23}^{(\text{out})} \approx 0$ in either limit.

Displaced thermal inputs: One important family of inputs which we will discuss are displaced thermal states, i.e. quantum states of the type, $\bigotimes_k \hat{D}_{\gamma_k}\hat{\Theta}_k\hat{D}_{\gamma_k}^\dagger$, where $\hat{D}_{\gamma_k}$ is the displacement operator for the kth mode with complex amplitude γ_k and $\hat{\Theta}_k$ is the single-mode thermal state. In the optical context, these inputs physically correspond to "noisy lasers". It is also good to consider this family of states as they are classical, and we want to generally consider how stimulating the Hawking process alters quantum features at the output.

Displaced thermal states have first and second moments,

$$\mathbf{r}^{(\text{in})} = \bigoplus_{k=1}^{3} \sqrt{2}\Big(\text{Re}\{\gamma_k\}, \text{Im}\{\gamma_k\}\Big)^\intercal \tag{4.29}$$

$$\sigma^{(\text{in})} = \bigoplus_{k=1}^{3} N_k \mathbb{I}_2, \tag{4.30}$$

where $N_k = 2\bar{n}_k(T_E) + 1$ and $\bar{n}_k(T_E)$ is the average number of Planckian-distributed, background photons in the kth input mode, when the background temperature is T_E (E for environment; note $N = 1$ only at zero temperature). Using these inputs into equation (4.28), I find the output covariance sub-matrices (ignoring first moments),

$$\begin{aligned}
\sigma_1^{(\text{out})} &= \Big((N_1 + N_2)\Gamma|\beta_H|^2 + (N_1 - N_3)\Gamma + N_3\Big)\mathbb{I}_2 \\
\sigma_2^{(\text{out})} &= \Big((N_1 + N_2)|\beta_H|^2 + N_2\Big)\mathbb{I}_2 \\
\sigma_3^{(\text{out})} &= \Big((N_1 + N_2)(1-\Gamma)|\beta_H|^2 + (N_3 - N_1)\Gamma + N_1\Big)\mathbb{I}_2 \\
\sigma_{12}^{(\text{out})} &= (N_1 + N_2)\sqrt{\Gamma|\beta_H|^2(|\beta_H|^2 + 1)}\sigma_z \\
\sigma_{23}^{(\text{out})} &= -(N_1 + N_2)\sqrt{(1-\Gamma)|\beta_H|^2(|\beta_H|^2 + 1)}\sigma_z \\
\sigma_{13}^{(\text{out})} &= \Big(N_3 - N_1 - (N_1 + N_2)|\beta_H|^2\Big)\sqrt{\Gamma(1-\Gamma)}\mathbb{I}_2.
\end{aligned} \tag{4.31}$$

Observe that each correlation matrix, $\sigma_{kj}^{(\text{out})}$, is non-trivial; hence, there are correlations – classical and quantum – between all mode pairs over nearly the entire parameter space. Also, notice that the displacement parameters $\{\gamma_k\}$ do not appear in the covariance matrix; they only appear at the level of first moments. This means that displacements do not change the (absolute) amount of correlations between the modes.

A simplified but highly instructive instance of noise, which I will focus on from here out, is that of isotropic noise, for which $N_k = N \;\forall\; k$. In this case, let me write the covariance

matrix explicitly in terms of the background photon number. For brevity, let $\bar{n}_E \overset{\text{def}}{=} \bar{n}(T_E)$ denote the (isotropic) number of background photons at temperature T_E. Then, $N = 2\bar{n}_E + 1$ and I find

$$\begin{aligned}
\sigma_1^{(\text{out})} &= (1+2\bar{n}_E)\left(2\Gamma|\beta_H|^2+1\right)\mathbb{I}_2 \\
\sigma_2^{(\text{out})} &= (1+2\bar{n}_E)\left(2|\beta_H|^2+1\right)\mathbb{I}_2 \\
\sigma_3^{(\text{out})} &= (1+2\bar{n}_E)\left(2(1-\Gamma)|\beta_H|^2+1\right)\mathbb{I}_2 \\
\sigma_{12}^{(\text{out})} &= 2\,(1+2\bar{n}_E)\sqrt{\Gamma|\beta_H|^2(|\beta_H|^2+1)}\sigma_z \\
\sigma_{23}^{(\text{out})} &= -2\,(1+2\bar{n}_E)\sqrt{(1-\Gamma)|\beta_H|^2(|\beta_H|^2+1)}\sigma_z \\
\sigma_{13}^{(\text{out})} &= -2\,(1+2\bar{n}_E)\,|\beta_H|^2\sqrt{\Gamma(1-\Gamma)}\mathbb{I}_2.
\end{aligned} \tag{4.32}$$

In Section 4.4, we will see that the background radiation can wash-out the quantum correlations generated in the Hawking process, if it is sufficiently large. A quantitative statement of "sufficiently large" will be made later.

Single-mode squeezed input: We will now consider a thermally seeded, single-mode squeezed input on the $k_1^{(\text{in})}$ in-mode. As I will show, using single-mode squeezing (a "non-classical" resource) in one input can enhance/revive entanglement generated in the Hawking process. Our input moments in this case are

$$\mathbf{r}^{(\text{in})} = \bigoplus_{k=1}^{3}\sqrt{2}\Big(\,\text{Re}\{\gamma_k\},\text{Im}\{\gamma_k\}\Big)^{\intercal} \tag{4.33}$$

$$\sigma_1^{(\text{in})} = (1+2\bar{n}_E)\,\tilde{\sigma}(R,\varphi) \tag{4.34}$$

$$\sigma_2^{(\text{in})} = (1+2\bar{n}_E)\,\mathbb{I}_2 \tag{4.35}$$

$$\sigma_3^{(\text{in})} = (1+2\bar{n}_E)\,\mathbb{I}_2, \tag{4.36}$$

where $\tilde{\sigma}(R,\varphi) \overset{\text{def}}{=} O_\varphi \text{e}^{2R\sigma_z} O_\varphi^{\intercal}$ is the covariance matrix for a single-mode squeezed vacuum, O_φ is a 2×2 rotation matrix, φ is the squeezing angle, and R is the squeezing strength. I note that the squeezing strength is often parameterized in terms of the amplification factor $z = \text{e}^R$, which is a scaling factor for the first moments of an input quantum state (e.g. $\langle x\rangle \to z\,\langle x\rangle$ for $\varphi = 0$). The output covariance matrix is then readily found per equation (4.28),

$$\begin{aligned}
\sigma_1^{(\text{out})} &= (1+2\bar{n}_E)\left((1-\Gamma)\mathbb{I}_2 + \Gamma\left((|\beta_H|^2+1)\tilde{\sigma} + |\beta_H|^2\right)\right) \\
\sigma_2^{(\text{out})} &= (1+2\bar{n}_E)\left(1+|\beta_H|^2\left(\mathbb{I}_2 + \sigma_z\tilde{\sigma}\sigma_z\right)\right) \\
\sigma_3^{(\text{out})} &= (1+2\bar{n}_E)\left(\Gamma\mathbb{I}_2 + (1-\Gamma)\left(\tilde{\sigma} + |\beta_H|^2(\tilde{\sigma}+\mathbb{I}_2)\right)\right) \\
\sigma_{12}^{(\text{out})} &= (1+2\bar{n}_E)\sqrt{\Gamma|\beta_H|^2(|\beta_H|^2+1)}(\tilde{\sigma}+\mathbb{I}_2)\sigma_z \\
\sigma_{23}^{(\text{out})} &= -\,(1+2\bar{n}_E)\sqrt{(1-\Gamma)|\beta_H|^2(|\beta_H|^2+1)}\sigma_z(\tilde{\sigma}+\mathbb{I}_2) \\
\sigma_{13}^{(\text{out})} &= -\,(1+2\bar{n}_E)\sqrt{\Gamma(1-\Gamma)}\left((1+|\beta_H|^2)\tilde{\sigma} - (1-|\beta_H|^2)\mathbb{I}_2\right),
\end{aligned} \tag{4.37}$$

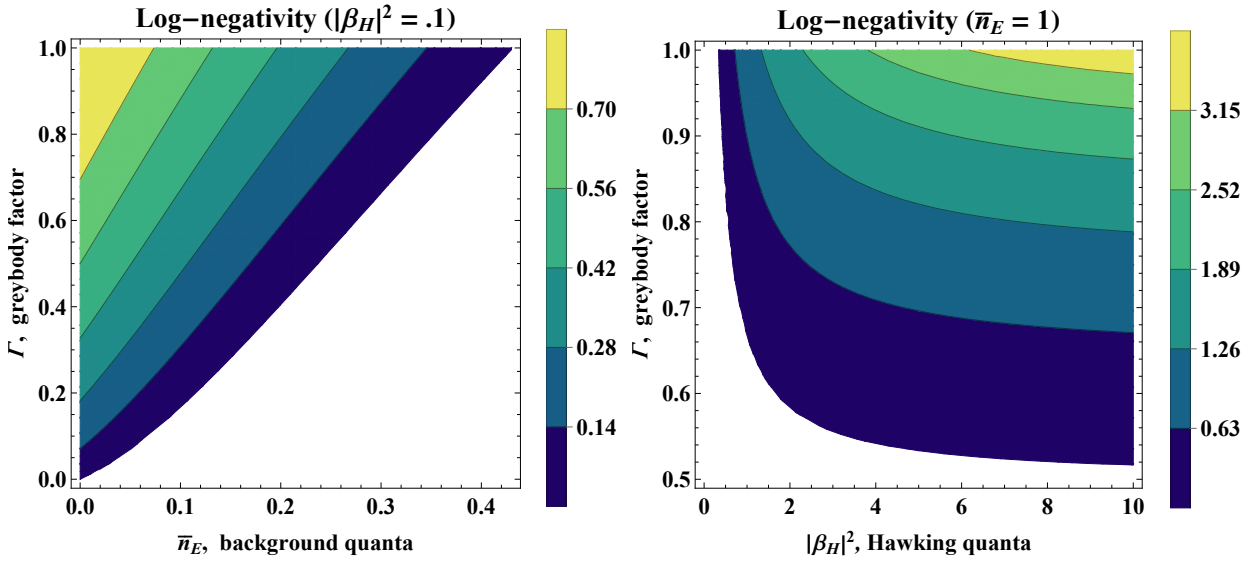

(a) (b)

Figure 4.5: Quantum entanglement in the Hawking pair, $(k_1^{(\text{out})}, k_2^{(\text{out})})$. These plots quantify the entanglement in the Hawking pair, as measured by the log-negativity, which roughly has units of ebits (entangled bits). In all plots, the white-space corresponds to zero-entanglement regions, which I will simply refer to as *null regions*. (a) Shows how the entanglement in the Hawking pairs vanishes, depending on the amount of backscattering (indicated by the greybody factor, Γ) and background noise (indicated by the number of background photons, $\bar{n}_E$). For $\Gamma = 1$, the entanglement completely vanishes when the condition $\bar{n}_E = 1/\left(\sqrt{(|\beta_H|^2+1)/|\beta_H|^2}-1\right)$ is met, which occurs for $\bar{n}_E \approx .43$ here. This point corresponds precisely to the sudden-death condition, $T_E^\star = 2T_H$, of equation (4.39). (b) Showing variations in entanglement over $(|\beta_H|^2, \Gamma)$ parameter space. Observe that, no matter how many Hawking quanta are produced, entanglement between the Hawking pairs vanishes whenever $\Gamma \leq 1/2$, consistent with the bound provided in equation (4.44) for $\bar{n}_E = 1$.

where, for brevity, I have suppressed the dependence on the squeezing strength and squeezing angle of the single-mode squeezed matrix, $\tilde{\sigma}$. Observe that these equations reduce to equations (4.30) for $R = 0$ ($\tilde{\sigma} = \mathbb{I}_2$). These equations are not very illuminating by themselves, but such are necessary in order to quantitatively discuss entanglement (to compute the log-negativity) between various mode pairs. So I add them here for completeness.

4.4 Quantum correlations

Here, I study quantum correlations between the Hawking-pair modes, $(k_1^{(\text{out})}, k_2^{(\text{out})})$, for different input states and varying system parameters, using the log-negativity as an entanglement quantifier. Though there generally exists multi-mode (3-mode) entanglement within our system, I restrict the analysis to a single mode-pair for simplicity, since, in practice, it may not be feasible to do a multi-mode correlation analysis. I further note that only dis-

cussing entanglement between Hawking pairs is equivalent to analyzing the entanglement between the interior and exterior regions of the black hole, when non-classical resources are absent at the input. This is so because the backscattered mode, $k_3^{(\text{out})}$, shares no quantum correlations with the outgoing Hawking mode, $k_1^{(\text{out})}$. Hence quantum correlations across the interior-exterior bipartition are solely a consequence of the correlations held between the $(k_1^{(\text{out})}, k_2^{(\text{out})})$ mode pair. This provides some justification for this restriction. Some qualitative discussion regarding entanglement in other modes and in the system as a whole is nevertheless provided. Still, a more comprehensive correlation-analysis, for various input quantum states, is subject to further study.

"Entanglement sudden-death": Ambient temperature and greybody effects

I plot the log-negativity of the Hawking pair, over various input parameters, in Figure 4.5. As shown in Figures 4.5b and 4.5a, there exists sharp lines in parameter space where the entanglement between Hawking pairs vanishes completely and never returns. This is a generic phenomena and has been dubbed "entanglement sudden-death" in the literature (see e.g. reference [175] for a generic discussion and reference [172] for a brief discussion in the context of analogue-gravity). What is physically happening in our scenario is that the number of background, Planckian-distributed photons is overwhelming the number of Hawking quanta and washing out any-and-all quantum correlations between Hawking pairs. Crudely, this occurs when the ambient temperature is much higher than the Hawking temperature of the underlying analogue-gravity system.

By examining the PPT criteria for the interior and exterior regions of the black hole, $(k_1^{(\text{out})}, k_2^{(\text{out})})$, one can make this description sharper and predict e.g. the temperature at which one expects the entanglement to suddenly vanish. Recall that, for two-mode Gaussian states, a non-zero logarithmic negativity corresponds to the smallest, partially transposed, symplectic eigenvalue condition, $\tilde{\nu}_- < 1$ (see the discussion surrounding equation (2.206)). Thus, the sudden death of entanglement occurs when $\tilde{\nu}_- = 1$, which we will call the *sudden-death condition*. Assume that the ambient, background photon-spectrum and the Hawking spectrum are Planckian distributed, and thus obey the Bose-Einstein relation

$$\bar{n}_E = 1/(\mathrm{e}^{\omega/T_E} - 1) \quad \text{and} \quad |\beta_H|^2 = 1/(\mathrm{e}^{\omega/T_H} - 1), \tag{4.38}$$

where T_E is the background temperature and T_H is the Hawking temperature, respectively. By computing $\tilde{\nu}_-$ with these relations and setting its value to one, one can find an explicit relationship between $T_E^\star$ and T_H, where $T_E = T_E^\star$ is the *sudden-death temperature*, at which point the sudden-death condition is satisfied and quantum correlations between Hawking pairs vanish.[9] For negligible backscattering ($\Gamma \approx 1$), I find

$$T_E^\star(T_H) = 2T_H, \tag{4.39}$$

which is consistent with the relationship found in reference [172]. Note that this calculation assumes that all interacting modes are of the same frequency, and thus all frequency modes experience the same sudden-death condition. This is slightly different than the expression

[9] I do not provide the explicit calculation here, as it is lengthy and not illuminating.

found in reference [172], where the authors consider scattering between different in and out frequency-modes.

I now include the greybody factor. Generally, backscattering will reduce the sudden-death temperature below the value given above, i.e.

$$T_E^\star(\Gamma, T_H) \leq 2T_H, \tag{4.40}$$

as one can qualitatively observe in Figure 4.5. To analytically see this, I analyze the sudden-death condition for non-negligible backscattering and find the transcendental equation,

$$\mathrm{e}^{\omega/T_H} = \mathrm{e}^{\omega/T_E^\star}\left(\Gamma_\omega\left(1+\mathrm{e}^{\omega/T_E^\star}\right)-1\right), \tag{4.41}$$

where I have hidden the dependence of $T_E^\star$ on the greybody factor and the Hawking temperature for brevity. Solving for $T_E^\star$ in the limit of low particle density (the Maxwell-Boltzmann limit; $\mathrm{e}^{\omega/T} \gg 1$ and $\bar{n} \approx \mathrm{e}^{-\omega/T}$) and assuming $\Gamma \gg \mathrm{e}^{-\omega/T_E}$, I find the greybody-corrected sudden-death temperature,

$$T_E^\star(\Gamma, T_H) \approx \frac{2T_H}{1-\frac{T_H}{\omega}\ln\Gamma} \leq 2T_H. \tag{4.42}$$

Observe that the sudden-death temperature is now frequency dependent by virtue of the greybody factor.

In order to gain more intuition of backscattering effects, I analyze the same situation but with focus turned towards the greybody factor. Independently of any approximation, the greybody factor is ultimately limited by the Boltzmann factor for the environmental photons, i.e.

$$\Gamma > \mathrm{e}^{-\omega/T_E}, \tag{4.43}$$

which can be derived from the transcendental equation (4.41) by taking the Hawking temperature to infinity. As long as this condition is satisfied, then there can exist entanglement between the interior and exterior regions of the black hole. For reference, I also write this in terms of the background photon number using the Bose-Einstein relation, $\bar{n}_E = 1/(\mathrm{e}^{\omega/T_E}-1)$,

$$\Gamma > \frac{\bar{n}_E}{\bar{n}_E+1}. \tag{4.44}$$

When these inequalities turn to equalities, the entanglement in the interior and exterior completely vanish, for all values of T_E and T_H.[10] Therefore, these inequalities place an intrinsic bound on the amount of backscattering permissible at finite background temperatures, if one wishes to observe quantum correlations between Hawking pairs.

In the low-temperature limit (or, equally, the high-frequency limit; $T_E/\omega \ll 1$), the only restriction on the greybody factor is that $\Gamma \gtrsim 0$. On the other hand, in high-temperature limit (or, equally, the low-frequency limit; $\omega/T_E \ll 1$), $\Gamma \gtrsim (1-\omega/T_E)$ must hold in order to observe entanglement between the Hawking pairs. In this high-temperature regime, the number of Hawking particles will be large, but the amount of quantum correlations can nevertheless vanish, even if T_E is significantly smaller than T_H (so long as $\omega/T_E \ll 1$).

[10] This can be thought of as a "sudden-death greybody factor", similar to the sudden-death temperature from before, but I do not use such language here

This emphasizes the significance that backscattering has on quantum correlations whenever background noise (though arbitrarily small but still finite) is present. See Figure 4.5 for numerical evidence of this.

The discussion thus far has focused on the Hawking pair (or equally, the interior and exterior of the black hole). However, this is not the full story, since backscattering corresponds to a physical transfer of particles and entanglement from the Hawking mode to the counter-propagating mode, such that, in the limit of $\Gamma \to 0$, the counter-propagating mode and the Hawking-partner mode share all correlations which originally resided in the Hawking pair (observe, for instance, Figure 4.4 and the covariance matrices in equation (4.32)). The question then becomes: if there is a loss of entanglement in the Hawking pair, due to the combined effects of background thermal radiation and backscattering, do correlations persist between the counter-propagating mode and partner mode? This is a good question to pose because we want to find entanglement somewhere within our system, if all such modes are experimentally accessible. To address this question, we could go through similar derivations for this mode-pair as we did for the Hawking pair, but this effectively reduces to a substitution $\Gamma \to 1 - \Gamma$ in all of the formulas above. So similar analyses carry over, with subtle changes in interpretation thus following. For instance, one observes that the greybody-dependent sudden-death temperature $T_E^\star(\Gamma, T_H)$ is then not a global signature of entanglement-death within the system as a whole (which one could also deduce by assessing Figure 4.4 with a keen eye). Only when we restrict ourselves to two modes is this quantity relevant. When considering entanglement between any-and-all modes, the most pertinent figure of merit is the sudden-death temperature, $T_E^\star = 2T_H$, as operating at this temperature means a vanishing of quantum correlations between any bipartition of the system, thus signifying a true global loss of entanglement. In some setups though, measuring and assessing multi-mode entanglement may not be feasible and observing two-mode correlations may be more practical. So it is good to keep these distinctions in mind.

Moreover, though I have structured the conversation around backscattering between the various modes in our analogue system, the results thus found correspond to more generic and practical scenarios as well. That is, similar discussions carry over if we regard the factor Γ as e.g. encoding the inefficiencies within an experimental setup, rather than viewing it as a greybody factor. For instance, say that backscattering is negligible, so that there are only two out-modes for our system – the Hawking mode and its partner, but there exists loss in the detector used to measure the Hawking mode. Furthermore, suppose the detector introduces some white-noise into the signal, comparable to the noise from the ambient thermal background. Then, this scenario is formally equivalent to the one prior regarding greybody effects, and therefore, all the same formulae apply. However, the conclusions of each scenario are slightly different because the now "loss-dependent sudden-death temperature", equation (4.42), which follows the same derivation as in the greybody scenario, signifies a global death of entanglement within the system, which was not the case when backscattering was included, since the the counter-propagating mode was, in principle, accessible.

Entanglement enhancement with non-classical resources

One thing which is clear is that stimulating an analogue-gravity system with "classical" states will generally degrade the amount of entanglement generated by the system itself,

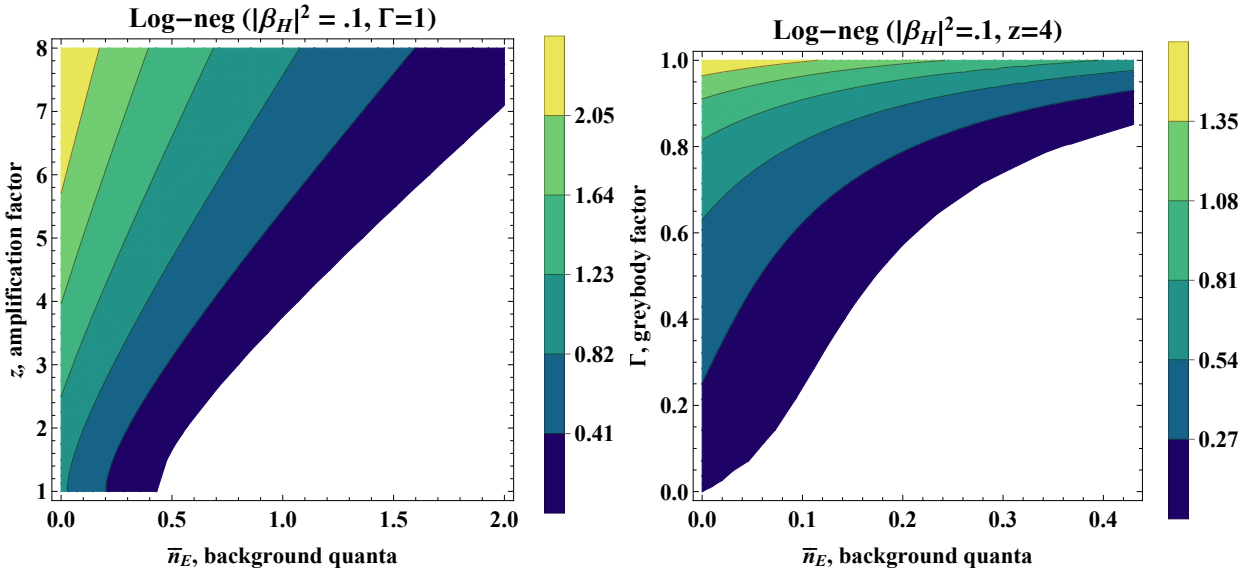

(a) (b)

Figure 4.6: Log-negativity of the Hawking pair, $(k_1^{(\text{out})}, k_2^{(\text{out})})$, for initial squeezing in the $k_1^{(\text{in})}$-mode. The amplification factor, z, quantifies the amount of squeezing (see discussion just above equation (4.37)). These plots are independent of the single-mode squeezing angle. (a) Log-negativity for $|\beta_H|^2 = 1$ and $\Gamma = 1$ in $(\bar{n}_E, z)$ parameter space. Not only does squeezing enhance the amount of correlations (relative to vacuum or thermal inputs), but it can also "revive" entanglement. For instance, when $z = 1$ (no initial squeezing), there are no quantum correlations when the number of background quanta $\bar{n}_E \gtrsim .4$. On the other hand, when squeezing is present and for any value of $\bar{n}_E$, there exists a value of z such that the log-negativity is non-zero. Qualitatively, one can see this by observing that, for $(\bar{n}_E, z) \gtrsim (.5, 2)$, the sudden-death line, which demarcates the boundary between the non-zero entanglement region and the null region, is linear. Therefore, the number of background quanta needed to kill the entanglement scales linearly with the amplification factor in this regime. (b) Log-negativity for $|\beta_H|^2 = 1$ and $z = 4$ in $(\bar{n}_E, \Gamma)$ parameter space. For a given value of z, the sudden-death line has an exponential-like tail, which carries the non-zero entanglement-region out to higher values of $\bar{n}_E$ as $\Gamma \to 1$. For $z = 4$ and at $\Gamma = 1$ as above, entanglement vanishes when $\bar{n}_E \approx 1$. This should be compared to the sudden-death value of $\bar{n}_E \approx .4$, when initial squeezing is not present. However, in the mid-region of parameter space, when approximately $\Gamma \in [.2, .7]$ and $\bar{n}_E \in [.1, .3]$, squeezing is actually detrimental, cf. to Figure 4.5a. This is due to the "bowing in" of the sudden-death line in this region, suggesting that a single-mode squeezed input is most beneficial when backscattering/loss is negligible, at least for $\bar{n}_E \gtrsim |\beta_H|^2$.

possibly leading to a complete death of entanglement over a large region of the analogue system's parameter space (see Figure 4.5 and the discussion on sudden-death entanglement in the previous subsection). A line of inquiry that follows this is then: (1) If we must operate in or close to a zero-entanglement region, perhaps dictated by spurious blackbody radiation, is there some way that we can push ourselves out of this barren region and into a nonzero-entanglement region, effectively reviving/enhancing the entanglement generated by the system? (2) And can we do so in such a way that still allows us make definitive statements about the physical nature of the analogue-gravity system under question? I.e. can we definitively say that Hawking process is "quantum" (produces entangled Hawking pairs) and still extract sought-after quantities, such as the Hawking temperature, with all these added complexities in hand? Providing conclusive answers to these questions is a bit tricky, but we can explore a few routes which are promising:

(i) *Lower the background temperature.* That is, operate at $T_E/T_H \ll 1$. This is the most obvious and, of course, the cleanest approach. This also greatly simplifies the problem because then we can just consider an initial quantum vacuum. In which case, any quanta and entanglement in the output would have to have been generated in the Hawking process, thus vindicating its quantum nature – i.e., vindicating the spontaneous Hawking effect. However, this amounts to operating at temperatures at or below the Hawking temperature of the analogue gravity system in question, which is likely to be quite low.

(ii) *Entanglement resonance.* One can revitalize entanglement by introducing another entangler (e.g. a separate two-mode squeezer) prior to the Hawking process, which is at resonance (phase-matched) with the Hawking process. This resonant condition allows for the successive entanglement-generation processes to add constructively, thus boosting the amount of entanglement in the output. The proviso is that precisely tuning the input resource to be at resonance with the Hawking process must be possible in order to observe constructive effects; otherwise, one could induce disentangling effects! Another aspect which one must consider is the ability to distinguish between the entanglement generation (and particle creation) mechanisms of the input resource and the Hawking process; for we wish to show that the Hawking process is a genuine quantum phenomena, in and of itself. Distinguishability between these processes is, perhaps, possible with sufficient control over the input resource and over the analogue-gravity system. This is a promising route, but we do not explore this possibility in detail here, as such has been discussed elsewhere in the literature (see, for instance, [172]).

(iii) *Leverage a single-mode resource.* Using a, e.g., single-mode squeezed state at the input can enhance entanglement generated by the Hawking process and even revive entanglement in regions of parameter space where there is none (see Figure 4.6), similar to entanglement-resonance phenomena. The benefit here is that the single-mode entanglement-enhancement effect does not rely on a resonance condition, and thus no tuning is necessary in order to see an enhancement/revival of entanglement. The drawback, however, is that this approach less robust to backscattering/loss, whenever the number of Hawking quanta is low. In any event, I view the utilization of a single-mode, non-classical resource as a promising avenue for enhancing/reviving quantum

correlations between generated Hawking-pairs. I thus provide a more detailed analysis of such in Figure 4.6.

The latter two prospects are indeed promising for enhancing the entangling effects of the Hawking process (and analogue-gravity systems in general). However, we must be careful about what conclusions we draw about the analogue-Hawking effect itself when such non-classical (even non-entangled) resources are in play. The reason is the following: There exists passive operations that can be done on non-classical, separable inputs, which can generate quantum correlations. For instance, linear optical networks – i.e., networks of orthogonal symplectic transformations (phase shifters and beamsplitters) – can generate quantum entanglement by using single-mode squeezing at the input [176, 177]. If we step back and consider this network as a blackbox, would one ascertain that the box is intrinsically quantum by nature, simply because there is quantum entanglement in the output? I would be skeptical of this conclusion, as one could rightly claim that the genuine quantum resource lies with the input states, not with the network operating on them. The question then becomes that, if we do allow for non-classical inputs to the Hawking process, is there a way to extract the quantum features of the output that are solely a consequence of the Hawking process and not necessarily due to our input resources? Perhaps the answer is yes, but this seems non-trivial to address and likely depends on the particular setup in question as well as the amount of control that we have over our input resources. One approach would be to show that the analogue system works as an amplifier (creates particles) for the entangled modes (Hawking pairs) under question. This is not something a linear optical network can do alone, as orthogonal symplectic transformations preserve particle number. Thus, concurrently observing entanglement, as well as amplification in the Hawking-pairs, would provide some support for the quantumness of the analogue-Hawking process, even in the presence of non-negligible, spurious background radiation. Although, more sophisticated methods may be warranted in practice.

4.5 White-black hole circuitry

The discussion so far has been restricted to the simple case of an analogue black hole. However, for several analogue-systems (optical systems in particular), there will exist a connected white-hole–black-hole pair, a *white-black hole*. See Figure 4.7 for an illustration. This occurs, e.g., in all optical setups where event horizons are formed by a refractive index front, which physically corresponds to a spatially-varying, background pump-pulse (see references [158, 159] and Figure 4.1). On trailing edge of the index front (see Figure 4.1 for an illustration) lies the white hole event horizon, while the black hole event horizon lies on the leading edge. The physics is quite rich in these setups because the black hole and white hole share the same interior, thus leading to an effective interaction between the black hole event horizon and the white hole event horizon. For instance, the particles created by the black hole, which fall into its interior, actually seed the particle-creation mechanism of the white hole. Since the white-hole dynamics is the inverse of the black-hole dynamics (see e.g. [178] and Figure 4.8), this can actually lead to cancellation effects. As example, when there is significant backscattering ($\Gamma \approx 0$) in an analogue white-black hole, all of the particles generated by the black hole fall into its interior and then get re-absorbed into the classical

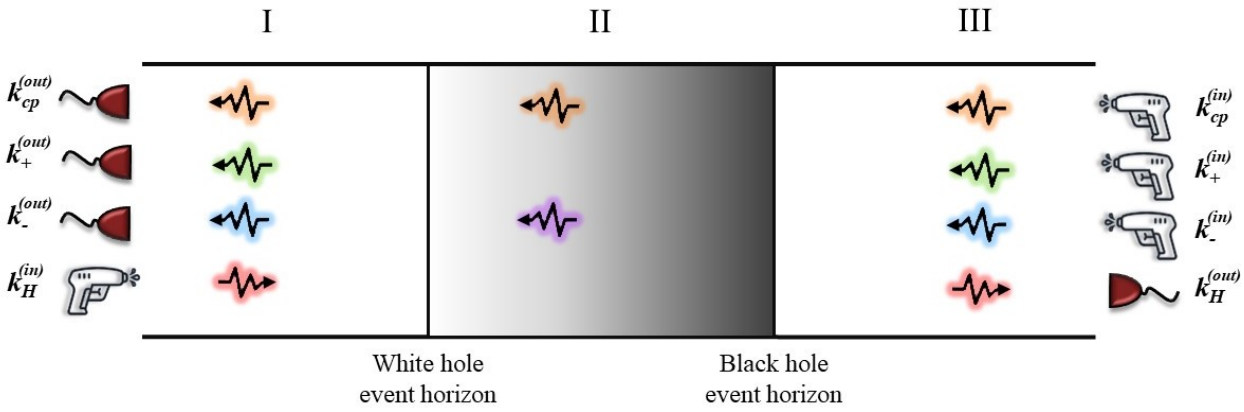

Figure 4.7: Scattering picture for an analogue white-black hole system. The original mode labels have been reintroduced, since the in/out mode spaces have been expanded from 3 modes to 4. The in/out regions correspond to I and III above, while the interaction region (the interior region) is restricted to the finite space-time region II. Photon guns illustrate the in-modes while detectors illustrate the out-modes. The flow from in to out is physically determined by the group velocity of the wavepackets. Observe that the in and out mode spaces are identical, due to the asymptotic regions, I and III, having the same mode structure. Note, for instance, that there are no white-black hole interior modes which connect the in Hawking-mode of the white hole, $k_H^{(\text{in})}$, to the out Hawking-mode of the black hole, $k_H^{(\text{out})}$. Such is a consequence of the causal structure, as no information sent to the white hole event horizon can ever go through and make it out to the other side; i.e. information can only flow from right to left! This is the signature of a "good" analogue white-black hole.

degrees of freedom of the hole itself. Thus, the white-black ole self-stabilizes! This is because the particle-creation mechanism at the white-hole event horizon is exactly undoing the particle-creation mechanism at the black hole event horizon (the squeezers are off-resonance). Note that similar phenomena do not occur when e.g. only an analogue black hole exists, since backscattering just amounts to a shifting of particles/correlations to other modes (the counter-propagating mode) and not to an actual decrease in particles created (cf. to Figure 4.4).

Though more quantitative and more qualitative descriptions of these complex scenarios is duly warranted, I will refrain from analyzing these systems any further, leaving more detailed studies for future work.

4.6 Summary and future work

In this work, I utilized the linear nature of the Hawking effect, as well as its apparent universality, to provide a conceptually simple description of the Hawking process (including backscattering) in terms of a discrete set of elementary operations – e.g. in terms of a network of squeezers and beamsplitters. The Bloch-Messiah decomposition provides the formal equivalence between this elementary set of operations and the actual physical process, from which one can draw physically intuitive diagrams (see e.g. Figure 4.3) that are just as well subject to a formal analysis per this equivalence. Hence, one can build a coherent and unobstructed landscape consisting of the nitty-gritty micro-physical details of the process, the conceptual diagrams used to gain intuition about the process, and the reduction of such into fundamental ingredients (squeezers, beamsplitters, etc.) that any user can digest. As an example, I applied this approach to the particularly simple case of an evaporating, optical-analogue black hole (see e.g. Figures 4.3 and 4.4). The black-hole evaporation dynamics was then translated into the language of symplectic transformations and the Gaussian formalism, which I further utilized to explore quantum correlations generated by the Hawking process, for various input states and in the face of debilitating, environmental effects such as a non-negligible thermal background and loss. From there, I showed precisely how a non-zero background temperature together with backscattering/loss can lead to "entanglement sudden-death", even when an arbitrary number of entangled Hawking-pairs are generated in the evaporation process. I then provided a way to enhance and even "revive" this entanglement with single-mode, non-classical resources. Following this, a broad discussion was given about the quantum aspects of the Hawking process itself, in the face of the extra complexities introduced through noise and non-classical resources. Though, any definitive statements to be made in this regard will likely be platform-dependent, and experiment should have a say here as well. Finally, I posed a set circuits corresponding to more complex scenarios than that of a simple evaporating black-hole (see Figure 4.8). Physically, any given circuit in Figure 4.8 corresponds to an analogue white-hole–black-hole pair (a white-black hole) which share an interior. These provide a rich playground for further study from many different routes. Yet, though these setups are certainly plausible, as one can argue on physical grounds, confirmation that they accurately provide a description of the scattering dynamics in the appropriate regimes is undoubtedly desirable, from an analytic and numerical perspective. Examining how good such dynamics (particularly Figure 4.8c) mimics recent results in the fiber-optical-analogue context (see, for instance, the experiment of [159] and the numerical

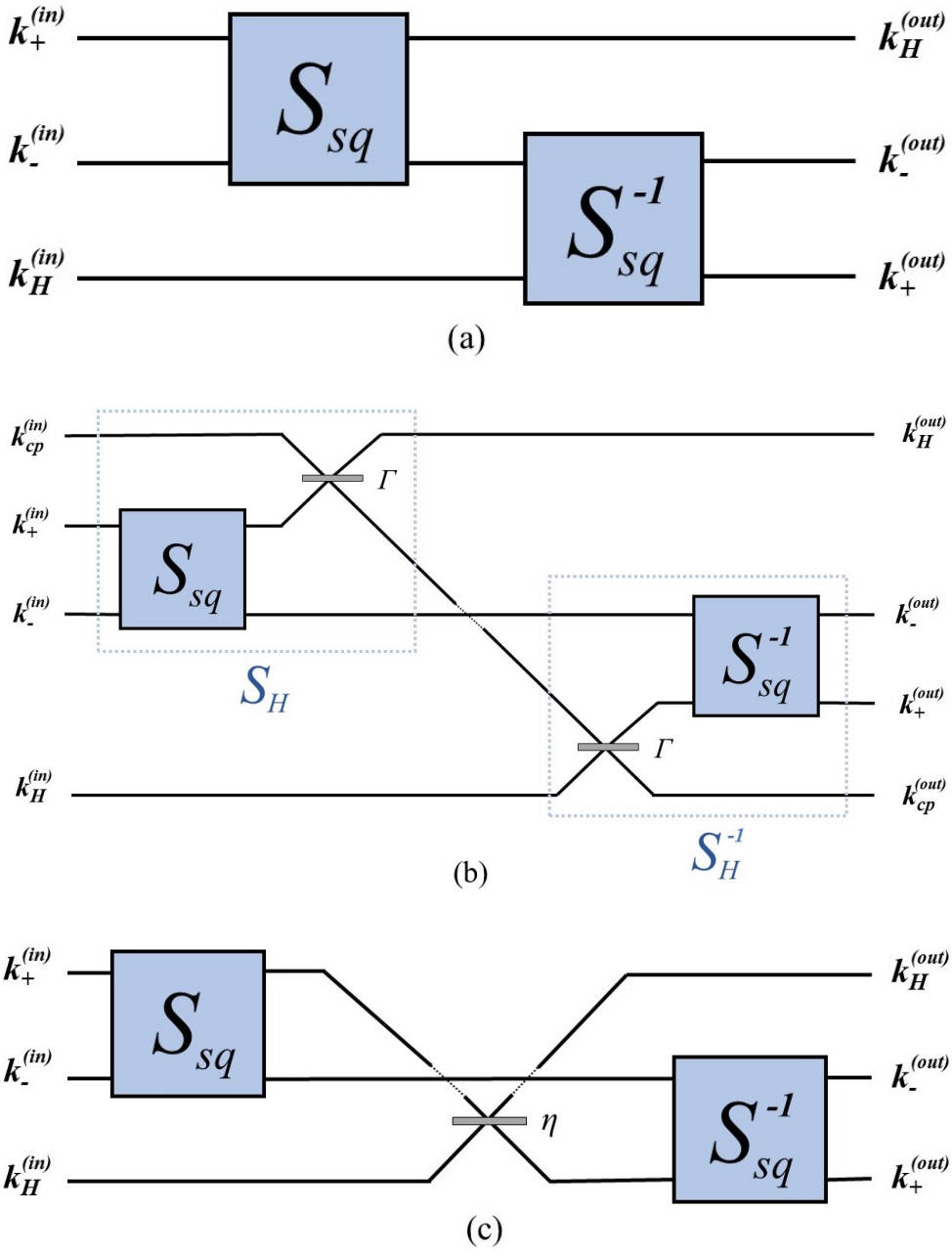

Figure 4.8: Circuit-equivalents for various white-black holes (white-hole–black-hole pair) systems. Circuits (a) and (b) assume that the white hole and black hole event horizons are well-separated, such that results of Section 4.2 simply carry over. (a) White-black hole with no backscattering. (b) White-black hole with backscattering. (c) A "partially transparent" white-black hole. In this case, the event horizons are not perfect (they are non-blocking, in the language of references [162, 163, 164]), and there is some finite probability, η, to tunnel through the white hole event horizon. This serves as a simple analytic model for imperfect, optical analogue-systems (cf. to references [163, 164, 159]).

studies of [163, 164]) is an interesting prospect as well. These are some avenues that I am currently exploring.

CHAPTER 5. EPILOGUE

I want to enforce a colloquial tone in this final chapter and also leave it a bit open-ended. Many use this opportunity to summarize research contributions and provide possible extensions for future work, but I already considered most of that in Sections 3.5 and 4.6, in the contexts of space-based quantum-communication and optical analogue-gravity. Perhaps, however, this is a good time to discuss current and future research directions not alluded to so far in (nor particularly in line with) this thesis.

One concrete direction, which I have been recently exploring, is the quantum error correction/protection properties of quantum information scramblers. In brief, quantum scrambling has to do with complex many-body interactions, which lead to the delocalization of quantum information into the degrees of freedom of the entire system. The complexity of these interactions provides a rich landscape for many research directions. To name a few: (i) The complexity of scramblers makes them novel physical systems to explore with near-to-mid term quantum simulators; (ii) This complexity also provides a novel encoding mechanism for robust protection of delicate quantum information, in the face of incoherent errors. For the latter, it has been shown that scramblers physically protect against projective-measurement errors, even when the errors occur on an extensive number of the encoded qubits [179]. Regimes of faithful and unfaithful protection have also been linked to entanglement phase-transitions in such systems, where e.g. faithful protection occurs when the system occupies a volume-law entanglement phase (whereby the entanglement scales linearly with the number of qubits). The transition to an area-law entanglement phase (sub-linear scaling with the number of qubits) in the face of projective measurements then signals the loss of delicate quantum information (unfaithful protection; see reference [179] for more details). I (and collaborators) have been working to generalize these results to include both measurement effects and decoherence as well as effects from noisy ancillae qubits which assist with encoding. These analyses seem pertinent as all such noise mechanisms will likely be present in near-term quantum devices and because one wishes to precisely observe how the entanglement structure of the scrambling system responds to a variety of deleterious effects.[1] As far as connections with this thesis goes, this topic has nothing remotely to do with photons, which has been the primary focus to this point! Nevertheless, from my perspective, this is an interesting topic to explore further.[2]

Shifting focus back towards the contents of this thesis, I have hoped to grant the reader with some perspective on the simplicity and breadth which one can ascribe to photons and their various endeavours – from the exploration of fundamental physics (see, e.g., Chapter 4) to the technological applications of near-term, long-distance quantum communications (see,

[1] As an aside, there are also interesting connections between these entanglement phase-transitions and "purification phase-transitions", whereby e.g. a thermalized system undergoes both unitary and projective-measurement dynamics. If the rate of projective measurements is large enough, the system can purify (go to a pure state) in some polynomial amount of time, depending on the nature of the unitary dynamics. For scrambling unitary dynamics, a large projective-measurement rate is required. The transition from the thermalized state to the purified state, for scrambling dynamics, evidently occurs at the same critical point as in entanglement phase-transitions; see, for instance, [179, 180].

[2] Recall that, in Chapter 1, I nearly blamed photons for my meandering in research, but no photons are to be found here. Perhaps the meandering is, alas, mine own.

e.g., Chapter 3). Simple and sufficiently ambiguous questions still remain: What more do photons have to offer us in the domain of quantum-technological applications? And also, what more can photons tell us, in general, about our world and the universe? Though ambiguous, these questions drive my research – keeping both my feet on the ground and my head in the clouds.

APPENDIX A. ENTANGLEMENT DISTRIBUTION: SUPPLEMENTARY METHODS

A.1 Extended noise model

We now consider photon transmission in the presence of background photons. We analyze the scenario in which a source generates an entangled photon pair and distributes the individual photons to two parties, Alice (A) and Bob (B). We allow the distributed photons to mix with spurious photons (noise) from an uncorrelated thermal source, assuming a low thermal background (which can be ensured via stringent filtering). We then determine, in the high loss and low noise regime, the fidelity of the distributed entangled photon pair.

First, consider a tensor product of thermal states for the horizontal and vertical polarization modes:

$$\Theta^{\bar{n}_H} \otimes \Theta^{\bar{n}_V} = \left(\sum_{n=0}^{\infty} \left(\frac{\bar{n}_H^n}{(\bar{n}_H + 1)^{n+1}} \right) |n\rangle\langle n| \right) \otimes \left(\sum_{n=0}^{\infty} \left(\frac{\bar{n}_V^n}{(\bar{n}_V + 1)^{n+1}} \right) |n\rangle\langle n| \right), \tag{A.1}$$

where $\bar{n}_k$ is the average number of photons in the thermal state for the polarization mode k. We assume this state comes from an incoherent source with no polarization preference (e.g., the sun), such that $\bar{n}_H = \bar{n}_V =: \bar{n}/2$. Furthermore, we assume some (non-polarization) filtering procedure, which reduces the number of background thermal photons, such that $\bar{n} \ll 1$. We then rewrite the above state to first order in the small parameter $\bar{n}$:

$$\Theta^{\frac{\bar{n}}{2}} \otimes \Theta^{\frac{\bar{n}}{2}} \approx \left(\left(1 - \frac{\bar{n}}{2}\right) |0\rangle\langle 0| + \frac{\bar{n}}{2} |1\rangle\langle 1| \right) \otimes \left(\left(1 - \frac{\bar{n}}{2}\right) |0\rangle\langle 0| + \frac{\bar{n}}{2} |1\rangle\langle 1| \right) \tag{A.2}$$

$$\approx (1 - \bar{n}) |\text{vac}\rangle\langle\text{vac}| + \frac{\bar{n}}{2} \left(|H\rangle\langle H| + |V\rangle\langle V| \right), \tag{A.3}$$

where $|\text{vac}\rangle = |0\rangle \otimes |0\rangle$, and

$$|H\rangle \stackrel{\text{def}}{=} |1\rangle \otimes |0\rangle, \tag{A.4}$$

$$|V\rangle \stackrel{\text{def}}{=} |0\rangle \otimes |1\rangle. \tag{A.5}$$

We thus define our approximate thermal background state as

$$\widetilde{\Theta}^{\bar{n}} \stackrel{\text{def}}{=} (1 - \bar{n}) |\text{vac}\rangle\langle\text{vac}| + \frac{\bar{n}}{2} \left(|H\rangle\langle H| + |V\rangle\langle V| \right), \tag{A.6}$$

which serves as a good approximation to a low thermal background. The transmission channel from the source to the ground is then approximately

$$\mathcal{L}_{\eta_{\text{sg}},\bar{n}}(\rho_{A_1A_2}) \stackrel{\text{def}}{=} \text{Tr}_{E_1E_2}[(U^{\eta_{\text{sg}}}_{A_1E_1} \otimes U^{\eta_{\text{sg}}}_{A_2E_2})(\rho_{A_1A_2} \otimes \widetilde{\Theta}^{\bar{n}}_{E_1E_2})(U^{\eta_{\text{sg}}}_{A_1E_1} \otimes U^{\eta_{\text{sg}}}_{A_2E_2})^\dagger], \tag{A.7}$$

where $U^{\eta_{\text{sg}}}$ is the beamsplitter unitary (see, e.g., Section 2.2), and A_1 and A_2 refer to the horizontal and vertical polarization modes, respectively, of the dual-rail quantum system being transmitted; similarly for E_1 and E_2. Note that for $\bar{n} = 0$, the transformation given by Eq. (A.7) is equal to the transformation in (2.195). For a source state ρ_{AB}^S, with $A \equiv A_1 A_2$ and $B \equiv B_1 B_2$, the quantum state shared by Alice and Bob after transmission of the state ρ_{AB}^S from the satellite to the ground stations is

$$(\mathcal{L}_{\eta_{\text{sg}}^{(1)},\bar{n}_1} \otimes \mathcal{L}_{\eta_{\text{sg}}^{(2)},\bar{n}_2})(\rho_{AB}^S). \tag{A.8}$$

Let us first assume that we have an ideal two-photon source, which generates one of the four two-photon polarization-entangled Bell states, i.e., a state of the form $\rho^S = \Phi^{\pm} \stackrel{\text{def}}{=} |\Phi^{\pm}\rangle\langle\Phi^{\pm}|$ or $\rho^S = \Psi^{\pm} \stackrel{\text{def}}{=} |\Psi^{\pm}\rangle\langle\Psi^{\pm}|$, where

$$\left|\Phi^{\pm}\right\rangle \stackrel{\text{def}}{=} \frac{1}{\sqrt{2}}(|H,H\rangle \pm |V,V\rangle), \tag{A.9}$$

$$\left|\Psi^{\pm}\right\rangle \stackrel{\text{def}}{=} \frac{1}{\sqrt{2}}(|H,V\rangle \pm |V,H\rangle). \tag{A.10}$$

After transmission, we assume post-selection on coincident events, along with high loss and low noise ($\eta_{\text{sg}}^{(1)}, \eta_{\text{sg}}^{(2)}, \bar{n} \ll 1$). The post-selection allows one to discard any occurrence in which one site registers a photon and the other does not. Furthermore, under the high-loss and low-noise assumptions, we can discard potential four-photon and three-photon occurrences, as these occur with negligible probability compared to the two-photon events. We thus focus our full attention on the two-photon state corresponding to one photon received at Alice's site and one photon received at Bob's site. Mathematically, this (unnormalized) state is given by

$$\Pi_{AB}(\mathcal{L}_{\eta_{\text{sg}}^{(1)},\bar{n}_1} \otimes \mathcal{L}_{\eta_{\text{sg}}^{(2)},\bar{n}_2})(\rho_{AB}^S)\Pi_{AB}, \tag{A.11}$$

where

$$\Pi_{AB} \stackrel{\text{def}}{=} (|H\rangle\langle H|_A + |V\rangle\langle V|_A) \otimes (|H\rangle\langle H|_B + |V\rangle\langle V|_B) \tag{A.12}$$

is the projection onto the two-photon-coincidence subspace. With $\rho_{AB}^S = \Phi_{AB}^{\pm}$, it is straightforward to show that

$$\begin{aligned}
&\Pi_{AB}(\mathcal{L}_{\eta_{\text{sg}}^{(1)},\bar{n}_1} \otimes \mathcal{L}_{\eta_{\text{sg}}^{(2)},\bar{n}_2})(\Phi_{AB}^{\pm})\Pi_{AB} \\
&\quad = \frac{1}{2}(x_1 x_2 + y_1 y_2 \pm z_1 z_2)\Phi_{AB}^{+} \\
&\qquad + \frac{1}{2}(x_1 x_2 + y_1 y_2 \mp z_1 z_2)\Phi_{AB}^{-} \\
&\qquad + \frac{1}{2}(x_1 y_2 + y_1 x_2)\Psi_{AB}^{+} \\
&\qquad + \frac{1}{2}(x_1 y_2 + y_1 x_2)\Psi_{AB}^{-},
\end{aligned} \tag{A.13}$$

where

$$x_1 \stackrel{\text{def}}{=} (1-\bar{n}_1)\eta_{\text{sg}}^{(1)} + \frac{\bar{n}_1}{2}((1-2\eta_{\text{sg}}^{(1)})^2 + (\eta_{\text{sg}}^{(1)})^2), \tag{A.14}$$

$$y_1 \stackrel{\text{def}}{=} \frac{\bar{n}_1}{2}(1-\eta_{\text{sg}}^{(1)})^2, \tag{A.15}$$

$$z_1 \stackrel{\text{def}}{=} (1-\bar{n}_1)\eta_{\text{sg}}^{(1)} - \bar{n}_1\eta_{\text{sg}}^{(1)}(1-2\eta_{\text{sg}}^{(1)}), \tag{A.16}$$

with analogous definitions for x_2, y_2, z_2. The fidelity of this quantum state conditioned on one photon received by Alice and one photon received by Bob is therefore

$$F_{\Phi^\pm} \stackrel{\text{def}}{=} \frac{\langle\Phi^+|\,\Pi(\mathcal{L}_{\eta_{\text{sg}}^{(1)},\bar{n}_1}\otimes\mathcal{L}_{\eta_{\text{sg}}^{(2)},\bar{n}_2})(\Phi_{AB}^\pm)\Pi\,|\Phi^+\rangle}{\text{Tr}\left[\Pi(\mathcal{L}_{\eta_{\text{sg}}^{(1)},\bar{n}_1}\otimes\mathcal{L}_{\eta_{\text{sg}}^{(2)},\bar{n}_2})(\Phi_{AB}^\pm)\Pi\right]} \tag{A.17}$$

$$= \frac{\frac{1}{2}(x_1x_2 + y_1y_2 \pm z_1z_2)}{(x_1+y_1)(x_2+y_2)}. \tag{A.18}$$

Assuming that $\eta_{\text{sg}}^{(1)} = \eta_{\text{sg}}^{(2)} = \eta_{\text{sg}}$ and $\bar{n}_1 = \bar{n}_2 = \bar{n}$, so that $x_1 = x_2$, $y_1 = y_2$, and $z_1 = z_2$, and under the high-loss and low-noise assumption, for $\rho^S = \Phi^+$ this reduces to

$$F_{\Phi^+} \approx \frac{1}{4}\left(1 + \frac{3}{\left(1+\frac{\bar{n}}{\eta_{\text{sg}}}\right)^2}\right). \tag{A.19}$$

The ratio $\frac{\eta_{\text{sg}}}{\bar{n}}$ is just the local signal-to-noise ratio (SNR). Thus, assuming a fidelity constraint $F \gtrsim F^\star$, we obtain the following bound on the SNR needed at each site in order to maintain a fidelity of $F^\star$ during operation:

$$\text{SNR} \stackrel{\text{def}}{=} \frac{\eta_{\text{sg}}}{\bar{n}} \gtrsim \frac{1}{\left(\sqrt{\frac{3}{4F^\star-1}} - 1\right)} \approx \frac{3}{2}(1-F^\star)^{-1}, \tag{A.20}$$

Here, we have assumed that the fidelity lies within some small range close to one (e.g., $.95 \leq F^\star \leq 1$) and expanded to first order in $1-F^\star$. As an example, consider $F^\star = .99$. Then, we must have SNR $\gtrsim 150$ at each site. Given that $\eta_{\text{sg}} \sim 10^{-3}$, this implies a constraint on the number of background photons per detection window of $\bar{n} \lesssim 7 \times 10^{-6}$.

A.1.1 Non-ideal Bell states

Let us now consider an initially imperfect Bell state generated by a non-ideal entangled photon-pair source. Specifically, we consider the state

$$\rho^S(f_0) \stackrel{\text{def}}{=} f_0\Phi^+ + \left(\frac{1-f_0}{3}\right)(\Phi^- + \Psi^+ + \Psi^-), \tag{A.21}$$

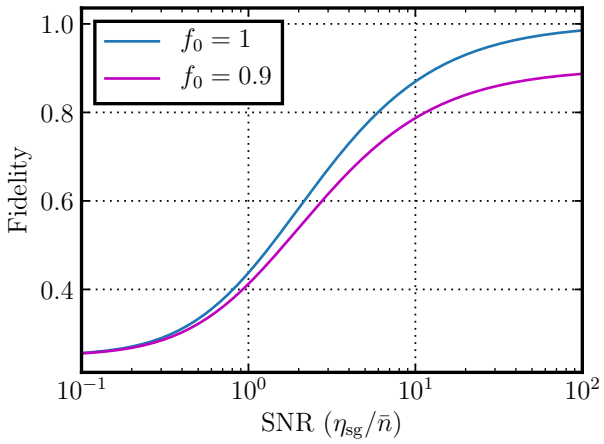

Figure A.1: Fidelity of satellite-to-ground entanglement transmission as a function of the signal-to-noise ratio (SNR) of the transmission medium. The source state is in Eq. (A.21), and the fidelity after transmission is given by Eq. (A.24).

where f_0 is the initial fidelity. Using the fact that

$$\begin{aligned}
&\Pi_{AB}(\mathcal{L}_{\eta_{\mathrm{sg}}^{(1)},\bar{n}_1} \otimes \mathcal{L}_{\eta_{\mathrm{sg}}^{(2)},\bar{n}_2})(\Psi_{AB}^{\pm})\Pi_{AB} \\
&\quad = \frac{1}{2}(x_1y_2 + y_1x_2)\Phi_{AB}^{+} \\
&\qquad + \frac{1}{2}(x_1y_2 + y_1x_2)\Phi_{AB}^{-} \\
&\qquad + \frac{1}{2}(x_1x_2 + y_1y_2 \pm z_1z_2)\Psi_{AB}^{+} \\
&\qquad + \frac{1}{2}(x_1x_2 + y_1y_2 \mp z_1z_2)\Psi_{AB}^{-},
\end{aligned} \tag{A.22}$$

in the high-loss low-noise regime, and in the symmetric case $\eta_{\mathrm{sg}}^{(1)} = \eta_{\mathrm{sg}}^{(2)} = \eta_{\mathrm{sg}}$ and $\bar{n}_1 = \bar{n}_2 = \bar{n}$, we obtain

$$\begin{aligned}
&F(f_0) \\
&\quad \stackrel{\mathrm{def}}{=} \frac{\langle\Phi^{+}|\,\Pi(\mathcal{L}_{\eta_{\mathrm{sg}}^{(1)},\bar{n}_1} \otimes \mathcal{L}_{\eta_{\mathrm{sg}}^{(2)},\bar{n}_2})(\rho^{S}(f_0))\Pi\,|\Phi^{+}\rangle}{\mathrm{Tr}\left[\Pi(\mathcal{L}_{\eta_{\mathrm{sg}}^{(1)},\bar{n}_1} \otimes \mathcal{L}_{\eta_{\mathrm{sg}}^{(2)},\bar{n}_2})(\rho^{S}(f_0))\Pi\right]} &\text{(A.23)} \\
&\quad \approx \frac{1}{4}\left(1 + \frac{4f_0 - 1}{\left(1 + \frac{\bar{n}}{\eta_{\mathrm{sg}}}\right)^2}\right). &\text{(A.24)}
\end{aligned}$$

Note that $1/4 \leq F \leq f_0$. See Fig. A.1 for a plot of this fidelity as a function of the signal-to-noise ratio.

A.1.2 Background photon flux

The background photon number $\bar{n}$ can be expressed in terms of the photon flux/rate at a receiving site. Let $\mathcal{R}$ be the number of background photons per second detected at a receiving site and ΔT be the coincidence time-window. Then, $\bar{n} = \mathcal{R}\Delta T$. Assuming background photons collected from, e.g., moonlight or sunlight, are the dominant source of noise, we have the following expression for the background photon rate [181, 182]:

$$\mathcal{R} = \frac{H\Omega_{\text{fov}}\pi r^2 \Delta\lambda}{hc/\lambda}, \tag{A.25}$$

where hc/λ is the photon energy at mean wavelength λ (h is Planck's constant and c is the speed of light), $\Delta\lambda$ is the filter bandwidth, Ω_{fov} is the field of view of a receiving telescope (in steradians, sr) with radius r, and H is the total spectral irradiance in units $\text{Wm}^{-2}\mu\text{m}^{-1}\text{sr}^{-1}$. In the case of daytime operating conditions, the total spectral irradiance includes direct solar irradiance as well as diffuse sky radiation, with the latter consisting mainly of solar light scattered by atmospheric constituents.

The spectral irradiance is generally a complicated function of atmospheric conditions, the sun/moon sky position relative to the telescope pointing angle, time of day and year, etc. Thus, for simplicity, in what follows we keep H as an open parameter but consider it to fall roughly within a typical range of $H \in [10^{-5}, 25]$ (in units $\text{Wm}^{-2}\mu\text{m}^{-1}\text{sr}^{-1}$), associated with clear-sky conditions, with the lower value corresponding to a moonless clear night and the upper value corresponding to clear daytime conditions, when the sun is in near-view of the optical receiver (see, e.g., Refs. [181, 182]).

Using the relation $\bar{n} = \mathcal{R}\Delta T$, with $\mathcal{R}$ given by Eq. (A.25), in Fig. A.2 we plot the fidelity in Eq. (A.19) as a function of the spectral irradiance H for several orbital altitudes h and ground-station separation distances d. To make the plot, we consider the situation depicted in Fig. 3.3, in which the satellite passes over the zenith of two ground stations and is at the midpoint between them. Note that spectral irradiance values on the order of 1 $\text{Wm}^{-2}\mu\text{m}^{-1}\text{sr}^{-1}$ (and above) correspond to clear daytime conditions [181, 95, 182]. Thus, for our chosen filter parameters, we see that entanglement distribution across, e.g., a ground-station separation distance of more than 2000 km, only seems feasible during the night ($H \lesssim 10^{-2}$ $\text{Wm}^{-2}\mu\text{m}^{-1}\text{sr}^{-1}$). We note, however, that these results are quite sensitive to the filtering parameters, owing to the steep slope of the fidelity in its mid-region.

An interesting extension of these results would be to consider a dynamic model, in which one parameterizes the satellite-to-ground transmittance and background photon rate in time. We do such a parameterization for the transmittance in this work; however, parameterizing the background photon rate requires real-time modeling of, e.g., the sun position relative to the satellite orbit, modeling diffuse sky radiation, etc. Work along these lines has already been done for satellite-to-ground quantum key distribution between a satellite and a lone ground station (see, e.g., Ref. [182]). A full, dynamical analysis of the fidelity for a noisy, global-scale satellite-to-ground entanglement distribution protocol—utilizing, e.g., the asymmetric noise model derived above—is an interesting direction for future research.

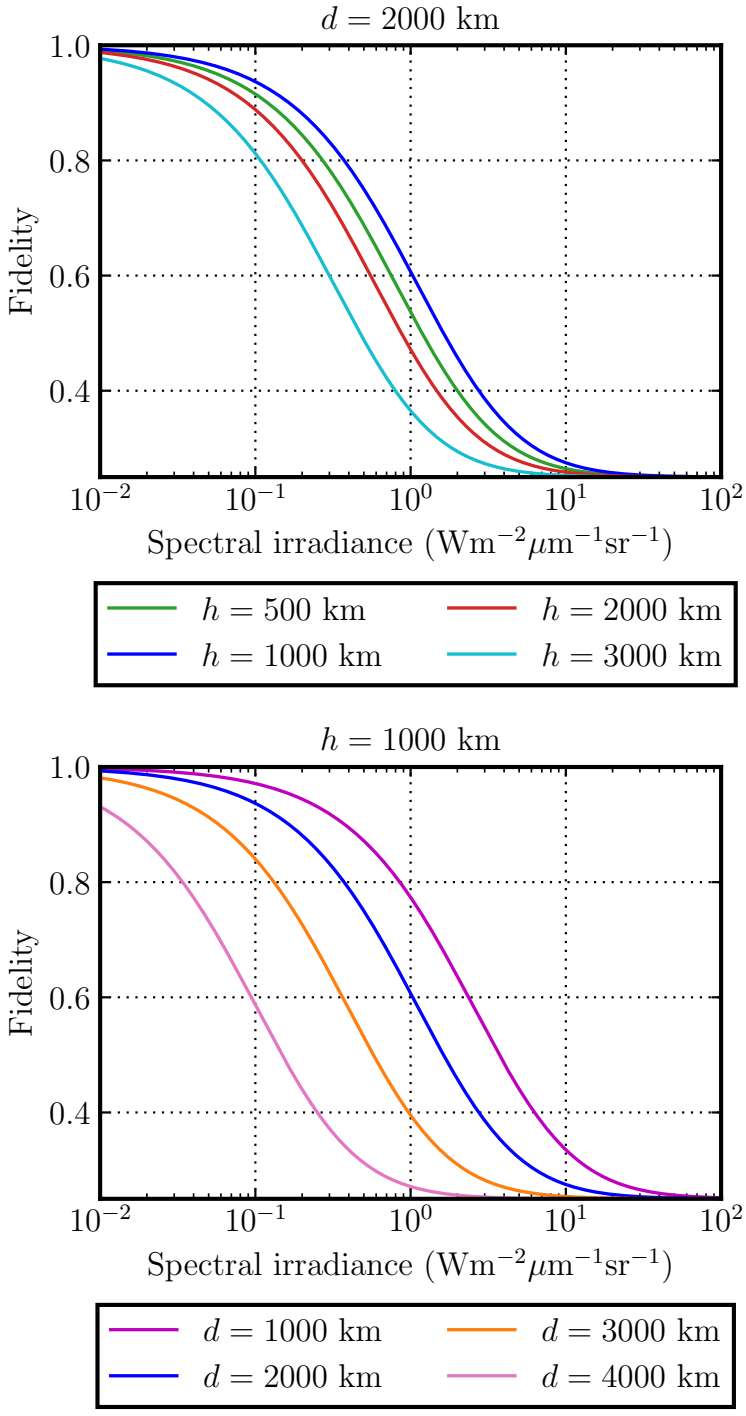

Figure A.2: Fidelity of satellite-to-ground entanglement transmission as a function of spectral irradiance. We consider transmission of the Bell state Φ^+ according to the scenario depicted in Fig. 3.3. The fidelity is given in Eq. (A.19), and the average background photon number is given by $\bar{n} = \mathcal{R}\Delta T$, with $\mathcal{R}$ given by Eq. (A.25). In order to calculate $\mathcal{R}$, we let $\lambda = 810$ nm, $\Delta\lambda = 1$ nm, $\Omega_{\text{fov}} = 100$ μsr, $r = 0.5$ m, and $\Delta T = 1$ ns; see, e.g., Refs. [182, 104, 131].

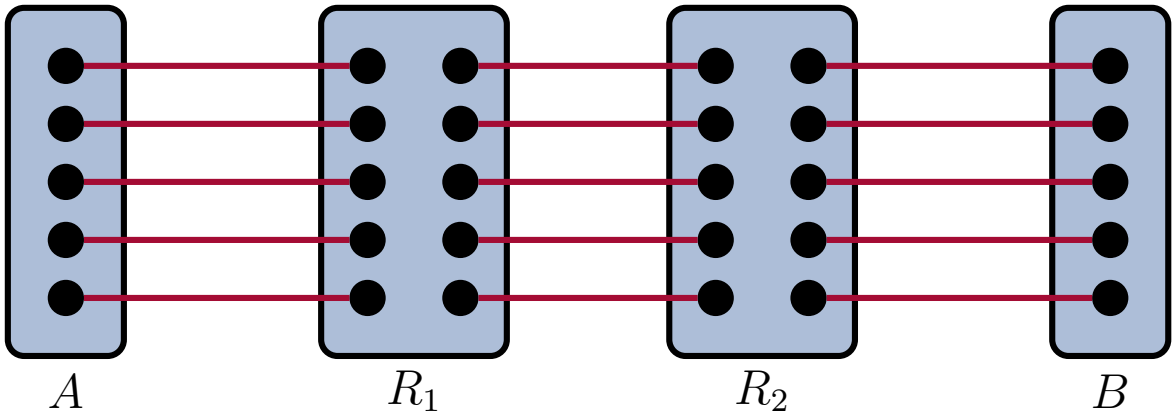

Figure A.3: A repeater chain with $M = 3$ elementary links. All of the elementary links have equal length, and there are $N_{\text{mem}} = 5$ quantum memories per repeater half-node.

A.2 Quantum repeater rates

In order to compare the satellite-based entanglement-distribution rates obtained in this work with rates that can be achieved using ground-based quantum repeater schemes, we consider a chain of quantum repeaters of total length d in which there are M elementary links and each repeater "half-node" has N_{mem} quantum memories; see Fig. A.3 for an example. This results in N_{mem} parallel quantum repeater chains between the end nodes. If we allow entanglement distribution to occur independently for each of the parallel chains, and we assume that the quantum memories have infinite coherence time, then the expected number of time steps until one end-to-end pair is obtained, i.e., the expected waiting time, has been shown in [183, Appendix B] to be

$$W_{N,N_{\text{mem}}} = \sum_{n=1}^{\infty} \left(1 - \left(1 - (1-p)^{n-1}\right)^{M}\right)^{N_{\text{mem}}}. \tag{A.26}$$

Now, the duration of each time step, i.e., the repetition rate, is limited by the classical communication time between neighboring nodes for heralding of the signals. (This is the best-case scenario. We do not consider other factors that affect the repetition rate, such as the memory read-write time.) The classical communication time is given by $\frac{2(d/M)}{c}$, resulting in a repetition rate of $\frac{c}{2(d/M)}$ for each of the N_{mem} parallel links of an elementary link. The total repetition rate is therefore $\frac{cN_{\text{mem}}}{2(d/M)}$. The formula in Eq. (3.11) for the rate then follows.

A higher rate than the one in Eq. (3.11) can be achieved by allowing for spatial multiplexing, i.e., by allowing cross connections between the different parallel chains [184]. An analytic expression for the waiting time in this scenario, in the case of $M = 2$ elementary links, has been derived in Ref. [185]. A general formula for the waiting time for an arbitrary number M of elementary links appears to be unknown.

REFERENCES

[1] Khatri Sumeet, Anthony J Brady, Renée A Desporte, Manon P Bart, and Jonathan P Dowling. Spooky action at a global distance: analysis of space-based entanglement distribution for the quantum internet. *NPJ Quantum Information*, 7(1), 2021.

[2] Lior Cohen, Anthony J Brady, Zichang Huang, Hongguang Liu, Dongxue Qu, Jonathan P Dowling, and Muxin Han. Efficient Simulation of Loop Quantum Gravity: A Scalable Linear-Optical Approach. *Physical Review Letters*, 126(2):020501, 2021.

[3] Manjit Kumar. *Quantum: Einstein, Bohr and the great debate about the nature of reality*. Icon Books Ltd, 2008.

[4] Hendrik Antoon Lorentz, Albert Einstein, Hermann Minkowski, Hermann Weyl, and Arnold Sommerfeld. *The principle of relativity: a collection of original memoirs on the special and general theory of relativity*. Courier Corporation, 1952.

[5] Charles W Misner, Kip S Thorne, and John Archibald Wheeler. *Gravitation*. Macmillan, 1973.

[6] Clifford M Will. *Theory and experiment in gravitational physics*. Cambridge University Press, 2018.

[7] Stuart J Freedman and John F Clauser. Experimental test of local hidden-variable theories. *Physical Review Letters*, 28(14):938, 1972.

[8] Alain Aspect, Philippe Grangier, and Gérard Roger. Experimental realization of Einstein-Podolsky-Rosen-Bohm Gedankenexperiment: a new violation of Bell's inequalities. *Physical Review Letters*, 49(2):91, 1982.

[9] Vincent Jacques, E Wu, Frédéric Grosshans, François Treussart, Philippe Grangier, Alain Aspect, and Jean-François Roch. Experimental realization of Wheeler's delayed-choice gedanken experiment. *Science*, 315(5814):966–968, 2007.

[10] Philip Ball. Squeezing more from gravitational-wave detectors. *Physics*, 12(139), 2019.

[11] Pieter Kok, William J Munro, Kae Nemoto, Timothy C Ralph, Jonathan P Dowling, and Gerard J Milburn. Linear optical quantum computing with photonic qubits. *Reviews of Modern Physics*, 79(1):135, 2007.

[12] Jianwei Wang, Fabio Sciarrino, Anthony Laing, and Mark G Thompson. Integrated photonic quantum technologies. *Nature Photonics*, 14(5):273–284, 2020.

[13] Sheng-Kai Liao, Wen-Qi Cai, Johannes Handsteiner, Bo Liu, et al. Satellite-relayed intercontinental quantum network. *Physical Review Letters*, 120:030501, January 2018.

[14] Juan Yin, Yuan Cao, Yu-Huai Li, Sheng-Kai Liao, et al. Satellite-based entanglement distribution over 1200 kilometers. *Science*, 356(6343):1140–1144, 2017.

[15] H. J. Kimble. The quantum internet. *Nature*, 453, 2008.

[16] Jonathan Dowling. *Schrödinger's Web: Race to Build the Quantum Internet*. Taylor & Francis, 2020.

[17] Anthony J Brady and Stav Haldar. Relativistic frame-dragging and the Hong-Ou-Mandel dip – a primitive to gravitational effects in multi-photon quantum-interference. *arXiv:2006.04221*, 2020.

[18] Herbert Goldstein, Charles P Poole, and John Safko. *Classical Mechanics*, volume 2. Addison-Wesley Reading, MA, 1950.

[19] Paul Adrien Maurice Dirac. *The Principles of Quantum Mechanics*. Oxford University Press, 1981.

[20] David Tong: Lectures on Quantum Field Theory. `https://www.damtp.cam.ac.uk/user/tong/qft.html`. Accessed: 2021-02-13.

[21] John Garrison and Raymond Chiao. *Quantum Optics*. Oxford University Press, 2008.

[22] Pieter Kok and Brendon W Lovett. *Introduction to Optical Quantum Information Processing*. Cambridge University Press, 2010.

[23] Izrail Moiseevitch Gelfand, Richard A Silverman, et al. *Calculus of Variations*. Courier Corporation, 2000.

[24] Alessio Serafini. *Quantum Coninuous Variables: A Primer of Theoretical Methods*. Taylor & Francis, 2017.

[25] Samuel L Braunstein. Squeezing as an irreducible resource. *Physical Review A*, 71(5):055801, 2005.

[26] Michael Reck, Anton Zeilinger, Herbert J Bernstein, and Philip Bertani. Experimental realization of any discrete unitary operator. *Physical Review Letters*, 73(1):58, 1994.

[27] Mark M Wilde. *Quantum Information Theory*. Cambridge University Press, 2013.

[28] Asher Peres. Separability criterion for density matrices. *Physical Review Letters*, 77(8):1413, 1996.

[29] Guifré Vidal and Reinhard F Werner. Computable measure of entanglement. *Physical Review A*, 65(3):032314, 2002.

[30] Martin B Plenio. Logarithmic negativity: A full entanglement monotone that is not convex. *Physical Review Letters*, 95(9):090503, 2005.

[31] Sumeet Khatri and Mark M Wilde. Principles of quantum communication theory: A modern approach. *arXiv:2011.04672*, 2020.

[32] Charles H Bennett, Gilles Brassard, Sandu Popescu, Benjamin Schumacher, John A Smolin, and William K Wootters. Purification of noisy entanglement and faithful teleportation via noisy channels. *Physical Review Letters*, 76(5):722, 1996.

[33] Norbert Kalb, Andreas A Reiserer, Peter C Humphreys, Jacob JW Bakermans, Sten J Kamerling, Naomi H Nickerson, Simon C Benjamin, Daniel J Twitchen, Matthew Markham, and Ronald Hanson. Entanglement distillation between solid-state quantum network nodes. *Science*, 356(6341):928–932, 2017.

[34] Charles H. Bennett and Gilles Brassard. Quantum cryptography: Public key distribution and coin tossing. In *International Conference on Computer System and Signal Processing, IEEE, 1984*, pages 175–179, 1984.

[35] Artur K. Ekert. Quantum cryptography based on Bell's theorem. *Physical Review Letters*, 67:661–663, August 1991.

[36] Nicolas Gisin, Grégoire Ribordy, Wolfgang Tittel, and Hugo Zbinden. Quantum cryptography. *Reviews of Modern Physics*, 74:145–195, March 2002.

[37] Valerio Scarani, Helle Bechmann-Pasquinucci, Nicolas J. Cerf, Miloslav Dušek, Norbert Lütkenhaus, and Momtchil Peev. The security of practical quantum key distribution. *Reviews of Modern Physics*, 81:1301–1350, September 2009.

[38] Peter Shor. Algorithms for quantum computation: discrete logarithms and factoring. In *Proceedings 35th Annual Symposium on Foundations of Computer Science*, pages 124–134, November 1994.

[39] Peter Shor. Polynomial-time algorithms for prime factorization and discrete logarithms on a quantum computer. *SIAM Journal on Computing*, 26(5):1484–1509, 1997.

[40] Vasileios Mavroeidis, Kamer Vishi, Mateusz D. Zych, and Audun Jøsang. The impact of quantum computing on present cryptography. *International Journal of Advanced Computer Science and Applications*, 9(3), 2018.

[41] M. Peev, C. Pacher, R. Alléaume, C. Barreiro, et al. The SECOQC quantum key distribution network in Vienna. *New Journal of Physics*, 11(7):075001, July 2009.

[42] Teng-Yun Chen, Jian Wang, Hao Liang, Wei-Yue Liu, et al. Metropolitan all-pass and inter-city quantum communication network. *Optics Express*, 18(26):27217–27225, December 2010.

[43] Abdul Mirza and Francesco Petruccione. Realizing long-term quantum cryptography. *Journal of the Optical Society of America B*, 27(6):A185–A188, June 2010.

[44] D. Stucki, M. Legré, F. Buntschu, B. Clausen, et al. Long-term performance of the SwissQuantum quantum key distribution network in a field environment. *New Journal of Physics*, 13(12):123001, December 2011.

[45] M. Sasaki, M. Fujiwara, H. Ishizuka, W. Klaus, et al. Field test of quantum key distribution in the Tokyo QKD Network. *Optics Express*, 19(11):10387–10409, May 2011.

[46] Shuang Wang, Wei Chen, Zhen-Qiang Yin, Hong-Wei Li, et al. Field and long-term demonstration of a wide area quantum key distribution network. *Optics Express*, 22(18):21739–21756, September 2014.

[47] Darius Bunandar, Anthony Lentine, Catherine Lee, Hong Cai, et al. Metropolitan quantum key distribution with silicon photonics. *Physical Review X*, 8:021009, April 2018.

[48] Qiang Zhang, Feihu Xu, Yu-Ao Chen, Cheng-Zhi Peng, and Jian-Wei Pan. Large scale quantum key distribution: challenges and solutions. *Optics Express*, 26(18):24260–24273, September 2018.

[49] Morten Kjaergaard, Mollie E. Schwartz, Jochen Braumüller, Philip Krantz, Joel I-Jan Wang, Simon Gustavsson, and William D. Oliver. Superconducting qubits: Current state of play. *arXiv:1905.13641*, 2019.

[50] Colin D. Bruzewicz, John Chiaverini, Robert McConnell, and Jeremy M. Sage. Trapped-ion quantum computing: Progress and challenges. *arXiv:1904.04178*, 2019.

[51] Frank Arute, Kunal Arya, Ryan Babbush, Dave Bacon, et al. Quantum supremacy using a programmable superconducting processor. *Nature*, 574(7779):505–510, 2019.

[52] Michele Mosca. Cybersecurity in an era with quantum computers: will we be ready? *Cryptology ePrint Archive, Report 2015/1075*, 2015.

[53] Michele Mosca Vlad Gheorghiu. Benchmarking the quantum cryptanalysis of symmetric, public-key and hash-based cryptographic schemes. *arXiv:1902.02332*, 2018.

[54] Michele Mosca and Marco Piani. Quantum threat timeline report. *Global Risk Institute*, 2019.

[55] Christoph Simon. Towards a global quantum network. *Nature Photonics*, 11:678–680, 2017.

[56] Davide Castelvecchi. The quantum internet has arrived (and it hasn't). *Nature*, 554:289–292, 2018.

[57] Stephanie Wehner, David Elkouss, and Ronald Hanson. Quantum internet: A vision for the road ahead. *Science*, 362(6412), 2018.

[58] Charles H. Bennett, Gilles Brassard, Claude Crépeau, Richard Jozsa, Asher Peres, and William K. Wootters. Teleporting an unknown quantum state via dual classical and Einstein-Podolsky-Rosen channels. *Physical Review Letters*, 70:1895–1899, March 1993.

[59] Samuel L. Braunstein, Christopher A. Fuchs, and H. J. Kimble. Criteria for continuous-variable quantum teleportation. *Journal of Modern Optics*, 47(2-3):267–278, 2000.

[60] Richard Jozsa, Daniel S. Abrams, Jonathan P. Dowling, and Colin P. Williams. Quantum clock synchronization based on shared prior entanglement. *Physical Review Letters*, 85:2010–2013, August 2000.

[61] Ulvi Yurtsever and Jonathan P. Dowling. Lorentz-invariant look at quantum clock-synchronization protocols based on distributed entanglement. *Physical Review A*, 65:052317, May 2002.

[62] Ebubechukwu O Ilo-Okeke, Louis Tessler, Jonathan P Dowling, and Tim Byrnes. Remote quantum clock synchronization without synchronized clocks. *npj Quantum Information*, 4(1):40, 2018.

[63] J. I. Cirac, A. K. Ekert, S. F. Huelga, and C. Macchiavello. Distributed quantum computation over noisy channels. *Physical Review A*, 59:4249–4254, June 1999.

[64] C. L. Degen, F. Reinhard, and P. Cappellaro. Quantum sensing. *Reviews of Modern Physics*, 89:035002, July 2017.

[65] Quntao Zhuang, Zheshen Zhang, and Jeffrey H. Shapiro. Distributed quantum sensing using continuous-variable multipartite entanglement. *Physical Review A*, 97:032329, March 2018.

[66] Yi Xia, Quntao Zhuang, William Clark, and Zheshen Zhang. Repeater-enhanced distributed quantum sensing based on continuous-variable multipartite entanglement. *Physical Review A*, 99:012328, January 2019.

[67] O. Svelto. *Principles of Lasers*. Springer US, 5 edition, 2010.

[68] Hemani Kaushal, V. K. Jain, and Subrat Kar. *Free Space Optical Communication*. Springer Nature, 2017.

[69] H.-J. Briegel, W. Dür, J. I. Cirac, and P. Zoller. Quantum repeaters: The role of imperfect local operations in quantum communication. *Physical Review Letters*, 81:5932–5935, December 1998.

[70] W. Dür, H.-J. Briegel, J. I. Cirac, and P. Zoller. Quantum repeaters based on entanglement purification. *Physical Review A*, 59:169–181, January 1999.

[71] Nicolas Sangouard, Christoph Simon, Hugues de Riedmatten, and Nicolas Gisin. Quantum repeaters based on atomic ensembles and linear optics. *Reviews of Modern Physics*, 83:33–80, March 2011.

[72] M. Żukowski, A. Zeilinger, M. A. Horne, and A. K. Ekert. 'Event-ready-detectors' Bell experiment via entanglement swapping. *Physical Review Letters*, 71:4287–4290, December 1993.

[73] Charles H. Bennett, Gilles Brassard, Sandu Popescu, Benjamin Schumacher, John A. Smolin, and William K. Wootters. Purification of noisy entanglement and faithful teleportation via noisy channels. *Physical Review Letters*, 76:722–725, January 1996.

[74] David Deutsch, Artur Ekert, Richard Jozsa, Chiara Macchiavello, Sandu Popescu, and Anna Sanpera. Quantum privacy amplification and the security of quantum cryptography over noisy channels. *Physical Review Letters*, 77:2818–2821, September 1996.

[75] Charles H. Bennett, David P. DiVincenzo, John A. Smolin, and William K. Wootters. Mixed-state entanglement and quantum error correction. *Physical Review A*, 54:3824–3851, November 1996.

[76] Barbara M. Terhal. Quantum error correction for quantum memories. *Reviews of Modern Physics*, 87:307–346, April 2015.

[77] Sreraman Muralidharan, Linshu Li, Jungsang Kim, Norbert Lütkenhaus, Mikhail D. Lukin, and Liang Jiang. Optimal architectures for long distance quantum communication. *Scientific Reports*, 6:20463, 2016.

[78] Peter C. Humphreys, Norbert Kalb, Jaco P. J. Morits, Raymond N. Schouten, Raymond F. L. Vermeulen, Daniel J. Twitchen, Matthew Markham, and Ronald Hanson. Deterministic delivery of remote entanglement on a quantum network. *Nature*, 558(7709):268, 2018.

[79] Norbert Kalb, Andreas A. Reiserer, Peter C. Humphreys, Jacob J. W. Bakermans, et al. Entanglement distillation between solid-state quantum network nodes. *Science*, 356(6341):928–932, 2017.

[80] Stephan Ritter, Christian Nölleke, Carolin Hahn, Andreas Reiserer, et al. An elementary quantum network of single atoms in optical cavities. *Nature*, 484(7393):195, 2012.

[81] Christoph Simon, Hugues de Riedmatten, Mikael Afzelius, Nicolas Sangouard, Hugo Zbinden, and Nicolas Gisin. Quantum repeaters with photon pair sources and multimode memories. *Physical Review Letters*, 98:190503, May 2007.

[82] Neil Sinclair, Erhan Saglamyurek, Hassan Mallahzadeh, Joshua A. Slater, Mathew George, Raimund Ricken, Morgan P. Hedges, Daniel Oblak, Christoph Simon, Wolfgang Sohler, et al. Spectral multiplexing for scalable quantum photonics using an atomic frequency comb quantum memory and feed-forward control. *Physical Review Letters*, 113(5):053603, 2014.

[83] Tian-Shu Yang, Zong-Quan Zhou, Yi-Lin Hua, Xiao Liu, et al. Multiplexed storage and real-time manipulation based on a multiple degree-of-freedom quantum memory. *Nature Communications*, 9(1):3407, 2018.

[84] David Edward Bruschi, Carlos Sabín, Angela White, Valentina Baccetti, Daniel K. L. Oi, and Ivette Fuentes. Testing the effects of gravity and motion on quantum entanglement in space-based experiments. *New Journal of Physics*, 16(5):053041, 2014.

[85] P. Kómár, E. M. Kessler, M. Bishof, L. Jiang, A. S. Sørensen, J. Ye, and M. D. Lukin. A quantum network of clocks. *Nature Physics*, 10:582, 2014.

[86] M. Aspelmeyer, T. Jennewein, M. Pfennigbauer, W. R. Leeb, and A. Zeilinger. Long-distance quantum communication with entangled photons using satellites. *IEEE Journal of Selected Topics in Quantum Electronics*, 9(6):1541–1551, November 2003.

[87] Thomas Jennewein and Brendon Higgins. The quantum space race. *Physics World*, 26(03):52, 2013.

[88] Robert Bedington, Juan Miguel Arrazola, and Alexander Ling. Progress in satellite quantum key distribution. *npj Quantum Information*, 3:30, 2017.

[89] Daniel K. L. Oi, Alex Ling, Giuseppe Vallone, Paolo Villoresi, et al. Cubesat quantum communications mission. *EPJ Quantum Technology*, 4(1):6, 2017.

[90] Erik Kerstel, Arnaud Gardelein, Mathieu Barthelemy, Matthias Fink, Siddarth Koduru Joshi, and Rupert Ursin. Nanobob: a cubesat mission concept for quantum communication experiments in an uplink configuration. *EPJ Quantum Technology*, 5(1):6, 2018.

[91] Daniel Gottesman, Thomas Jennewein, and Sarah Croke. Longer-baseline telescopes using quantum repeaters. *Physical Review Letters*, 109:070503, August 2012.

[92] E. T. Khabiboulline, J. Borregaard, K. De Greve, and M. D. Lukin. Optical interferometry with quantum networks. *Physical Review Letters*, 123:070504, August 2019.

[93] E. T. Khabiboulline, J. Borregaard, K. De Greve, and M. D. Lukin. Quantum-assisted telescope arrays. *Physical Review A*, 100:022316, August 2019.

[94] David Rideout, Thomas Jennewein, Giovanni Amelino-Camelia, Tommaso F. Demarie, et al. Fundamental quantum optics experiments conceivable with satellites–reaching relativistic distances and velocities. *Classical and Quantum Gravity*, 29(22):224011, 2012.

[95] C. Bonato, A. Tomaello, V. Da Deppo, G. Naletto, and P. Villoresi. Feasibility of satellite quantum key distribution. *New Journal of Physics*, 11(4):045017, April 2009.

[96] Dominique Elser, Stefan Seel, Frank Heine, Thomas Länger, Momtchil Peev, Daniele Finocchiaro, Roberta Campo, Annamaria Recchia, Alessandro Le Pera Thomas Scheidl, and Rupert Ursin. Network architectures for space-optical quantum cryptopgraphy services. In *Proc. International Conference on Space Optical Systems and Applications (ICSOS)*, 2012.

[97] J.-P. Bourgoin, E. Meyer-Scott, B. L. Higgins, B. Helou, et al. A comprehensive design and performance analysis of low earth orbit satellite quantum communication. *New Journal of Physics*, 15(2):023006, 2013.

[98] K. Boone, J.-P. Bourgoin, E. Meyer-Scott, K. Heshami, T. Jennewein, and C. Simon. Entanglement over global distances via quantum repeaters with satellite links. *Physical Review A*, 91:052325, May 2015.

[99] Zhongkan Tang, Rakhitha Chandrasekara, Yue Chuan Tan, Cliff Cheng, et al. Generation and analysis of correlated pairs of photons aboard a nanosatellite. *Physical Review Applied*, 5:054022, May 2016.

[100] Robert Bedington, Xueliang Bai, Edward Truong-Cao, Yue Chuan Tan, et al. Nanosatellite experiments to enable future space-based QKD missions. *EPJ Quantum Technology*, 3(1):12, 2016.

[101] Mingjian He, Robert Malaney, and Jonathan Green. Quantum communications via satellite with photon subtraction. *arXiv:1806.00924*, 2018.

[102] Mingjian He, Robert Malaney, and Jonathan Green. Photonic Engineering for CV-QKD over Earth-Satellite Channels. *arXiv:1902.09175*, 2019.

[103] Tom Vergoossen, Sergio Loarte, Robert Bedington, Hans Kuiper, and Alexander Ling. Satellite constellations for trusted node QKD networks. *arXiv:1903.07845*, 2019.

[104] Sheng-Kai Liao, Hai-Lin Yong, Chang Liu, Guo-Liang Shentu, et al. Long-distance free-space quantum key distribution in daylight towards inter-satellite communication. *Nature Photonics*, 11(8):509, 2017.

[105] Sheng-Kai Liao, Wen-Qi Cai, Wei-Yue Liu, Liang Zhang, et al. Satellite-to-ground quantum key distribution. *Nature*, 549:43, 2017.

[106] Hideki Takenaka, Alberto Carrasco-Casado, Mikio Fujiwara, Mitsuo Kitamura, Masahide Sasaki, and Morio Toyoshima. Satellite-to-ground quantum-limited communication using a 50-kg-class microsatellite. *Nature Photonics*, 11(8):502, 2017.

[107] Ji-Gang Ren, Ping Xu, Hai-Lin Yong, Liang Zhang, Sheng-Kai Liao, Juan Yin, Wei-Yue Liu, Wen-Qi Cai, Meng Yang, Li Li, et al. Ground-to-satellite quantum teleportation. *Nature*, 549(7670):70, 2017.

[108] Luca Calderaro, Costantino Agnesi, Daniele Dequal, Francesco Vedovato, et al. Towards quantum communication from global navigation satellite system. *Quantum Science and Technology*, 4(1):015012, December 2018.

[109] Olivia Lee and Tom Vergoossen. An updated analysis of satellite quantum-key distribution missions. *arXiv:1909.13061*, 2019.

[110] Luca Mazzarella, Christopher Lowe, David Lowndes, Siddarth K. Joshi, et al. QUARC: Quantum Research Cubesat—A Constellation for Quantum Communication. *Cryptography*, 4:7, 2020.

[111] J. G. Walker. Circular orbit patterns providing continuous whole earth coverage. *Royal Aircraft Establishment Techical Report*, 70211, 1970.

[112] Raymond J. Leopold. The Iridium Communications Systems. In *Communications on the Move : Singapore ICCS/ISITA '92, 16-20 November 1992*, pages 451–455. IEEE, 1992.

[113] S. R. Pratt, R. A. Raines, C. E. Fossa, and M. A. Temple. An operational and performance overview of the IRIDIUM low earth orbit satellite system. *IEEE Communications Surveys*, 2(2):2–10, 1999.

[114] R. David Luders. Satellite networks for continuous zonal coverage. *ARS Journal*, 31(2):179–184, 1961.

[115] Thomas J. Lang and William S. Adams. A Comparison of Satellite Constellations for Continuous Global Coverage. In Jozef C. van der Ha, editor, *Mission Design & Implementation of Satellite Constellations*, pages 51–62, Dordrecht, 1998. Springer Netherlands.

[116] Erick Lansard, Eric Frayssinhes, and Jean-Luc Palmade. Global design of satellite constellations: a multi-criteria performance comparison of classical walker patterns and new design patterns. *Acta Astronautica*, 42(9):555–564, 1998.

[117] Mark Handley. Delay is not an option: Low latency routing in space. In *Proceedings of the 17th ACM Workshop on Hot Topics in Networks*, HotNets '18, pages 85–91, New York, NY, USA, 2018. Association for Computing Machinery.

[118] Carlo Liorni, Hermann Kampermann, and Dagmar Bruss. Quantum repeaters in space. *arXiv:2005.10146*, 2020.

[119] Mustafa Gündoğan, Jasminder S. Sidhu, Victoria Henderson, Luca Mazzarella, Janik Wolters, Daniel K.L. Oi, and Markus Krutzik. Space-borne quantum memories for global quantum communication. *arXiv:2006.10636*, 2020.

[120] Rolf T. Horn, Piotr Kolenderski, Dongpeng Kang, Payam Abolghasem, et al. Inherent polarization entanglement generated from a monolithic semiconductor chip. *Scientific Reports*, 3:2314, 2013.

[121] Nobuyuki Matsuda, Hanna Le Jeannic, Hiroshi Fukuda, Tai Tsuchizawa, et al. A monolithically integrated polarization entangled photon pair source on a silicon chip. *Scientific Reports*, 2:817, 2012.

[122] Dongpeng Kang, Ankita Anirban, and Amr S. Helmy. Monolithic semiconductor chips as a source for broadband wavelength-multiplexed polarization entangled photons. *Optics Express*, 24(13):15160–15170, June 2016.

[123] Michael Kues, Christian Reimer, Piotr Roztocki, Luis Romero Cortés, et al. On-chip generation of high-dimensional entangled quantum states and their coherent control. *Nature*, 546:622, 2017.

[124] J. F. Dynes, H. Takesue, Z. L. Yuan, A. W. Sharpe, et al. Efficient entanglement distribution over 200 kilometers. *Optics Express*, 17(14):11440–11449, July 2009.

[125] Juan Yin, Ji-Gang Ren, He Lu, Yuan Cao, et al. Quantum teleportation and entanglement distribution over 100-kilometre free-space channels. *Nature*, 488:185–188, 2012.

[126] Takahiro Inagaki, Nobuyuki Matsuda, Osamu Tadanaga, Masaki Asobe, and Hiroki Takesue. Entanglement distribution over 300 km of fiber. *Optics Express*, 21(20):23241–23249, Oct 2013.

[127] Sören Wengerowsky, Siddarth Koduru Joshi, Fabian Steinlechner, Julien R. Zichi, et al. Entanglement distribution over a 96-km-long submarine optical fiber. *Proceedings of the National Academy of Sciences*, 116(14):6684–6688, 2019.

[128] D. Vasylyev, A. A. Semenov, W. Vogel, K. Günthner, A. Thurn, Ö. Bayraktar, and Ch. Marquardt. Free-space quantum links under diverse weather conditions. *Physical Review A*, 96:043856, Oct 2017.

[129] Carlo Liorni, Hermann Kampermann, and Dagmar Bruß. Satellite-based links for quantum key distribution: beam effects and weather dependence. *New Journal of Physics*, 21(9):093055, September 2019.

[130] Mateusz Polnik, Luca Mazzarella, Marilena Di Carlo, Daniel K. L. Oi, Annalisa Riccardi, and Ashwin Arulselvan. Scheduling of space to ground quantum key distribution. *EPJ Quantum Technology*, 7:3, 2020.

[131] Heasin Ko, Kap-Joong Kim, Joong-Seon Choe, Byung-Seok Choi, Jong-Hoi Kim, Yongsoon Baek, and Chun Ju Youn. Experimental filtering effect on the daylight operation of a free-space quantum key distribution. *Scientific Reports*, 8(1):15315, 2018.

[132] Adam Bognat and Patrick Hayden. *Privacy from Accelerating Eavesdroppers: The Impact of Losses*, pages 180–190. Springer International Publishing, Cham, 2014.

[133] Siddhartha Das, Sumeet Khatri, and Jonathan P. Dowling. Robust quantum network architectures and topologies for entanglement distribution. *Physical Review A*, 97:012335, January 2018.

[134] D. Vasylyev, W. Vogel, and F. Moll. Satellite-mediated quantum atmospheric links. *Physical Review A*, 99(5):053830, 2019.

[135] Craig F. Bohren and Donald R. Huffman. *Absorption and scattering of light by small particles*. John Wiley & Sons, 2008.

[136] Larry C. Andrews and Ronald L. Phillips. *Laser beam propagation through random media*, volume 152. SPIE press, 2005.

[137] Yuan Cao, Yu-Huai Li, Wen-Jie Zou, Zheng-Ping Li, et al. Bell Test over Extremely High-Loss Channels: Towards Distributing Entangled Photon Pairs between Earth and the Moon. *Physical Review Letters*, 120:140405, April 2018.

[138] V. V. Gounder, R. Prakash, and H. Abu-Amara. Routing in LEO-based satellite networks. In *1999 IEEE Emerging Technologies Symposium. Wireless Communications and Systems (IEEE Cat. No.99EX297)*, pages 22.1–22.6, 1999.

[139] Jae-Wook Lee, Jun-Woo Lee, Tae-Wan Kim, and Dae-Ung Kim. Satellite over satellite (SOS) network: a novel concept of hierarchical architecture and routing in satellite network. In *Proceedings 25th Annual IEEE Conference on Local Computer Networks. LCN 2000*, pages 392–399, 2000.

[140] Caleb Ho, Antia Lamas-Linares, and Christian Kurtsiefer. Clock synchronization by remote detection of correlated photon pairs. *New Journal of Physics*, 11(4):045011, 2009.

[141] Jianwei Lee, Lijiong Shen, Alessandro Cerè, James Troupe, Antia Lamas-Linares, and Christian Kurtsiefer. Symmetrical clock synchronization with time-correlated photon pairs. *Applied Physics Letters*, 114(10):101102, 2019.

[142] Hui Dai, Qi Shen, Chao-Ze Wang, Shuang-Lin Li, Wei-Yue Liu, Wen-Qi Cai, Sheng-Kai Liao, Ji-Gang Ren, Juan Yin, Yu-Ao Chen, et al. Towards satellite-based quantum-secure time transfer. *Nature Physics*, 16(8):848–852, 2020.

[143] Hawking, Stephen W. Black hole explosions? *Nature*, 248(5443):30–31, 1974.

[144] Hawking, Stephen W. Particle creation by black holes. *Communications in Mathematical Physics*, 43(3):199–220, 1975.

[145] Unruh, William G and Wald, Robert M. Information loss. *Reports on Progress in Physics*, 80(9):092002, 2017.

[146] Visser, Matt. Essential and inessential features of hawking radiation. *International Journal of Modern Physics D*, 12(04):649–661, 2003.

[147] Unruh, William G. Notes on black-hole evaporation. *Physical Review D*, 14(4):870, 1976.

[148] Crispino, Luis CB and Higuchi, Atsushi and Matsas, George EA. The unruh effect and its applications. *Reviews of Modern Physics*, 80(3):787, 2008.

[149] Novello, Mário and Visser, Matt and Volovik, Grigory E. *Artificial black holes*. World Scientific, 2002.

[150] Barceló, Carlos and Liberati, Stefano and Visser, Matt. Analogue gravity. *Living Reviews in Relativity*, 14(1):1–159, 2011.

[151] Barceló, Carlos. Analogue black-hole horizons. *Nature Physics*, 15(3):210–213, 2019.

[152] Unruh, William George. Experimental black-hole evaporation? *Physical Review Letters*, 46(21):1351, 1981.

[153] Weinfurtner, Silke and Tedford, Edmund W and Penrice, Matthew CJ and Unruh, William G and Lawrence, Gregory A. Measurement of stimulated hawking emission in an analogue system. *Physical Review Letters*, 106(2):021302, 2011.

[154] Jean Macher and Renaud Parentani. Black-hole radiation in bose-einstein condensates. *Physical Review A*, 80(4):043601, 2009.

[155] Steinhauer, Jeff. Observation of quantum hawking radiation and its entanglement in an analogue black hole. *Nature Physics*, 12(10):959–965, 2016.

[156] De Nova, Juan Ramon Munoz and Golubkov, Katrine and Kolobov, Victor I and Steinhauer, Jeff. Observation of thermal hawking radiation and its temperature in an analogue black hole. *Nature*, 569(7758):688–691, 2019.

[157] Kolobov, Victor I and Golubkov, Katrine and de Nova, Juan Ramón Muñoz and Steinhauer, Jeff. Observation of stationary spontaneous hawking radiation and the time evolution of an analogue black hole. *Nature Physics*, pages 1–6, 2021.

[158] Philbin, Thomas G and Kuklewicz, Chris and Robertson, Scott and Hill, Stephen and König, Friedrich and Leonhardt, Ulf. Fiber-optical analog of the event horizon. *Science*, 319(5868):1367–1370, 2008.

[159] Drori, Jonathan and Rosenberg, Yuval and Bermudez, David and Silberberg, Yaron and Leonhardt, Ulf. Observation of stimulated hawking radiation in an optical analogue. *Physical Review Letters*, 122(1):010404, 2019.

[160] Rosenberg, Yuval. Optical analogues of black-hole horizons. *Philosophical Transactions of the Royal Society A*, 378(2177):20190232, 2020.

[161] Jacquet, Maxime J and Weinfurtner, Silke and Koenig, Friedrich. The next generation of analogue gravity experiments, 2020.

[162] Demircan, A and Amiranashvili, Sh and Steinmeyer, G. Controlling light by light with an optical event horizon. *Physical Review Letters*, 106(16):163901, 2011.

[163] Rubino, Elenora and Lotti, A and Belgiorno, F and Cacciatori, SL and Couairon, Arnaud and Leonhardt, Ulf and Faccio, D. Soliton-induced relativistic-scattering and amplification. *Scientific Reports*, 2(1):1–4, 2012.

[164] Petev, Mike and Westerberg, Niclas and Moss, Daniel and Rubino, Elenora and Rimoldi, C and Cacciatori, SL and Belgiorno, F and Faccio, D. Blackbody emission from light interacting with an effective moving dispersive medium. *Physical Review Letters*, 111(4):043902, 2013.

[165] Stefano Finazzi and Iacopo Carusotto. Quantum vacuum emission in a nonlinear optical medium illuminated by a strong laser pulse. *Physical Review A*, 87(2):023803, 2013.

[166] Belgiorno, F and Cacciatori, SL and Dalla Piazza, F. Hawking effect in dielectric media and the hopfield model. *Physical Review D*, 91(12):124063, 2015.

[167] Linder, Malte F and Schützhold, Ralf and Unruh, William G. Derivation of Hawking radiation in dispersive dielectric media. *Physical Review D*, 93(10):104010, 2016.

[168] Jacquet, Maxime J and König, Friedrich. Analytical description of quantum emission in optical analogs to gravity. *Physical Review A*, 102(1):013725, 2020.

[169] Alessio Serafini. *Quantum continuous variables: a primer of theoretical methods*. CRC press, 2017.

[170] Mark Fox. Optical properties of solids, 2002.

[171] Fabbri, Alessandro and Navarro-Salas, José. *Modeling black hole evaporation*. World Scientific, 2005.

[172] Bruschi, David Edward and Friis, Nicolai and Fuentes, Ivette and Weinfurtner, Silke. On the robustness of entanglement in analogue gravity systems. *New Journal of Physics*, 15(11):113016, 2013.

[173] Xavier Busch and Renaud Parentani. Quantum entanglement in analogue hawking radiation: When is the final state nonseparable? *Physical Review D*, 89(10):105024, 2014.

[174] Nambu, Yasusada and Osawa, Yuki. Tripartite entanglement of hawking radiation in dispersive model. *arXiv:2101.11764*, 2021.

[175] Yu, Ting and Eberly, JH. Sudden death of entanglement. *Science*, 323(5914):598–601, 2009.

[176] MS Kim, W Son, Vladimír Bužek, and PL Knight. Entanglement by a beam splitter: Nonclassicality as a prerequisite for entanglement. *Physical Review A*, 65(3):032323, 2002.

[177] Zhang Jiang, Matthias D Lang, and Carlton M Caves. Mixing nonclassical pure states in a linear-optical network almost always generates modal entanglement. *Physical Review A*, 88(4):044301, 2013.

[178] Jean Macher and Renaud Parentani. Black/white hole radiation from dispersive theories. *Physical Review D*, 79(12):124008, 2009.

[179] Soonwon Choi, Yimu Bao, Xiao-Liang Qi, and Ehud Altman. Quantum Error Correction in Scrambling Dynamics and Measurement-Induced Phase Transition. *Physical Review Letters*, 125:030505, Jul 2020.

[180] Michael J Gullans and David A Huse. Dynamical purification phase transition induced by quantum measurements. *Physical Review X*, 10(4):041020, 2020.

[181] Miao Er-long, Han Zheng-fu, Gong Shun-sheng, Zhang Tao, Diao Da-Sheng, and Guo Guang-Can. Background noise of satellite-to-ground quantum key distribution. *New Journal of Physics*, 7(1):215, 2005.

[182] Mark T Gruneisen, Michael B Flanagan, Brett A Sickmiller, James P Black, Kurt E Stoltenberg, and Alexander W Duchane. Modeling daytime sky access for a satellite quantum key distribution downlink. *Optics Express*, 23(18):23924–23934, 2015.

[183] Sumeet Khatri, Corey T. Matyas, Aliza U. Siddiqui, and Jonathan P. Dowling. Practical figures of merit and thresholds for entanglement distribution in quantum networks. *Physical Review Research*, 1:023032, September 2019.

[184] O. A. Collins, S. D. Jenkins, A. Kuzmich, and T. A. B. Kennedy. Multiplexed memory-insensitive quantum repeaters. *Physical Review Letters*, 98(6):060502, 2007.

[185] Nadja K. Bernardes, Ludmiła Praxmeyer, and Peter van Loock. Rate analysis for a hybrid quantum repeater. *Physical Review A*, 83:012323, January 2011.

VITA

Anthony J. Brady was born in the beautiful mountains of Northeast Georgia in 1992. In 2016, he received his Bachelor's of science in physics from the University of North Georgia and, shortly thereafter, accepted an offer to join the physics graduate program at Louisiana State University (LSU). He is a member of the Quantum Science and Technologies group at LSU and frequently collaborates with the gravity theory group there as well. He is the father of two beautiful girls and expecting another in the Spring/Summer of 2021. Anthony enjoys mixed martial arts, a good anime, and a belly full of laughter.